UNIVERSIDAD NACIONAL AUTÓNOMA DE MÉXICO
PROGRAMA DE MAESTRÍA Y DOCTORADO EN INGENIERÍA
INGENIERÍA ELÉCTRICA - CONTROL

Dynamic State Estimation in Electric Power Systems

TESIS
QUE PARA OPTAR POR EL GRADO DE:
DOCTOR EN INGENIERÍA

PRESENTA:
Natanael Vieyra Valencia

TUTOR PRINCIPAL
Dr. Paul Rolando Maya Ortiz, Facultad de Ingeniería, UNAM

COMITÉ TUTOR
Dr. Jesús Alvarez Calderón, UAM-I
Dr. Luis Miguel Castro González, Facultad de Ingeniería, UNAM
Dr. Gerardo René Espinosa Peréz, Facultad de Ingeniería, UNAM

CIUDAD UNIVERSITARIA, CIUDAD DE MÉXICO, MAYO DE 2021

JURADO ASIGNADO:

Presidente: Dr. Jesús Alvarez Calderón

Secretario: Dr. Gerardo René Espinosa Perez

Vocal: Dr. Paul Rolando Maya Ortiz

1er. Suplente: Dr. Luis Miguel Castro González

2o. Suplente: Dr. Claudio Rubén Fuerte Esquivel

La tesis se realizó en el Laboratorio de control no lineal perteneciente al Posgrado de la Facultad de Ingeniería, UNAM.

TUTOR DE TESIS:

Dr. Paul Rolando Maya Ortiz, Facultad de Ingeniería, UNAM

In memory of my grandfather Pedro Valencia,
you will always be remembered.

Acknowledgements

To my mother and father, for their endless support and sacrifices.

To Dr. Paul Maya for his friendship and guidance since I was an undergrad student.

To Dr. Jesús Álvarez for his friendship and support, for adopting me as an academic son, I learned a lot from you.

To Dr. Luis M. Castro for their invaluable support and comments through my Ph.D. studies and for teaching me how fascinating electric power systems are.

Declaración de autenticidad

Por la presente declaro que, salvo cuando se haga referencia específica al trabajo de otras personas, el contenido de esta tesis es original y no se ha presentado total o parcialmente para su consideración para cualquier otro título o grado en esta o cualquier otra Universidad. Esta tesis es resultado de mi propio trabajo y no incluye nada que sea el resultado de algún trabajo realizado en colaboración, salvo que se indique específicamente en el texto.

Natanael Vieyra Valencia. Ciudad Universitaria, Ciudad de México, Mayo de 2021,

Abstract

Nowadays, the electric industries face an unprecedented growth of new technologies for generating energy. Microturbines, photovoltaic cells, wind turbines, wave energy converters are examples of renewable energy generators used to supply clean energy in a distributed manner. Moreover, microgrids (MGs) and, more precisely, islanded microgrids (IMGs) have been proposed as a viable alternative, especially for small remote cities, in contraposition to large generation units and large electric power systems, which often require enormous investments. However, new phenomena appear in MGs with distributed generation, and new challenges are faced in grid planning and operation.

Energy Management Systems (EMSs) are responsible for the operation, control, and protection of Electric Power Systems (EPSs). Within this heading are the also known multimachine power systems (MPSs), the single-machine infinite-bus (the most straightforward power system under some restrictive considerations) as well as the MGs (including the IMG structures). For these tasks, precise information is needed, for example, bus voltages and phase angles, electrical frequency, mechanical speed of the rotating machinery, generated active and reactive power. Despite the improved quality of the measurement devices, it is always necessary to count on a suitable tool able to deliver information about the system state for adequate control and operation of the grid; admittedly, a state estimator is a convenient tool for these purposes. The power system community has widely studied the power system state estimation for many years. Commonly, this task is done under the steady-state assumption. The nodal voltage phasors are reconstructed through a set of measurements which are nonlinear functions of the state at specific time intervals. This state estimation approach strongly depends on available measurements (redundancy is needed), and it cannot capture the dynamic phenomena related to the system. Thus, it is essential to count on detailed nonlinear models and estimation schemes that dynamically estimate the state.

The topic addressed in this present dissertation is the design of state estimation schemes for dynamic systems such that the MPSs and IMG structures. Firstly, adopting a differential-algebraic (DA) representation for an IMG consisting of a set of hydroelectric and wind generators, a polynomial load model as well as the network restrictions, two centralized estimators based on Kalman Filter theory are proposed which are easy to construct and robust against measurement noise and model uncertainties. Both

estimators, through a set of measurements given by bus voltage phasors and power outputs of generators, can depict in real-time the dynamic variables (load angles, internal voltages, mechanical speeds) of generators together with the algebraic variables (bus voltage magnitudes and phase angles) through the same estimation scheme, thus reducing the number of the employed sensors. Furthermore, the estimation schemes can recover the transient and steady-state regimes associated with the operation of the IMG. Finally, both estimators' performance is evaluated using practical IMG models containing wind power and hydroelectric generators, under load and wind variations, and three-phase faults.

Secondly, the problem of estimating the states of an MPS consisting of interconnected synchronous generators through a purely inductive transmission network and a constant impedance load model is addressed within a constructive framework by combining notions and tools from electrical engineering, model design for a specific purpose at hand, the nonlinear estimation. The estimation of dynamic variables (load angle, relative speed, and electrical power variation) of each generator is carried out using the load angle as individual measured output and not requiring the knowledge of the global system, the result is a design with (i) systematic construction, (ii) solvability in terms of observability and robust convergence in the presence of modeling-measurement error criterion coupled with a conventional-like simple pole placement-based tuning, and (iii) robust functioning underlain by an adequate compromise between reconstruction speed, robustness concerning model error and measurement noise, as well as on-line computational load. The proposed design methodology is: (i) put in perspective with previous sliding modes (SM) and extended Kalman filter (EKF) techniques, and (ii) illustrated through numerical simulation with a representative case example, including favorable comparison against the conventional EKF.

Contents

List of Figures

List of Tables

Notation and Acronyms

Variables and Constant Definitions

δ_i	—	Power angle of the synchronous generator
ω_i, f_0	—	Rotor speed of the synchronous generator and synchronous frequency
P_i	—	Difference between the electrical power minus mechanical input power
E'_{q_i}	—	q- transient voltage of the synchronous generator
P_{m_i}	—	Per unit mechanical input power
E_{f_i}	—	Per unit field voltage
H_i, D_i	—	Inertia constant and damping factor per unit
x_{d_i}, x_{q_i}	—	Direct- and quadratic-axis reactance
x'_{d_i}	—	Direct-axis transient reactance
τ_i	—	Direct-axis transient open-circuit time constant of the synchronous generator
P_{g_i}, Q_{g_i}	—	Generated active and generated reactive powers by the synchronous generator
P_{gs_i}, Q_{gs_i}	—	Generated active and generated reactive powers by the wind generator
P_{wt}, ρ	—	Mechanical power developed by the wind turbine's rotor and air density
A, V_w	—	Swept area of the blades and wind speed
λ, n_{gb}	–	Tip speed ratio and gear box ratio
R, β	—	Rotor blade radius of the turbine and pitch angle
e'_{d_i}, e'_{q_i}	—	d- and q- transient voltage of the induction generator
ω_{m_i}, ω_b	—	Mechanical speed of the induction generator and base angular speed
ω_s, R_r	—	Electrical rotating speed of the stator and rotor resistance
T'_0	—	Transient open-circuit time constant of the induction generator
L_{m_i}, L_{rr_i}	—	Mutual inductance and rotor inductance of the induction generator
X'	—	Transient reactance of the induction generator
H_{eq_i}	—	Equivalent inertia of the turbine-generator group
T_{e_i}, θ_e	—	Per unit electromagnetic torque and electrical angle
V_i, θ_i	—	Terminal bus voltage and phase angle
$\boldsymbol{f}, \boldsymbol{g}$	—	Nonlinear differential equations related to the generators and nonlinear algebraic equations related to the network restrictions

Acronyms

MG	—	Microgrid
IMG	—	Islanded Microgrid
DAEs	—	Differential Algebraic Equations
DA	—	Differential Algebraic
ODEs	—	Ordinary Differential Equations
DERs	—	Distributed Energy Resources
IG	—	Induction Generator
SG	—	Synchronous Generator
WLS	—	Weighted Least-Squares
E.M.F	—	Electromotive Force
RMSE	—	Root Mean Square Error
IS	—	Input-to-State
SE	—	State Estimation
R	—	Robust
NL	—	Nonlinear
GE	—	Geometric Estimator
MPS	—	Multimachine Power System
OL	—	Open Loop
CL	—	Closed Loop
EKF	—	Extended Kalman Filter
UKF	—	Unscented Kalman Filter
SPT	—	Singular Perturbation Theory
IS	—	Input-to-State
EU	—	Exponentially Ultimate
SS	—	Steady State
SMPO	—	Sliding Mode Perturbation Observer
SM	—	Sliding Modes

Extended Kalman Filter - Islanded Microgrids

$\boldsymbol{x}$	—	Dynamic variables
$\boldsymbol{z}$	—	Algebraic variables
n_d	—	Dimension of dynamic variables
n_z	—	Dimension of algebraic variables
$\hat{\boldsymbol{x}}$	—	Estimated value of $\boldsymbol{x}$
$\hat{\boldsymbol{z}}$	—	Estimated value of $\boldsymbol{z}$
$\boldsymbol{x}^{aug}$	—	Grouping of dynamic and algebraic variables
$\hat{\boldsymbol{x}}^{aug}$	—	Estimated value of x^{aug}
$\boldsymbol{\Lambda}$	—	Representation of augmented system
$\boldsymbol{\phi}$	—	Transition matrix of augmented system
$\boldsymbol{H}^{aug}$	—	Jacobian of measurement model with respect to the augmented state

UKF-SPT - Islanded Microgrids

$\boldsymbol{x}$	—	Dynamic variables
$\boldsymbol{z}$	—	Algebraic variables
n_d	—	Dimension of dynamic variables
n_z	—	Dimension of algebraic variables
n_{aug}	—	Dimension of augmented state (dynamic variables together with algebraic variables)
$\hat{\boldsymbol{x}}$	—	Estimated value of $\boldsymbol{x}$
$\hat{\boldsymbol{z}}$	—	Estimated value of $\boldsymbol{z}$
$\boldsymbol{x}^{aug}$	—	Grouping of dynamic and algebraic variables
$\boldsymbol{P}_{k+1}^{yy}$	—	Covariance of the measurement
$\boldsymbol{P}_{k+1}^{xy}$	—	Cross covariance of the state and measurement
$\boldsymbol{P}_{k+1}^{aug}$	—	Predicted estimation error covariance of the augmented state
$\boldsymbol{P}_{k+1|k+1}^{aug}$	—	Updated estimation error covariance of the augmented state
$\boldsymbol{W}^m, \boldsymbol{W}^c$	—	Weights for the mean and the covariance of the state or measurement
$\hat{\boldsymbol{X}}_k^{aug}$	—	Sigma points of the augmented state
$\hat{\boldsymbol{X}}_{k+1|k}^{aug}$	—	Predicted sigma points of the augmented state

Thesis Contribution and Outlines

1.1 Introduction and Thesis Motivation

Nowadays, the electric industry faces an unprecedented growth of new technologies for the generation and distribution of energy. Microturbines, photovoltaic cells, wind turbines, wave energy converters are examples of renewable energy generators used to supply clean energy in a distributed manner. Moreover, microgrids (MGs) have been proposed as a viable alternative, especially for small remote cities, in contraposition to large generation units and large electric power systems, which often require enormous investments. However, new phenomena appear in MGs (either when they work connected to the main grid or as an islanded system) with distributed generation, and new challenges are faced in grid planning, and operation [1, 2].

Energy Management Systems (EMSs) are responsible for monitoring, controlling, and protecting the MPSs, including their variants; the MGs can operate connected to the main grid or as an islanded system (IMGs). For this, the EMSs require information about the state variables of the system [2], which are associated with bus voltages and phase angles, electrical frequency, mechanical speeds of rotating machinery. Despite the improved quality of the measurement devices, it is always necessary to count on a suitable tool able to deliver information about the system state variables for adequate control and operation of the grid; admittedly, a state estimator is a convenient tool for these purposes [3, 4]. The estimated values of state variables can be used as references for local controllers or oscillation monitoring [5].

Usually, the estimation task has been carried out through the traditional static state estimation (SSE) approach under the steady-state assumption. The estimator refines the information received from the Supervisory Control And Data Acquisition (SCADA) systems and Phasor Measurement Unit (PMU) devices to obtain the best estimate of bus voltage magnitudes, and phase angles, which represent the algebraic variables of the system [5, 6].

The estimators designed under this approach strongly depends on available measurements, besides those estimators that only adopt measurements from SCADA systems

measurements (whose sampling rate is slower than those provided by PMUs) could not provide an estimate of transient behavior associated with the operation of generators, which correspond to the dynamic part of the system. It is also essential to consider these dynamic variables and algebraic variables (i.e., the network bus voltage phasors), allowing a general overview of the system. Therefore, it is necessary to count on dynamic models, and dynamic state estimation (DSE) algorithms that can provide enhanced dynamic visibility for power system monitoring [5].

In this research work, a set of non-linear differential-algebraic equations (DAEs) and a set of non-linear ordinary differential equations (ODEs) are employed for describing power system dynamics, and they are used to design the dynamic estimators.

1.2 Thesis Hypotheses

The research work presented in this dissertation is derived under the following hypotheses:

- The nonlinear dynamic systems describe the behavior of electrical power networks correctly. A set of nonlinear differential-algebraic equations or a set of nonlinear ordinary differential equations can be employed to represent the associated phenomena.

- A set of measurements that guaranteed the system's observability can be employed to design dynamic estimators that reconstruct the state variables of these mathematical representations.

1.3 Research Objectives

The research work has as the main objective to design robust dynamic state estimation schemes for dynamic systems that represent electric power systems, such as MPSs or IMG structures, considering:

- The proposed estimators should have the capacity to estimate the transient and steady-state regimes associated with the operation of these systems.

- The proposed estimators should include an observability analysis to determine the required measurements to reconstruct the state.

- The proposed estimation schemes should be generic to network decomposition, which means that it can integrate different topologies, generator units, loads.

- For a dynamic system that represents an IMG consisting of a set of hydroelectric and wind generators interconnected with another set of loads (polynomial load

model) through power lines and whose interaction is described by a differential-algebraic system (also known as structure-preserving models). The dynamic variables (load angles, internal voltages of generators, mechanical speeds) and algebraic variables (bus voltage magnitudes and phase angles) should be estimated in real-time in the presence of system disturbances through a minimum number of measurements (only the minimal amount to guarantee observability properties), which are based on bus voltage phasors and power outputs of generators. In turn, for the estimator design, the IMG structure can be assumed as a positive sequence balanced electrical network. It is assumed to know the parameters (those related to the generators and the electrical network). Moreover, a nominal control input should be considered such that the IMG can operate within the established limits.

○ For a dynamic system that represents a MPS consisting of a set of interconnected synchronous generators through a purely inductive transmission network and including a constant impedance load model, thus all zero injection nodes are removed considering only the generator nodes and whose dynamic behavior is described by a set of nonlinear differential ordinary equations. The estimation of dynamic variables (load angle, relative speed, and electrical power variation) of every generator should be carried out using the load angle as unique measured output and not requiring the global system's knowledge. The proposed estimator should reconstruct in a fast and robust way the state, even in the presence of measurement noise and parametric uncertainty coupled with a precise and systematic industrial-like tuning. Besides, the convergence must be guaranteed.

1.4 Contributions

The contributions of the thesis are divided into two main challenges, which are stated as follows.

1. The first addressed challenge is the design of robust dynamic estimators for IMG structures highlighting the following four main contributions: (i) the proposed estimators based on a centralized approach are able to depict in real-time the dynamic variables (load angles, internal voltages, mechanical speeds) of generators together with the algebraic variables (bus voltage magnitudes and phase angles) through the same estimation scheme thus reducing the number of the employed sensors, (ii) the developed dynamic estimators allows estimating the transient and steady-state regimes of an IMG, (iii) the design of estimator is generic concerning the network decompositions as well as the nonlinear dynamics associated with generators are considered, and (iv) the proposed variant of the Unscented Kalman Filter (UKF) significantly reduces the creation of algebraic loops in comparison with the traditional UKF for differential-algebraic systems, thus decreasing the simulation time and the computational load.

2. The second addressed challenge focuses on designing a dynamic state estimator for a MPS highlighting the following contributions: (i) based on a state-unmeasured input observable model of the MPS the dynamic variables of generators (load angles, relative speeds, and electrical power variations) are reconstructed in a decentralized way by using load angle as the unique measured output, (ii) the developed estimator retains the low-dimensionality (low online computational load), disturbance rejection capability, and formal assessment of robust convergence of a sliding mode observer, and the robustness of the Extended Kalman Filter concerning measurement noise but coupled with a conventional-like simple tuning scheme, (iii) identification of the underlying state-input observability property that justifies the feasibility of quickly and robustly the reconstruction of the augmented state in the presence of measurement noise which clearly leads to upper and lower observer gains that are equivalent to the ultimate gains in the industrial application tunings, (iv) the presented convergence analysis of estimation error dynamics is based on input-to-state stability sense with respect to model errors and measurement noise yielding to robust convergence conditions of the type small gains which is sharper, more transparent and with greater interpretability than those based on Lyapunov functions, and (v) the proposed estimation methodology can be easily implemented in power grids with traditional and renewable sources (like those documented in [7]) allowing the estimation of dynamic variables of generators and inverters in a decentralized way through local information with a conventional-like simple tuning scheme.

1.5   Thesis Outline

The outline of the present thesis is organized into five chapters boarding the two challenges mentioned earlier.

Chapter 2:   The state estimation problem is presented, and the dynamic model of IMG structures and MPSs employed in the analysis of the design of state estimation algorithms are introduced.

Chapter 3: The dynamic state estimation algorithms for IMGs structures based on Kalman Filter theory are presented.

Chapter 4: A new decentralized dynamic state estimator for MPS is introduced with a comparative study case with the conventional EKF.

Chapter 5: The concluding remarks of this thesis work are given, and future work ideas are established.

1.6   List of Publications

The research work contained in this thesis has given rise to the following refereed publications:

Journal Papers

1. **Natanael Vieyra**, Paul Maya, and Luis M. Castro. "Dynamic State Estimation for Microgrid Structures.", Electric Power Components and Systems, Vol. 48, 2020, pp. 1-13.

2. **Natanael Vieyra**, Paul Maya, and Luis M. Castro. "Effective dynamic state estimation algorithm for Islanded microgrid structures based on singular perturbation theory.", Electric Power Systems Research, Vol. 187, 2020, pp. 106455.

3. **Natanael Vieyra**, Jesús Álvarez, and Paul Maya-Ortiz. "Decentralized Robust State Estimation of Multimachine Power Systems.", International Journal of Electrical Power & Energy Systems, *Status- Under Review, second round.*

Conference papers

1. Michael Rojas, **Natanael Vieyra**. "A Comparative Study of State Estimation Methodologies for Electric Power Systems.", Congreso AMCA 2019, Octubre 2019, Puebla, México.

2. **Natanael Vieyra**, Paul Maya, Luis M. Castro. "Modelado Dinámico de Microrredes con Generacion Eólica: Enfoque Práctico.", Congreso AMCA 2018, Octubre 2018, San Luis Potosí, México.

3. **Natanael Vieyra**, Paul Maya, Luis M. Castro. "Comparación de Dos Métodos para Estimación Dinámica en Sistemas Eléctricos de Potencia.", Congreso AMCA 2017, Octubre 2017, Monterrey, Nuevo León, México.

State Estimation Problem and Power System Description

Abstract: This chapter is devoted to present the dynamic state estimation problem for IMG structures and MPSs. They are viewed as dynamic systems represented by a set of nonlinear ODEs or nonlinear DAEs. Firstly, the IMG model based on the differential-algebraic (DA) model is presented considering hydro generators, wind power generators, and those algebraic restrictions that describe the nodal power balance equations. Secondly, a new representation of an MPS is introduced, usually used for stability analysis for large-scale power systems. The introduced models represent the starting point to design the state estimation schemes.

2.1 Dynamic State Estimation

2.1.1 Model Under Consideration

Generally, the dynamic behavior of an electric power system, either be an IMG or an MPS, can be described through a set of nonlinear DAEs:

$$
\begin{aligned}
\dot{\boldsymbol{x}}(t) &= \boldsymbol{f}(t, \boldsymbol{x}, \boldsymbol{z}, \boldsymbol{u}), & \boldsymbol{x}(t_0) &= \boldsymbol{x}_0 \\
0 &= \boldsymbol{g}(t, \boldsymbol{x}, \boldsymbol{z}), & \boldsymbol{z}(t_0) &= \boldsymbol{z}_0 \\
\boldsymbol{y}(t) &= \boldsymbol{h}(t, \boldsymbol{x}, \boldsymbol{z})
\end{aligned}
\tag{2.1}
$$

where $\boldsymbol{x} \in \mathbb{R}^{n_d}$ are the state variables associated with the generation unit dynamics; these can be, for instance, the internal variables of a power plant (say hydroelectric or wind turbine) such as the rotor angle, mechanical speed, and internal voltages, $\boldsymbol{z} \in \mathbb{R}^{n_z}$ are variables related to the algebraic interconnection constraints, such as voltage magnitude, and voltage phase angle on each network bus, including load buses, $\boldsymbol{f} \in \mathbb{R}^{n_d}$

are the nonlinear local Lipschitz functions that describe the dynamic behavior of generators, $\boldsymbol{g} \in \mathbb{R}^{n_z}$ is the set of algebraic equations representing the network restrictions, $\boldsymbol{u} \in \mathbb{R}^p$ is the input vector (e.g., field voltage, mechanical input power) and $\boldsymbol{y} \in \mathbb{R}^m$ are the nonlinear observation equations (outputs) which can be the state or nonlinear functions of the state.

The next section the observation problem for DA systems is derived from the ideas presented in [8].

2.1.2   Observation Problem

Given a dynamic system described by a representation (2.1) the observation problem is reduced to find an estimated $(\hat{\boldsymbol{x}}(t), \hat{\boldsymbol{z}}(t))$ for $(\boldsymbol{x}(t), \boldsymbol{z}(t))$ from the knowledge of $\boldsymbol{y}(\tau)$, $\boldsymbol{u}(\tau)$ for an specific time interval $0 \leq \tau \leq \infty$.

The observation problem for dynamic systems is divided into two parts [8].

Observability: Considering only the available information $(\boldsymbol{u}, \boldsymbol{y})$, it should be possible to retrieve the real value of $\boldsymbol{x}(t)$ and $\boldsymbol{z}(t)$, over a specific time interval $\boldsymbol{t} \in [t_0, t_0 + T]$, $T > 0$.

Observer design: An observer is given by an auxiliary system for $(\boldsymbol{x}, \boldsymbol{z})$ such that

$$
\begin{aligned}
&(i) \;\; \hat{\boldsymbol{x}}(0) = \boldsymbol{x}_0 \Rightarrow \hat{\boldsymbol{x}}(t) = \boldsymbol{x}(t), && \forall t \geq 0; \\
&(ii) \;\; \hat{\boldsymbol{z}}(0) = \boldsymbol{z}_0 \Rightarrow \hat{\boldsymbol{z}}(t) = \boldsymbol{z}(t), && \forall t \geq 0; \\
&(iii) \;\; ||\boldsymbol{e}_{n_d}|| = ||\hat{\boldsymbol{x}}(t) - \boldsymbol{x}(t)|| \to 0, && \text{as} \quad t \to \infty; \\
&(iv) \;\; ||\boldsymbol{e}_{n_z}|| = ||\hat{\boldsymbol{z}}(t) - \boldsymbol{z}(t)|| \to 0, && \text{as} \quad t \to \infty
\end{aligned}
$$

If i) and ii) hold for any $\hat{\boldsymbol{x}}(0), \boldsymbol{x}(0), \hat{\boldsymbol{z}}(0), \boldsymbol{z}(0)$, the *observer is global.*

If iii) and iv) hold with exponential convergence, *the observer is exponential.*

If iii) and iv) hold with a convergence rate which can be tuned, *the observer is tunable.*

2.1.3   State Estimation Problem for IMG structures and MPSs

The IMG estimation problem whose mathematical representation is given by (2.1) turns to be a problem of observer design to estimate the state variables, $\boldsymbol{x}(t)$ and $\boldsymbol{z}(t)$ in real-time using a set of measurements that guarantee the IMG's observability. Depending on each electrical power grid and its components, these measurements may be given by bus voltage phasors and the power outputs of generators. In turn, for estimator design, it is assumed the knowledge of the parameters (those related to the generators and the electrical network), for a MPS consisting of a set of interconnected synchronous generators through a purely inductive transmission network and whose dynamic behavior is described by a set of nonlinear ODEs (for this all zero injection nodes are removed considering only the generator nodes). The estimation problem is

reduced to estimate the $\boldsymbol{x}(t)$ variables (load angle, relative speed, and electrical power variation) of each generator employing the load angle as individual measured output (one per generator).

Here below, in Section 2.2, the IMG mathematical model is presented, and in Section 2.3, a MPS dynamic model is introduced.

2.2 Microgrid Description

2.2.1 Microgrid Architecture

An MG can operate in two ways: connected to the main grid or islanded. When it operates in isolation, it can be disconnected from the main network and operate autonomously [1] and its main characteristics are:

- The MGs are composed of distributed energy resources (DERs), storage assets, and loads.

- Local control over DERs without the necessity of a dispatch center.

- Likewise, the IMG is susceptible to frequency variations due to the marked difference between the inertias of generation units; conventional generation sources (hydroelectric generation - synchronous generators), distributed energy resources (wind, solar), and those inverted sources (without inertia)[9].

To ensure the correct operation of an IMG, the EMSs require precise information about IMG state variables allowing its protection and control [10]. There are different methods and tools to achieve the correct operation of an IMG: (i) *state estimation schemes* (to provide accurate information about the IMG state), (ii) backup (batteries, capacitor bank), and (iii) control approach (centralized or decentralized) through speed governors, automatic voltage regulators, flywheel backup generators, "droop control", etc [1, 9].

Figure 2.1 shows a typical MG including DERs, industrial and residential loads, local producers, some fossil energy-based producers, and one Point of Common Coupling (PCC) with the grid.

2.2.2 Microgrid Model Incorporating Renewable Energy Resources

As previously mentioned, the mathematical model emerging from an IMG may be described by a nonlinear semi-explicit DAE (2.1). For this, the nonlinear differential functions $\boldsymbol{f}(t, \boldsymbol{x}, \boldsymbol{z}, \boldsymbol{u})$ and nonlinear algebraic constraints $\boldsymbol{g}(t, \boldsymbol{x}, \boldsymbol{z})$ are given by the expressions derived in Sections 2.2.2.1, 2.2.2.2 and 2.2.2.3, whereas, the model of measured outputs $\boldsymbol{y}$ are presented in Section 2.2.2.4.
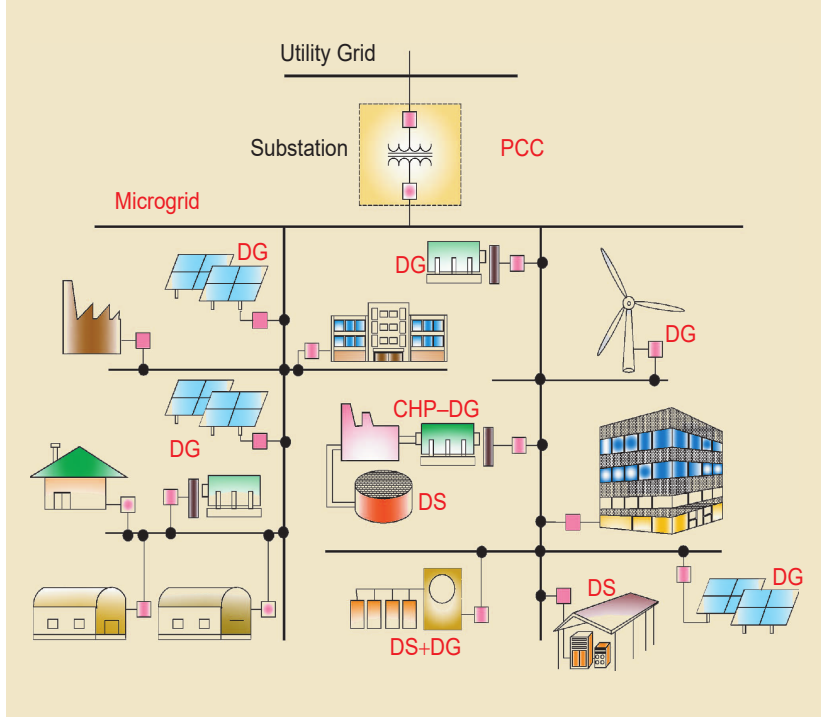
Figure 2.1: A typical MR usually includes loads and DERs units [9]

2.2.2.1 Hydroelectric Generators

Synchronous generators convert the mechanical input power from a prime mover into electrical power to supply the demand [11]. This generator is characterized by its ability to vary its power production within a few second, an important feature which is helpful for electrical frequency regulation purposes in IMG structures.

Assuming that a synchronous generator (SG) is connected to a generic node "i" of the microgrid, its dynamics may be described through the widely used flux-decay model, which involves the swing equations together with the transient voltage dynamics [12, 13]:

$$\dot{\delta}_i = \omega_i - 2\pi f_0 \tag{2.2a}$$

$$2H_i\dot{\omega}_i = P_{m_i} - D_i(\omega_i - 2\pi f_0) - P_{g_i} \tag{2.2b}$$

$$\tau_i\dot{E}'_{q_i} = -\frac{x_{d_i}}{x'_{d_i}}E'_{q_i} + \frac{x_{d_i} - x'_{d_i}}{x'_{d_i}}V_i\cos(\delta_i - \theta_i) + E_{F_i} \tag{2.2c}$$

where δ_i, ω_i and E'_{q_i}, are the rotor angle, the rotor speed, and the quadrature axis internal electromotive force (E.M.F), respectively. The terms V_i and θ_i are the terminal voltage magnitude and the phase angle, f_0 is the synchronous frequency (Hz), P_{m_i} is

the mechanical power, P_{g_i} is the active power injected by the synchronous generator, H_i, D_i are the inertia constant and the damping coefficient, respectively, x_{d_i}, x_{q_i} are the direct and quadrature axis synchronous reactance, x'_{d_i} is the direct axis transient reactance, τ_i represents the direct axis transient open-circuit time constant and E_{F_i} is the field voltage.

The active and reactive powers delivered by the generator are given by

$$P_{g_i} = \frac{E'_{q_i} V_i}{x'_{d_i}} \sin(\delta_i - \theta_i) + \frac{x'_{d_i} - x_{q_i}}{2x_{q_i} x'_{d_i}} V_i^2 \sin(2(\delta_i - \theta_i)) \tag{2.3a}$$

$$Q_{g_i} = \left(\frac{x'_{d_i} + x_{q_i}}{2x_{q_i} x'_{d_i}} - \frac{x'_{d_i} - x_{q_i}}{2x_{q_i} x'_{d_i}} \cos(2(\delta_i - \theta_i)) \right) V_i^2 - \frac{E'_{q_i} V_i}{x'_{d_i}} \cos(\delta_i - \theta_i) \tag{2.3b}$$

The mechanical input power P_{m_i} and the field voltage E_{F_i} can be modified by including speed governors and automatic voltage regulators.

2.2.2.2 Wind Power Generators

Wind power sources are one of the fastest-growing sources worldwide, especially suitable for remote areas. In this present thesis, to test the proposed state estimators, different practical IMGs with wind generation have been considered. Each wind power generator is represented by a fixed-speed wind generator based on a squirrel-cage induction generator (SCIG) driven by a wind turbine. The stator terminals are directly connected to the grid through a coupling power transformer. Since the speed is almost fixed to the grid frequency and is not controllable, an alternative to the frequency regulation can include doubly-fed induction generators with their local controls by including a converter model.

Firstly, the aerodynamic model of the wind turbine rotor includes the conversion of the kinetic energy from the wind into mechanical power developed by the wind turbine's rotor is computed by [14].

$$P_{wt} = \frac{1}{2} \rho \cdot c_1 \left(\frac{c_2}{\lambda_\alpha} - c_3 \beta - c_4 \beta^{c_5} - c_6 \right) \cdot e^{\frac{-c_7}{\lambda_\alpha}} A \cdot V_w^3 \tag{2.4}$$

with

$$\lambda_\alpha = \left[\left(\frac{1}{\lambda + c_8 \beta} \right) - \left(\frac{c_9}{\beta^3 + 1} \right) \right]^{-1}, \qquad \lambda = \frac{R \cdot n_{gb} \cdot \omega_m}{V_w} \tag{2.5}$$

where P_{wt} is the mechanical power developed by the wind turbine, ρ is the air density (kg/m^3), A is the swept area of the blades (m^2) and V_w is the wind speed (m/s), β is the pitch angle of the rotor blades (degrees) and λ is the tip speed ratio, n_{gb} is the gearbox ratio, ω_m is the angular mechanical speed (rad/s), R is the rotor blade radius of the turbine (m) and the constants c_1 to c_9 are the design parameters of the wind turbine.

Assuming an induction generator (IG)-based on wind generator, the two electrical equations describing the machine's dynamics in the dq reference frame, are [11]:

$$T'_{0_i}\frac{de'_{d_i}}{dt} = \omega_{s_i}L_{m_i}i_{qr_i} + \frac{(\omega_{s_i} - \omega_{m_i})L_{rr_i}}{R_{r_i}}e'_{q_i} \tag{2.6a}$$

$$T'_{0_i}\frac{de'_{q_i}}{dt} = -\omega_{s_i}L_{m_i}i_{dr_i} - \frac{(\omega_{s_i} - \omega_{m_i})L_{rr_i}}{R_{r_i}}e'_{d_i} \tag{2.6b}$$

where "i" is the counter index which depends on the node of the islanded microgrid where the induction generator is connected, the subscripts s and r represent quantities corresponding to the stator and rotor, respectively, e'_{d_i} and e'_{q_i} are the per-unit electromotive force behind the transient reactance, ω_{s_i} is the electrical rotating speed of the stator, ω_{m_i} is the mechanical speed of the generator rotor, ω_{b_i} is the base angular speed used to calculate the inductive reactances (rad/s), R_{r_i} represents the rotor resistance and T'_{0_i} is the transient open-circuit time constant (seconds) [3, 4].

The machine's rotor motion equation is given by swing equation describing the accelerations and the decelerations of wind generators

$$\frac{d\omega_{m_i}}{dt} = \frac{T_{e_i} - T_{m_i}}{2H_{eq_i}} \tag{2.7}$$

where H_{eq_i} is the equivalent inertia of the turbine-generator group, it includes the inertia constants of the generator and turbine. The per-unit electromagnetic torque T_{e_i} is expressed as,

$$T_{e_i} = \frac{-R_{s_i}(e'^2_{d_i} + e'^2_{q_i} + e'_{d_i}V_i\sin(\theta_i - \theta_e) - e'_{q_i}V_i\cos(\theta_i - \theta_e)) + X'_iV_i(e'_{d_i}\cos(\theta_i - \theta_e) + e'_{q_i}\sin(\theta_i - \theta_e))}{\omega_{s_i}(R^2_{s_i} + X'^2_i)} \tag{2.8}$$

where X'_i is the transient reactance, it is given by $X'_i = (L_{ss_i} - L^2_{m_i}/L_{rr_i})\omega_{s_i}$, of which $L_{ss_i} = L_{s\sigma_i} + L_{m_i}$. The subscripts r, m, s and σ stand for the rotor, mutual, stator and leakage inductances, respectively. The mechanical torque T_m (p.u) is determined by $T_{m_i} = P_{wt_i}/\omega_{m_i}$.

Finally, the active and reactive powers injected by each wind generator are expressed in terms of dynamic and algebraic variables to attain the correspondence between the network and the wind generator as follows:

$$P_{gs_i} = V_i\left(\frac{R_{s_i}(V_i + e'_{d_i}\sin(\theta_i - \theta_e) - e'_{q_i}\cos(\theta_i - \theta_e)) + X'_i(e'_{d_i}\cos(\theta_i - \theta_e) + e'_{q_i}\sin(\theta_i - \theta_e))}{R^2_{s_i} + X'^2_i}\right) \tag{2.9a}$$

$$Q_{gs_i} = V_i\left(\frac{-R_{s_i}(e'_{d_i}\cos(\theta_i - \theta_e) + e'_{q_i}\sin(\theta_i - \theta_e)) + X'_i(V_i + \sin(\theta_i - \theta_e)e'_{d_i} - \cos(\theta_i - \theta_e)e'_{q_i})}{R^2_{s_i} + X'^2_i}\right) \tag{2.9b}$$

where the terms e'_{d_i}, e'_{q_i} and ω_{m_i} are the dynamics states of the induction genera-
tor, these states together with those of hydroelectric generators, will represent the set
of dynamic variables to be estimated by this introduced dynamic estate estimation
approach.

2.2.2.3   Microgrid's Nodal Power Balance Equations

The power transmission line is one of the major components of an electric power system.
Its major function is to transport electric energy, with minimal losses, from power
sources to loads. The design of a transmission line depends on four electrical parameters
[15]:

1. Series resistance

2. Series inductance

3. Shunt capacitance

4. Shunt conductance

For estimation purposes, a medium-length transmission line model is adopted whose
single-phase equivalent model can be represented by π configuration (the shunt capac-
itance of the line is divided into two equals parts placed at the sending and receiving
ends of the line) [15]. Thus, the active and reactive powers, P_i^{cal} and Q_i^{cal}, at bus "i"
are nonlinear functions of nodal voltages and network impedances, as cited as follows:

$$P_i^{cal} = V_i^2 G_{ii} + \sum_{j=1,j\neq i}^{N} V_i V_j [G_{ij}\cos(\theta_i - \theta_j) + B_{ij}\sin(\theta_i - \theta_j)] \tag{2.10a}$$

$$Q_i^{cal} = -V_i^2 B_{ii} + \sum_{j=1,j\neq i}^{N} V_i V_j [G_{ij}\sin(\theta_i - \theta_j) - B_{ij}\cos(\theta_i - \theta_j)] \tag{2.10b}$$

where G_{ij} and B_{ij} are the conductance and the susceptance between the bus "i" and
"j", θ_j is the nodal phase angle and V_j is the nodal voltage magnitude at bus "j".
The nodal balance equations are defined as:

$$\Delta P_i = P_{G_i} - P_{L_i} - P_i^{cal} = 0 \tag{2.11a}$$

$$\Delta Q_i = Q_{G_i} - Q_{L_i} - Q_i^{cal} = 0 \tag{2.11b}$$

Notice that (2.11a)-(2.11b) imply that there is a generator connected to the cor-
responding bus "i", the terms P_{G_i} and Q_{Gi} represent the active and reactive powers
injected by the generator unit at bus "i". This generator may be either synchronous or
asynchronous depending on the type of power plant to be considered, i.e., hydroelectric
generator (2.3a)-(2.3b) or wind power generator (2.9a)-(2.9b). P_{L_i} and Q_{L_i} are the

active and reactive powers drawn by the load at bus "i". Respectively, for this, it has been considered a polynomial load model.

Remark 2.1 For a hydro generator the nonlinear functions $\boldsymbol{f}$ are given by (2.2a)-(2.2c), the dynamic and algebraic variables will be, $\boldsymbol{x} := \left[\delta_i, \omega_i, E'_{q_i}\right]^\top \in \mathbb{R}^{n_d}$ and $\boldsymbol{z} := \left[\theta_i, V_i\right]^\top \in \mathbb{R}^{n_z}$, respectively, and the inputs $\boldsymbol{u} := \left[P_{m_i}, E_{F_i}\right]$. Whereas for a fixed speed wind generator, the nonlinear functions $\boldsymbol{f}$ are given by (2.6a)-(2.7), the dynamic and algebraic variables will be, $\boldsymbol{x} := \left[\omega_{m_i}, e'_{d_i}, e'_{q_i}\right]^\top \in \mathbb{R}^{n_d}$ and $\boldsymbol{z} := \left[\theta_i, V_i\right]^\top \in \mathbb{R}^{n_z}$, respectively. The nonlinear algebraic equations $\boldsymbol{g}(t, \boldsymbol{x}, \boldsymbol{z})$ related to the microgrid's nodal power balance equations are given by (2.11a)-(2.11b) and the measured outputs $\boldsymbol{y} = \boldsymbol{h}(t, \boldsymbol{x}, \boldsymbol{z})$ used for estimators design is cited in the following Section 2.2.2.4.

2.2.2.4 Observation Model and Bad Data Detection Analysis

The dynamic estate estimation algorithms introduced in this research work based on the Kalman filter theory consider four measured outputs (2.12), provided by a measurement device installed at the generic bus "i"(assuming a synchronous generator connected to this bus) [3, 4]:

$$
\begin{aligned}
h_1 &= \frac{E'_{q_i} V_i}{x'_{d_i}} \sin(\delta_i - \theta_i) + \frac{x'_{d_i} - x_{q_i}}{2 x_{q_i} x'_{d_i}} V_i^2 \sin(2(\delta_i - \theta_i)) \\
h_2 &= \left(\frac{x'_{d_i} + x_{q_i}}{2 x_{q_i} x'_{d_i}} - \frac{x'_{d_i} - x_{q_i}}{2 x_{q_i} x'_{d_i}} \cos(2(\delta_i - \theta_i)) \right) V_i^2 - \frac{E'_{q_i} V_i}{x'_{d_i}} \cos(\delta_i - \theta_i) \\
h_3 &= V_i, \qquad h_4 = \theta_i
\end{aligned}
\tag{2.12}
$$

For the 3-bus IMG (employed in study cases of Sections 3.2.3 and 3.3.3), the observability property is guaranteed using these four measurements from bus one. Depending on each electrical power grid and their components, for the 7-bus IMG (used in simulation results of Subsections 3.2.3.2, 3.3.3.1 and 3.3.3.2), the set of measurements (2.12) can be completed with those signals associated with the output powers of wind generators (2.9a)-(2.9b). With these measurements, the reconstruction of IMG state variables is guaranteed under the observability criterion for DA systems presented in [16, 17].

The dynamic state estimation algorithms must include a bad data analysis to detect and handle the effects of gross measurement errors. The proposed estimators based on the Kalman Filter theory can identify the gross errors through a normalized innovation vector. Following the ideas presented in [18], a measurement must be discarded if it is more significant than 1.5 p.u.

2.3   A Multimachine Power System Dynamic Model

A modified model of a MPS made of N interconnected generators, considering the electrical power as the third state instead of the internal voltage, whose dynamics are described under standard assumptions [19–23], by following mechanical and energy balances:

$$\dot{\delta}_i = \omega_i, \qquad\qquad\qquad \delta_i(0) = \delta_{i0}, \quad y_i = \delta_i, \qquad i = 1, ..., \mathrm{N} \quad (2.13\mathrm{a})$$

$$\dot{\omega}_i = -a_i\omega_i - b_iP_i + d_{\omega_i}, \qquad\qquad \omega_i(0) = \omega_{i0} \qquad\qquad\qquad (2.13\mathrm{b})$$

$$\dot{P}_i = -c_iP_i + \gamma_i(\boldsymbol{\delta}, \boldsymbol{\omega}, \boldsymbol{d}_\gamma, \boldsymbol{p}_i, \boldsymbol{p}_{I_i}) + u_i, \quad P_i(0) = P_{i0} \qquad\qquad\qquad (2.13\mathrm{c})$$

where

$$\boldsymbol{\delta} = [\delta_1, ..., \delta_\mathrm{N}]^\top, \quad \boldsymbol{\omega} = [\omega_1, ..., \omega_\mathrm{N}]^\top, \quad P_i = \Delta P_{e_i} = P_{e_i} - P_{m_i} \qquad (2.13\mathrm{d})$$

$$\delta_i \in A = [0, 2\pi], \quad \omega_i \in \Omega_i = [0, \omega_i^+], \quad u_i \in U_i = [u_i^-, u_i^+] \qquad (2.13\mathrm{e})$$

$$a_i = D_i/M_i, \quad b_i = 1/M_i, \quad c_i = 1/T'_{d_i}, \quad u_i = c_iI_{q_i}E_{f_i} \qquad (2.13\mathrm{f})$$

$$\mathbf{w} = [I_{d_i}, E'_{q_i}, E'_{q_j}, \dot{E}'_{q_j}, Q_{e_i}]^\top, \quad \boldsymbol{\eta}_i = [P_{m_i}, I_{q_i}]^\top \quad \boldsymbol{d}_\gamma = [\mathbf{w}, \boldsymbol{\eta}_i]^\top \qquad (2.13\mathrm{g})$$

$$\boldsymbol{p}_i = [a_i, b_i, c_i, \rho_i, \rho_{t_i}]^\top, \quad \boldsymbol{p}_{I_i} = B_{ij} \qquad (2.13\mathrm{h})$$

$$\gamma_i(\boldsymbol{\delta}, \boldsymbol{\omega}, \boldsymbol{d}_\gamma, \boldsymbol{p}_i, \boldsymbol{p}_{I_i}) = -c_i(\rho_i - \rho_{t_i})(I_{q_i}I_{d_i}) - c_iP_{m_i} - Q_{e_i}\omega_i$$
$$+ E'_{q_i}\left[\sum_{j=1}^\mathrm{N} \dot{E}'_{q_j}B_{ij}\sin(\delta_i - \delta_j) - \sum_{j=1}^\mathrm{N} E'_{q_j}B_{ij}\cos(\delta_i - \delta_j)\omega_j\right]$$
$$(2.13\mathrm{i})$$

For the i-th generator: δ_i is the load angle [rad], ω_i is the relative speed [p.u.] (with respect to the synchronous speed), P_i is the electrical power (P_{e_i}) minus mechanical input (P_{m_i} known and constant) power [p.u.], d_{w_i} is a known persistent disturbance [p.u.], $\boldsymbol{\eta}_i$ (or $\mathbf{w}$) is the measured vector (or unmeasured vector) input [p.u.], y_i (or u_i) is the measured output [rad] (or control input [p.u.]) associated with E_{f_i}, which is an equivalent EMF in the excitation coil, g_i is a (Lipschitz bounded) nonlinear function, ρ_i (or ρ_{t_i}) is the direct axis (or transient) reactance [p.u.], D_i is the per unit damping factor, M_i is the inertia constant [s], T'_{di} is the direct axis transient short circuit time constant [s], I_{d_i} (or I_{q_i}) is the direct (or quadratic) axis current [p.u.], Q_{e_i} is the reactive power [p.u.], E'_{q_i} is the transient EMF in the quadrature axis [p.u.], and B_{ij} is the i-th row and j-th column element of nodal susceptance matrix at the internal nodes after eliminating all physical buses, $\boldsymbol{p}_i$ (or $\boldsymbol{p}_{I_i}$) are the local (or interaction) parameters and

N is the number of generators connected to the grid.

In per-machine vector notation, the MPS NL model (2.13) is written as

$$\dot{\boldsymbol{x}}_i = \mathcal{A}_i \boldsymbol{x}_i + \boldsymbol{b}_d d_{\omega_i} + \boldsymbol{b}_u [\gamma_i(\boldsymbol{x}, \boldsymbol{d}_\gamma) + u_i], \quad \boldsymbol{x}_i(0) = \boldsymbol{x}_{i_0}, \quad y_i = \boldsymbol{c}_y \boldsymbol{x}_i, \quad i = 1, ..., \text{N} \quad (2.14)$$

where

$$\boldsymbol{x}_i = \begin{bmatrix} \delta_i \\ \omega_i \\ P_i \end{bmatrix}, \quad \mathcal{A}_i = \begin{bmatrix} 0 & 1 & 0 \\ 0 & -a_i & -b_i \\ 0 & 0 & -c_i \end{bmatrix}, \quad \boldsymbol{b}_u = \begin{bmatrix} 0 \\ 0 \\ 1 \end{bmatrix}, \quad \boldsymbol{b}_d = \begin{bmatrix} 0 \\ 1 \\ 0 \end{bmatrix}, \quad \boldsymbol{c}_y = [1, 0, 0]$$

In compact form, the MPS NL model (2.14) is rewritten as

$$\dot{\boldsymbol{x}} = \boldsymbol{f}(\boldsymbol{x}, \boldsymbol{d}_x), \quad \boldsymbol{x}(0) = \boldsymbol{x}_0, \quad \boldsymbol{y} = \boldsymbol{C}\boldsymbol{x}, \quad \boldsymbol{x}_0 \in X_0 \subseteq X, \quad \boldsymbol{x} \in X, \quad \boldsymbol{d}_x \in D_x \quad (2.15a)$$

where (*bd*: block diagonal matrix)

$$\boldsymbol{f}(\bar{\boldsymbol{x}}, \bar{\boldsymbol{d}}_x) = \mathcal{A}\boldsymbol{x} + \boldsymbol{B}_d \boldsymbol{d}_\omega + \boldsymbol{B}_u [\boldsymbol{u} + \boldsymbol{\gamma}(\boldsymbol{x}, \boldsymbol{d}_\gamma)] = 0 \quad (2.15b)$$

$$||\boldsymbol{\gamma}(\boldsymbol{x}, \boldsymbol{d}_\gamma) - \boldsymbol{\gamma}(\bar{\boldsymbol{x}}, \bar{\boldsymbol{d}}_\gamma)|| \le l_{\boldsymbol{x}}^\gamma ||\boldsymbol{x} - \bar{\boldsymbol{x}}|| + l_{\boldsymbol{d}_\gamma}^\gamma ||\boldsymbol{d}_\gamma - \bar{\boldsymbol{d}}_\gamma|| \quad (2.15c)$$

$$\boldsymbol{x} = \begin{bmatrix} \boldsymbol{x}_1 \\ \vdots \\ \boldsymbol{x}_\text{N} \end{bmatrix}, \quad \boldsymbol{d}_\gamma = \begin{bmatrix} \boldsymbol{d}_{\gamma_1} \\ \vdots \\ \boldsymbol{d}_{\gamma_\text{N}} \end{bmatrix}, \quad \boldsymbol{u} = \begin{bmatrix} \boldsymbol{u}_1 \\ \vdots \\ \boldsymbol{u}_\text{N} \end{bmatrix}, \quad \boldsymbol{d}_\omega = \begin{bmatrix} \boldsymbol{d}_{\omega_1} \\ \vdots \\ \boldsymbol{d}_{\omega_\text{N}} \end{bmatrix}, \quad \boldsymbol{d}_x = \begin{bmatrix} \boldsymbol{d}_\omega \\ \boldsymbol{u} \\ \boldsymbol{d}_\gamma \end{bmatrix}$$

$$\mathcal{A} = bd[\mathcal{A}_1, \ldots, \mathcal{A}_\text{N}], \quad \boldsymbol{B}_d = bd[\boldsymbol{b}_{d_1}, \ldots, \boldsymbol{b}_{d_\text{N}}]$$

$$\boldsymbol{B}_u = bd[\boldsymbol{b}_{u_1}, \ldots, \boldsymbol{b}_{u_\text{N}}], \quad \boldsymbol{C} = bd[\boldsymbol{c}_{y_1}, \ldots, \boldsymbol{c}_{y_\text{N}}]$$

$\bar{\boldsymbol{x}}$ is unique robustly stable nominal steady-state (SS) given by the nonlinear algebraic equation (AE) (2.15b) and $\bar{\boldsymbol{d}}_x$ is the associated nominal input. Since $\boldsymbol{\gamma}$ is a Lipschitz bounded function (2.15c) about the nominal operation, for each admissible initial-input pair $[\boldsymbol{x}_0, \boldsymbol{d}_x(t)]$ the NL ODE has a unique state motion $\boldsymbol{x}(t)$ and a unique measured output trajectory $\boldsymbol{y}(t)$:

$$\boldsymbol{x}(t) = \boldsymbol{\tau}_x[t, \boldsymbol{x}_0, \boldsymbol{d}_x(\cdot)] \in X, \qquad \boldsymbol{y}(t) \in \boldsymbol{C}\boldsymbol{x}(t) \quad (2.16)$$

when the exogenous input $\boldsymbol{d}_x(t)$ reaches asymptotically its nominal value $\bar{\boldsymbol{d}}_x$, the state motion $\boldsymbol{x}(t)$ and the measured output $y(t)$ reach asymptotically their nominal values, i.e.,

$$\boldsymbol{x}_0 \in X_0 \setminus \boldsymbol{x}_0, \qquad \boldsymbol{d}_x(t) \to \bar{\boldsymbol{d}}_x, \quad \Longrightarrow \boldsymbol{x}(t) \to \bar{\boldsymbol{x}} \in X, \quad \boldsymbol{y}(t) \to \bar{\boldsymbol{y}} \quad (2.17)$$

subjected to bounded -in the sense of the Euclidian norm $|(\cdot)|$ of $(\cdot)$- initial state-input

disturbances

$$|\boldsymbol{x}_0 - \bar{\boldsymbol{x}}| \leq \epsilon_0^+, \qquad |\boldsymbol{d}_x(t) - \bar{\boldsymbol{d}}_x| \leq \epsilon_{\boldsymbol{d}_x}^+ \tag{2.18}$$

the state motion and output signal are exponentially ultimate (EU) bounded about their nominal values $\bar{\boldsymbol{x}}$ and $\bar{\boldsymbol{y}}$, respectively:

$$|\boldsymbol{x}(t) - \bar{\boldsymbol{x}}| = |\boldsymbol{y}(t) - \bar{\boldsymbol{y}}| \leq a_x e^{-\lambda_x t} \epsilon_0^+ + b_x \epsilon_{\boldsymbol{d}_x}^+ := \epsilon_x, \quad a_x, b_x, \lambda_x > 0 \tag{2.19}$$

and the motion rate of change is EU bounded as

$$|\dot{\boldsymbol{x}}(t)| \leq \lambda_x^+ \epsilon_x + b_x^+ \epsilon_{\boldsymbol{d}_x} := \epsilon_{\dot{x}} \tag{2.20}$$

Remark 2.2 In comparison with the synchronous generator model (2.2c)-(2.2c) presented in Subsection 2.2.2.1, which is employed specifically in the IMG studies derived in Chapter 3.The state variable ω_i (2.13b) of the MPS dynamic model (2.13) stands for the generator relative speed, and it should be taking into account in the estimation methodology proposed in Chapter 4.

Dynamic State Estimation for Islanded Microgrid Structures

Abstract: This chapter presents the centralized dynamic state estimation algorithms for DA models whose methodology relies on the Kalman Filter theory. Firstly, an estimator based on the Extended Kalman Filter is introduced. Secondly, an Unscented Kalman Filter adopting the Singular Perturbation Theory is presented. Both estimators can recover the dynamic and algebraic variables of an IMG through the same estimation scheme. The proposed methodology uses fewer measurements concerning the conventional static estimators as well, as the transient and steady-state regimes are captured.

This chapter is based on the work:

1. **Natanael Vieyra**, Paul Maya, and Luis M. Castro. "Dynamic State Estimation for Microgrid Structures.", Electric Power Components and Systems, Vol. 48, 2020, pp. 1-13.

2. **Natanael Vieyra**, Paul Maya, and Luis M. Castro. "Effective dynamic state estimation algorithm for Islanded microgrid structures based on singular perturbation theory.", Electric Power Systems Research, Vol. 187, 2020, pp. 106455.

3.1 Introduction

An MG can operate either connected to a large power system or as an islanded system supplying off-grid areas or islands. When the MG operates as an islanded system, the frequency and voltage regulation are carried out through local controls over distributed generation resources without a central dispatcher's necessity. The present dissertation deals with MGs operating as isolated systems (IMGs), which implies that they are more susceptible to frequency and voltage variations.

To ensure the correct operation of an IMG, the EMSs require precise information about IMG state variables associated with bus voltages and phase angles, electrical frequency, mechanical speeds of rotating machinery allowing its protection and control [10]. Despite the improved quality of the measurement devices, it is always necessary to count on a suitable tool able to deliver information about the system variables for adequate control and operation of the grid; admittedly, a state estimator is a convenient tool for these purposes.

For this, different state estimation algorithms have been proposed. In [10], for instance, a distributed dynamic state estimator is proposed to estimate the dynamic variables of energy resources. Then the estimated values of each component are converted to phasor data with time, and the EMS collects them. This data, together with those provided by conventional meters, are used as input to the static state estimation, ultimately generating real-time operating conditions of MGs. In [24], two techniques for state estimation are used in a droop-controlled IMG, an Unscented Kalman Filter and a nonlinear Particle Filter are reported; authors assure that their algorithms can deal with Gaussian noise in all measurements, and some numerical simulations show it. The results are reduced to a specific droop-controlled IMG. For an electrical system including multiple microgrids, a state estimation algorithm based on the WLS method is proposed [25]. However, there are three main drawbacks: it adopts a steady-state approach, the strong dependency on the available measurements, and the high computational burden. Thus, to reduce the required computational load, a decentralized estimator has been developed in [26–28]. However, the employed dynamic models and grid topologies may not be so practical, thus introducing frailty in the formulation [3, 4]. In [29] assuming that the system has slowly changing states and not considering the nonlinear dynamics of distributed energy resources (DERs), a quasi-dynamic approach is adopted. The voltages values of an island microgrid are reconstructed through a modified nodal load observer (NLO).

In the context of the state estimation problem for IMG structures consisting of hydroelectric and wind generators interconnected with another set of loads (polynomial load model) through power lines and whose interaction is described by a differential-algebraic system (also known as structure-preserving models). This detailed mathematical representation of the IMG allows capturing different dynamic phenomena associated with generators and the electrical grid. The dynamic variables (load angles, internal voltages of generators, and mechanical speeds) and algebraic variables (bus voltage magnitudes and phase angles) are estimated in real-time in the presence of system disturbances (wind and load variations, three-phase faults) using two estimators based on Kalman Filter theory through a minimum number of measurements (only the minimal amount to guarantee observability properties), which are based on bus voltage phasors and power outputs of generators. The parameters of generators as well as of the electrical network are known to design the state estimators. Moreover, the IMG is considered as a positive sequence balanced network.

3.2 Dynamic State Estimation Algorithm for IMG structures based on Extended Kalman Filter

Firstly, in this thesis work, a dynamic state estimator based on Extended Kalman Filter (EKF) ad-hoc for DAEs is proposed. It should be highlighted that the EKF is a broadly used technique that has shown its usefulness in nonlinear systems, represented by ODEs, of different nature [30]. However, when a set of nonlinear differential-algebraic equations represent the system, its implementation is more complex and rarely used [3]. Specifically, in electric power systems, few research works are reported in the scientific literature, but none for IMG structures [31–34].

Using a nonlinear representation of an IMG (2.1) allowed the design of an estimator based on EKF (Subsection 3.2.2), which recovers the transient and steady-state regimes associated with the IMG operation, contrary to other existing approaches [25, 35, 36]. It should be highlighted that the design of the state estimation algorithm is generic concerning the network decomposition, where the nonlinear dynamics associated with the DERs are also considered in contrast with [26–28, 37, 38]. Furthermore, the adopted DA representation of an IMG (2.1) allows considering the nodal voltage phasors as a part of the state variables to be estimated. Thus, the estimation of dynamic variables of each generator (load angles, internal voltages, and mechanical speeds) is independent of the existence of a measurement device (delivering information about the voltage and current phasors) in that generator terminal for this instance; the proposed dynamic estimator uses a minimum number of measurements (only the minimal amount to guarantee observability properties - Subsection 2.2.2.4). In this way, the proposed in this dissertation is different to other existing dynamic approaches [31–34, 39–47] , which assume that the all nodal voltage phasors are known or are available through measurement devices.

3.2.1 Structure-Preserving Model in Discrete Form

To design an state estimation scheme based on EKF for a DA system that allows estimating the dynamic and algebraic state variables arising from an IMG represented by a set of DAEs (2.1) is necessary to obtain its discrete equivalent representation due to that the measurements (Subsection 2.2.2.4) are available only during specific time intervals. Furthermore, the following assumptions should be taken into account [3]:

1. All the inputs are considered constants.

2. The measurements are obtained at intervals of Δt, the discrete measurements may be expressed by

$$\boldsymbol{y}_{k+1} = \boldsymbol{h}(\boldsymbol{x}_{k+1}, \boldsymbol{z}_{k+1}) + \boldsymbol{v}_{k+1} \tag{3.1}$$

   where $\boldsymbol{v}_k \in \mathbb{R}^m$ represents the noise that affects the measurements, it may be modeled as Gaussian white noise with zero-mean whose covariance matrix $\boldsymbol{R}_k$ is

known.

Thus, the stochastic nonlinear discrete-time DA system is described as [48]:

$$\boldsymbol{x}_{k+1} = \boldsymbol{x}_k + \int_{(k)\Delta t}^{(k+1)\Delta t} \boldsymbol{f}(\boldsymbol{x}(t), \boldsymbol{z}(t))dt + \boldsymbol{w}_{k+1}, \qquad \boldsymbol{x} \in \mathbb{R}^{n_d}, \quad \boldsymbol{z} \in \mathbb{R}^{n_z} \qquad (3.2a)$$

$$0 = \boldsymbol{g}(\boldsymbol{x}_{k+1}, \boldsymbol{z}_{k+1}) \qquad (3.2b)$$

which, in turn, may be expressed in compact form as:

$$\boldsymbol{x}_{k+1} = \boldsymbol{F}(\boldsymbol{x}_k, \boldsymbol{z}_k, \boldsymbol{w}_k), \qquad \boldsymbol{x} \in \mathbb{R}^{n_d}, \quad \boldsymbol{z} \in \mathbb{R}^{n_z} \qquad (3.3a)$$

$$0 = \boldsymbol{g}(\boldsymbol{x}_{k+1}, \boldsymbol{z}_{k+1}) \qquad (3.3b)$$

where $\boldsymbol{w}_k \in \mathbb{R}^{n_d}$ is a noise vector affecting the system state variables and whose covariance matrix $\boldsymbol{Q}_k$ is known. Expressions (3.3a)-(3.3b) are represented by (2.2a)-(2.2c) and (2.6a)-(2.7) in their discrete form, and $\boldsymbol{g}$ are the network restrictions, given by (2.11a) and (2.11b), whereas, the discrete measured outputs (3.1) are based on measurement models reported in Subsection 2.2.2.4.

The estimation problem of an IMG whose discrete mathematical representation is given by (3.3a)-(3.3b) and considering a set of measurements (bus voltage phasors and power outputs of generators) turns to be a problem of observer design to estimate the state variables, those related to generators, $\boldsymbol{x}$ (load angle, mechanical speeds, internal voltages, electrical frequency) and electrical network, $\boldsymbol{z}$ (bus voltage phasors) in real-time despite the presence of system disturbances. The parameters of generators and the electrical network are assumed known. Moreover, a nominal control input for the synchronous generators (mechanical input power and field voltage) is considered to obtain a correct transient behavior.

3.2.2 Dynamic State Estimation Algorithm based on EKF

The estimation problem for IMG structures derived in Subsection 2.1.3 is solved through a unique adaptation of the EKF algorithm for DA systems documented in [48]. Compared with the mentioned scheme, the proposed estimator is based on the full discrete representation of the DA system. For the estimator reported in [48], it is assumed that only the measurements are in their discrete form while the associated dynamics are continuous. Thus, the prediction step strongly depends on the selected DA solver directly affecting the execution times. Moreover, this reported approach may not be suitable to capture the fast dynamics of an IMG. This problem is avoided by adopting the full discrete representation of the IMG (3.4a)-(3.4b) due to that the prediction step is done more appropriately because the filter performance does not depend on the selected solver.

The proposed dynamic state estimation algorithm is able to provide an estimated

of $(\boldsymbol{x}_k, \boldsymbol{z}_k)$ at time k, given the initial estimate $(\boldsymbol{x}_0, \boldsymbol{z}_0)$, the series of measurements, $\boldsymbol{y}_1, ..., \boldsymbol{y}_k$, and the information of the DA system $\boldsymbol{F}, \boldsymbol{g}, \boldsymbol{h}$, $\boldsymbol{Q}_k$ and $\boldsymbol{R}_k$. The estimation scheme is summarized in the following steps:

Prediction Step [3, 48] - The predicted mean values of dynamic and algebraic variables together with the error covariance matrix are computed.

- The initial conditions $(\boldsymbol{x}_0, \boldsymbol{z}_0)$ of dynamic and algebraic variables are set as well as the covariance matrix $\boldsymbol{P}_0^{aug}$ associated with the estimation errors of both state variables is initiated. Also, the covariance matrices $\boldsymbol{Q}_k$ and $\boldsymbol{R}_k$ should be precised, which are tuning to improve the EKF performance.

- Consider $(\hat{\boldsymbol{x}}_{k|k}, \hat{\boldsymbol{z}}_{k|k})$ as the estimated state variable at the instant k with information at the same time instant. Solve (3.4a)-(3.4b) to obtain the estimated state variable with the previous step information $(\hat{\boldsymbol{x}}_{k+1|k}, \hat{\boldsymbol{z}}_{k+1|k})$. This prediction also could be carried out using a DAE solver [49, 50] or any other integration algorithms such as [51, 52].

$$\hat{\boldsymbol{x}}_{k+1|k} = \boldsymbol{F}(\hat{\boldsymbol{x}}_{k|k}, \hat{\boldsymbol{z}}_{k|k}) \tag{3.4a}$$

$$0 = \boldsymbol{g}(\hat{\boldsymbol{x}}_{k+1|k}, \hat{\boldsymbol{z}}_{k+1|k}) \tag{3.4b}$$

the augmented state variable estimated is then obtained by

$$\hat{\boldsymbol{x}}_{k+1|k}^{aug} = \begin{bmatrix} \hat{\boldsymbol{x}}_{k+1|k} & \hat{\boldsymbol{z}}_{k+1|k} \end{bmatrix}^{\top}$$

- A linear approximation of the DA model is used to obtain the error covariance matrix of the augmented state variable:

$$\dot{\boldsymbol{x}} = \boldsymbol{A}\boldsymbol{x} + \boldsymbol{B}\boldsymbol{z} \tag{3.5a}$$

$$0 = \boldsymbol{C}\boldsymbol{x} + \boldsymbol{D}\boldsymbol{z} \tag{3.5b}$$

where

$$\begin{bmatrix} \boldsymbol{A} & \boldsymbol{B} \\ \boldsymbol{C} & \boldsymbol{D} \end{bmatrix} = \begin{bmatrix} \frac{\partial \boldsymbol{f}}{\partial \boldsymbol{x}} & \frac{\partial \boldsymbol{f}}{\partial \boldsymbol{z}} \\ \frac{\partial \boldsymbol{g}}{\partial \boldsymbol{x}} & \frac{\partial \boldsymbol{g}}{\partial \boldsymbol{z}} \end{bmatrix}\Bigg|_{\hat{\boldsymbol{x}}_{k|k}^{aug}} \tag{3.5c}$$

$\boldsymbol{f}$ and $\boldsymbol{g}$ are given by the expressions presented in Subsections 2.2.2.1, 2.2.2.2 and 2.2.2.3, respectively.

Specifically, according to the algebraic restrictions derived from Subsection 2.2.2.3, the term $\partial \boldsymbol{g}/\partial \boldsymbol{z}$ is invertible, (3.5b) is differentiated once to obtain:

$$\dot{\boldsymbol{z}} = -\boldsymbol{D}^{-1}\boldsymbol{C}\dot{\boldsymbol{x}}$$

$$= -\boldsymbol{D}^{-1}\boldsymbol{C}\boldsymbol{A}\boldsymbol{x} - \boldsymbol{D}^{-1}\boldsymbol{C}\boldsymbol{B}\boldsymbol{z} \tag{3.6}$$

which in matrix form becomes

$$\begin{bmatrix} \dot{\boldsymbol{x}} \\ \dot{\boldsymbol{z}} \end{bmatrix} = \begin{bmatrix} \boldsymbol{A} & \boldsymbol{B} \\ -\boldsymbol{D^{-1}CA} & -\boldsymbol{D^{-1}CB} \end{bmatrix} \begin{bmatrix} \boldsymbol{x} \\ \boldsymbol{z} \end{bmatrix} \tag{3.7}$$

in compact form,

$$\dot{\boldsymbol{x}}^{aug} = \Lambda_k x^{aug} \tag{3.8}$$

The state transition matrix is given by

$$\boldsymbol{\phi}_k = exp(\Lambda_k \Delta t) \tag{3.9}$$

The error covariance matrix associated with the state estimation is calculated as:

$$\boldsymbol{P}_{k+1|k}^{aug} = \boldsymbol{\phi}_k \boldsymbol{P}_{k|k}^{aug} \boldsymbol{\phi}_k^\top + \boldsymbol{\Gamma}_k \boldsymbol{Q}_k \boldsymbol{\Gamma}_k^\top \tag{3.10a}$$

where

$$\boldsymbol{\Gamma} = \begin{bmatrix} \boldsymbol{I} \\ -\boldsymbol{D^{-1}C} \end{bmatrix} \bigg|_{\hat{\boldsymbol{x}}_{k|k}^{aug}} \tag{3.10b}$$

Equation (3.10b) is related to the noise effects on the augmented state variable, and $\boldsymbol{I}$ is a $n_d \times n_d$ identity matrix.

Correction Step [3, 48] - The updated mean and the updated covariance matrix are obtained.

- The Kalman filter gain of the augmented state variable is obtained as:

$$\boldsymbol{K}_{k+1}^{aug} = \boldsymbol{P}_{k+1|k}^{aug} \boldsymbol{H}_{k+1}^{aug\top} (\boldsymbol{H}_{k+1}^{aug} \boldsymbol{P}_{k+1|k}^{aug} \boldsymbol{H}_{k+1}^{aug\top} + \boldsymbol{R}_{k+1})^{-1} \tag{3.11}$$

where $\boldsymbol{H}_{k+1}^{aug}$ is the linearized measurement model evaluated at $\hat{\boldsymbol{x}}_{k+1|k}^{aug}$.

- The update of the estimated state variable is given by

$$\hat{\boldsymbol{x}}_{k+1|k+1}^{aug} = \hat{\boldsymbol{x}}_{k+1|k}^{aug} + \boldsymbol{K}_{k+1}^{aug}(\boldsymbol{y}_{k+1} - \boldsymbol{h}(\hat{\boldsymbol{x}}_{k+1|k}^{aug})) \tag{3.12}$$

Notice that (3.12) suggests that only the differential variables are considered $\hat{\boldsymbol{x}}_{k+1|k+1}$.

- Given $\hat{\boldsymbol{x}}_{k+1|k+1}$ the update of algebraic variables $\hat{\boldsymbol{z}}_{k+1|k+1}$ is calculated as

$$\boldsymbol{g}(\hat{\boldsymbol{x}}_{k+1|k+1}, \hat{\boldsymbol{z}}_{k+1|k+1}) = 0 \tag{3.13}$$

- Finally the covariance matrix has to be updated

$$\boldsymbol{P}_{k+1|k+1}^{aug} = (\boldsymbol{I} - \boldsymbol{K}_{k+1}^{aug} \boldsymbol{H}_{k+1}^{aug}) \boldsymbol{P}_{k+1|k}^{aug} \qquad (3.14)$$

3.2.2.1 Bad Data Analysis

The estimation algorithm based on EKF for DA systems also includes a bad data detection analysis that can detect and handle the gross errors affecting the measurements used in the estimation task (Subsection 2.2.2.4). The proposed EKF, through a normalized innovation vector, identifies the gross errors:

$$\gamma_{k+1,j} = \frac{|y_{k+1,j} - \hat{y}_{k+1,j}|}{\sqrt{\boldsymbol{H}_{k+1,j}^{aug} \boldsymbol{P}_{k+1}^{aug} \boldsymbol{H}_{k+1,j}^{aug} + \boldsymbol{R}_{k,j}^2}} \leq \Upsilon \qquad (3.15)$$

where k indicates the k-th time step, the index j corresponds to the j-th measurement, in the case of $\boldsymbol{R}_k$, represents the j-th diagonal element.

The innovation vector associated with each measurement must be within a range of values delimited by a threshold value Υ. According to [18], the measurement has to be discarded if it is more significant than 1.5 p.u. Thus, the y_{k+1} is discarded and replaced by y_k to update the estimated state.

3.2.3 Simulation Results

The EKF for DA systems proposed in Section (3.2) is assessed through two practical IMGs (three and seven buses) considering hydroelectric and wind generators and a set of loads (polynomial load model) under different scenarios; under load and wind variations as well as are considered process and measurement noises (modeled as white Gaussian noises). It should be highlighted that in comparison with [26–28, 37, 38] the present work used a nonlinear model to represent the dynamic behavior of an IMG, considering the dynamics associated with generators as well as the network restrictions. Thus, the mathematical representation adopted allows capturing a wide variety of nonlinear phenomena.

3.2.3.1 Dynamic State Estimation with Wind Speed and Load Variations

In the first instance, the performance of the proposed estimation scheme is evaluated using a meshed 3-bus IMG containing a 5-MW hydro generator and a 0.9-MW wind generator, initially operating at $V_w = 12$ m/s. Generation units are feeding into a load rated at 3+j1 MVA. The system's base is 10 MVA, and the microgrid's nominal frequency is 50 Hz. Based on the observability criterion for DAEs [16, 17]. For this IMG, the observability is guaranteed using the measurement model given by (2.12) previously presented in Subsection 2.2.2.4. The considered measurements are obtained through a measurement device installed at bus one using a sampling rate of 120 samples/s [53].
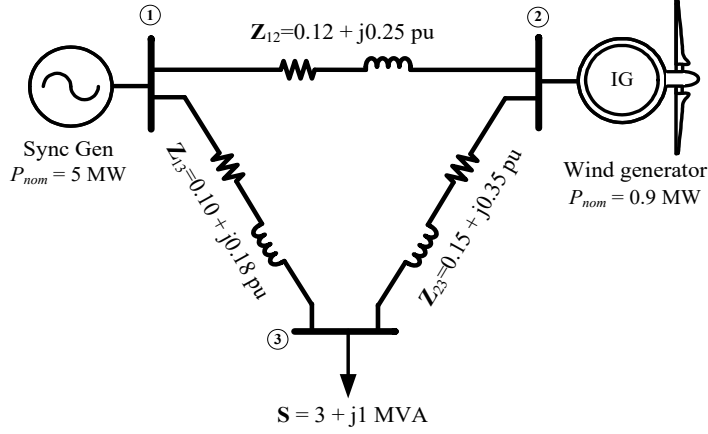
Figure 3.1: Microgrid with hydro generation and wind generation.

Two disturbances affect the microgrid operation. It is considered to wind speed changes from 12 m/s to 14 m/s, whereas the load connected to node three is subjected to 3 % variations approximately. Both study cases are simulated for 40 seconds where the initial steady-state equilibrium point, shown in (3.16), is obtained through a conventional power-flow algorithm [3].

$$
x = \begin{cases} \delta_1 = 0.3945\text{rad} \\ \omega_1 = 1\text{p.u.} \\ E'_{q_1} = 0.9117\text{p.u.} \\ \omega_{m_2} = 1.0094\text{p.u.} \\ e'_{d_2} = -0.1548\text{p.u.} \\ e'_{q_2} = 0.9048\text{p.u.} \end{cases} \quad z = \begin{cases} \theta_1 = 0\text{rad} \\ \theta_2 = -0.0014\text{rad} \\ \theta_3 = -0.0396\text{rad} \\ V_1 = 1\text{p.u.} \\ V_2 = 0.9789\text{p.u.} \\ V_3 = 0.9540\text{p.u.} \end{cases} \tag{3.16}
$$

The covariances matrices assocaited with the process and measurement noises are set to $\boldsymbol{Q}_k = diag([3 \times 10^{-7}, 3 \times 10^{-6}, 3 \times 10^{-7}, 3 \times 10^{-6}, 3 \times 10^{-7}, 3 \times 10^{-7}])$ and $\boldsymbol{R}_k = diag([5 \times 10^{-6}, 5 \times 10^{-6}, 5 \times 10^{-5}, 5 \times 10^{-5}])$ and the initial covariance matrix is established as $\boldsymbol{P}_0^{aug} = 4.5 \times 10^{-6} \boldsymbol{I}_{12 \times 12}$. Moreover, the mechanical input power P_{m_i} and the field voltage E_{F_i} are considered known and constants during time simulation.

Figure 3.2 shows the performance of the proposed estimator for the dynamic variables associated with the hydroelectric generator connected to bus one. It is noted that the estimator can adequately capture the transient behavior of these variables quite well. Similarly, the dynamic variables of the wind generator are suitably estimated, as shown in Fig. 3.3, where it is observed that the proposed approach can recover the transients of the wind generator.
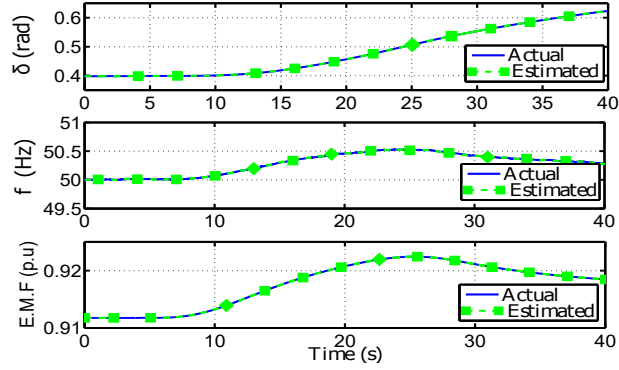
Figure 3.2: Load angle, electrical frequency and q-axis E.M.F of hydro generator.
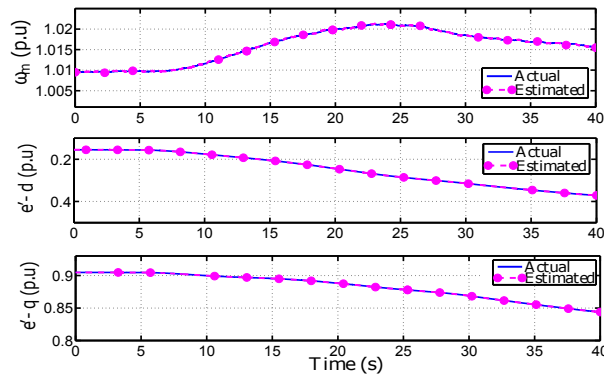
Figure 3.3: Mechanical speed of WG, d-axis E.M.F of WG and q-axis E.M.F of WG.
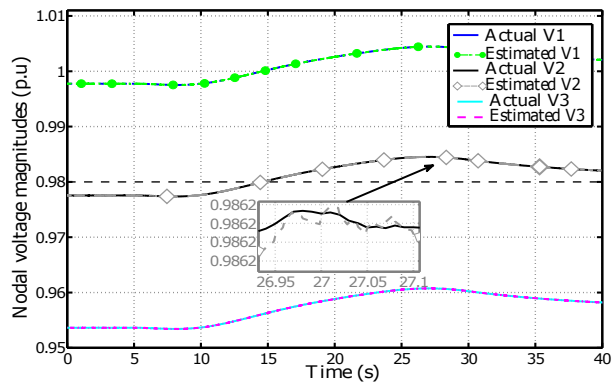
Figure 3.4: Nodal voltage magnitudes of the Microgrid.

Fig. 3.4 further demonstrate the dynamic state estimator's good capabilities concerning the transient behavior of the system's nodal voltage magnitudes. The root means square errors (RMSE) obtained by the dynamic performances of the proposed estimator reported in this simulation study are quite inferior to 1×10^{-8} p.u.

The proposed dynamic state estimation algorithm allows estimating the dynamic and algebraic variables through the same estimation scheme. In this way, following the proposed methodology, estimating all the states arising from an IMG is carried out employing fewer measurements than static estimators, thus properly capturing the estimation of both the steady-state and transient operation of MGs with fewer computing requirements. This method may represent a vital tool for ensuring the overall stability of new microgrid structures subject to disturbances.

3.2.3.2 Dynamic State Estimation with Load and Wind Variations

The new approach's usefulness and suitability are demonstrated using the IMG shown in Fig. 3.5. It is an electrical grid containing three wind generators and one hydro generator that supplies power to two distributed loads. The distribution line impedance is $z = 0.12 + j0.25 \ p.u/km$ whose length is shown in Fig. 3.5. The system's base is 10 MVA, and the microgrid's nominal frequency is 50 Hz.
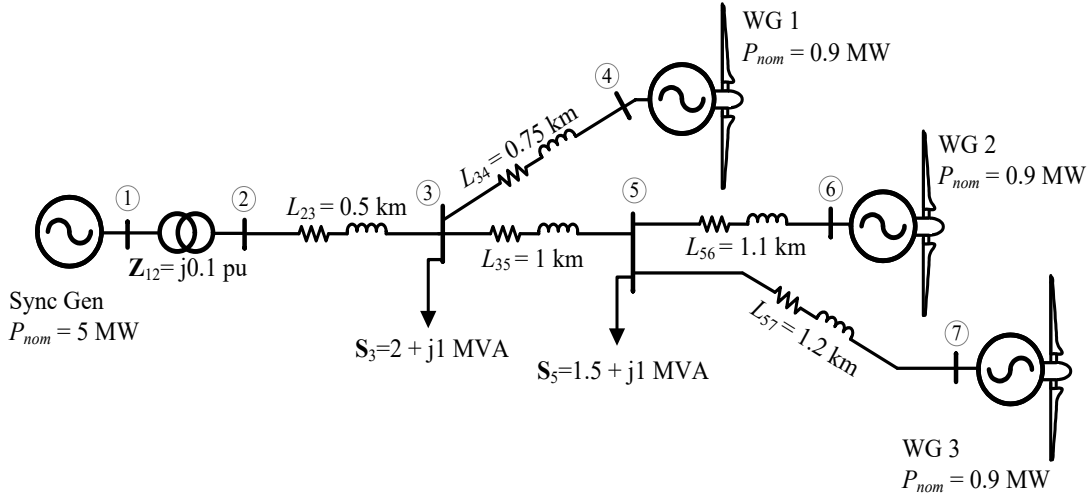
Figure 3.5: Microgrid with hydro generation and wind generation.

The dynamic variables to be estimated are given by:

$$\boldsymbol{x} := [\delta_1 \quad \omega_1 \quad E'_{q_1} \quad \omega_{m_1} \quad e'_{d_1} \quad e'_{q_1} \quad \omega_{m_2} \quad e'_{d_2} \quad e'_{q_2} \quad \omega_{m_3} \quad e'_{d_3} \quad e'_{q_3} \quad \omega_{m_4} \quad e'_{d_4} \quad e'_{q_4}]^\top$$

whereas the algebraic variables to be estimated correspond to the nodal voltages:

$$z := [\theta_1 \quad \theta_2 \quad \theta_3 \quad \theta_4 \quad \theta_5 \quad \theta_6 \quad \theta_7 \quad V_1 \quad V_2 \quad V_3 \quad V_4 \quad V_5 \quad V_6 \quad V_7]^\top$$

The state estimation algorithm considers a set of ten measurements; the first four measurements are given by (2.12), which are obtained through a sensor installed at bus 1. The remaining generator buses have considered three sensors at buses 4, 6, and 7, delivering information about the active and reactive power injected by each wind generator. These output signals are given by (2.9a) and (2.9b), respectively.

The proposed state estimation algorithm used the following covariance matrices: $Q_k = diag([4 \times 10^{-5}, 4 \times 10^{-5}, 4 \times 10^{-5}, 4 \times 10^{-5}, 4 \times 10^{-5}, 4 \times 10^{-5}, 9 \times 10^{-6}, 9 \times 10^{-6}, 9 \times 10^{-6}, 9 \times 10^{-6}, 9 \times 10^{-6}, 9 \times 10^{-6}])$, $R_k = 3 \times 10^{-6} I_{10 \times 10}$ and the initial covariance matrix is set as $P_0^{aug} = 4.5 \times 10^{-11} I_{26 \times 26}$. The performance of the method is tested by tracking the system dynamics when the IMG is affected by wind speed variations in the wind turbines and load changes, as shown in Fig. 3.6.
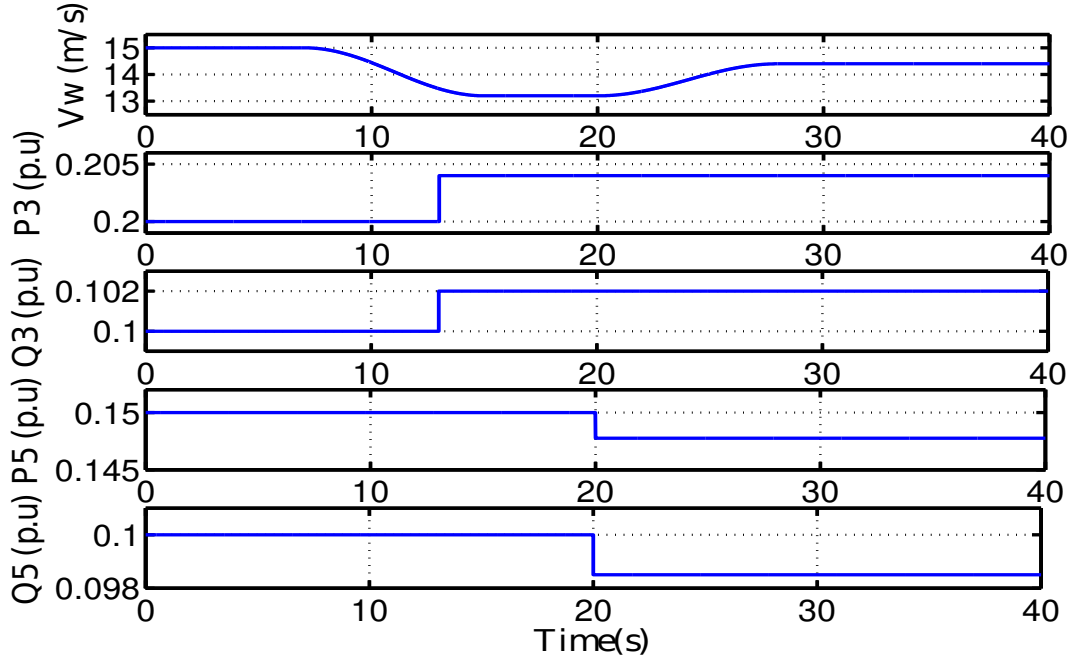
Figure 3.6: Wind speed variations and load profile variations.

The solid line in Fig. 3.7 represents actual values; the magenta dashed line is the estimated value from EKF. The generators experiment transient fluctuations due to wind speed and load variations. In Fig. 3.7, the islanded microgrid shows a transient behavior adequately estimated by the state estimation algorithm. Figure 3.7 shows the filter's performance estimating the electrical frequency and wind generators' mechanical speed.
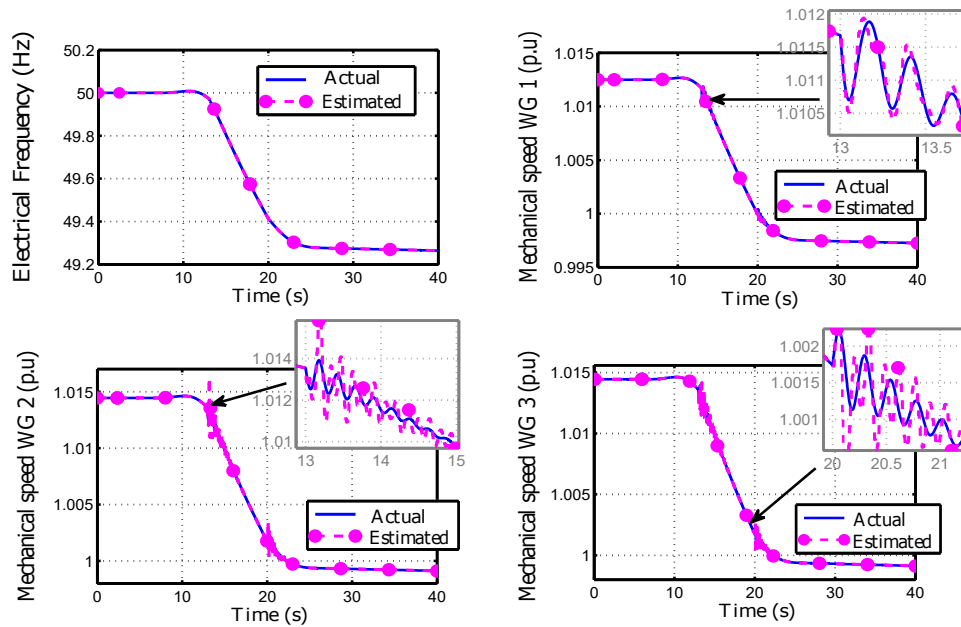
Figure 3.7: Electrical frequency, Mechanical speed of WG 1, Mechanical speed of WG 2, Mechanical speed of WG 3.
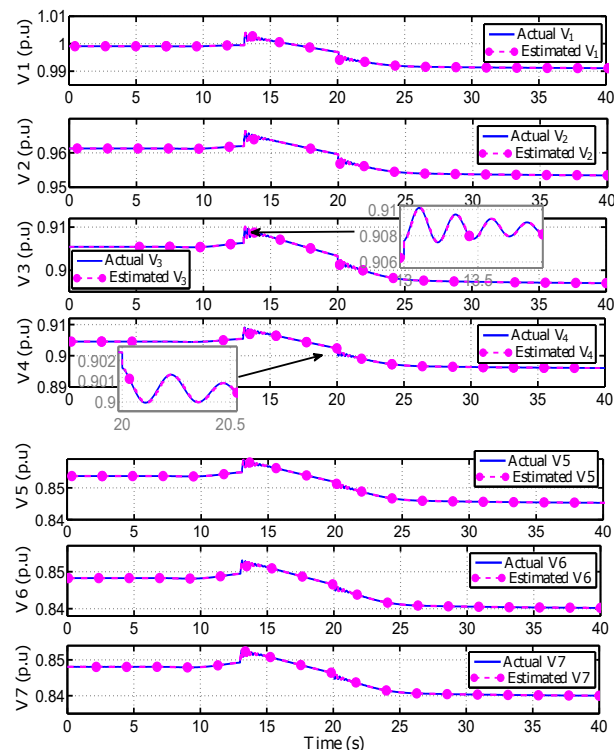
Figure 3.8: Nodal voltage magnitudes of the Microgrid.

Figure 3.8 shows the estimation of bus voltage magnitudes. Again, it is corroborated
that the introduced dynamic state estimator approach estimates the dynamic voltage
performance correctly in the face of rather extreme variations in wind speed and load
profile.

To offer an alternative to the estimation task for IMG given by a set nonlinear
DAEs. An estimator based on UKF, which dismisses the main drawbacks associated
with the EKF, is presented in the following section.

3.3 Dynamic State Estimation Algorithm for IMG Structures based on Singular Perturbation Theory

For state estimation, the EKF requires the computation of Jacobian matrices to ap-
proximate the nonlinear functions, resulting in a nontrivial task. Moreover, the EKF
performance is degraded in highly nonlinear systems because of uncertainty propagation
through the system. The Unscented Kalman filter emerged to overcome the drawbacks
above of EKF, which is based on producing several sampling points (also known as
sigma points) around the current state estimate based on its covariance. These points
are propagated through the nonlinear functions to better approximate the mean and
covariance associated with the mapping results [54, 55].

The estimation of the dynamic and algebraic variables of an IMG is carried out
using a modified version of the Unscented Kalman Filter (UKF) for DAEs. Few works
reported in the scientific literature are focused on adapting the UKF for differential-
algebraic (DA) systems [48, 55, 56].

Indeed, it is well-known that the main drawback of the UKF for DA systems is
that it requires calculating a set of consistent sigma points in every prediction and
correction step, reflecting in algebraic loops and a high computational load. Later,
this aspect affects the execution times, representing a problem if the estimated values
are used for monitoring and control purposes. Thus, a new dynamic state estimation
based on UKF for DA systems is presented in this present dissertation. Firstly, in
Subsection 3.3.1 the proposed estimator employs the Singular Perturbation Theory
(SPT) to rewrite the set of DAEs (IMG model - (2.1)) into a set of ODEs as wells its
discrete equivalent is generated. Then, the new representation of the IMG is considered
for the state estimation algorithm presented in Subsection 3.3.2, which reduces the
creation of algebraic loops considerably compared with the traditional UKF for DA
systems [48].

The main features of the proposed methodology are summarized as: (i) like the pre-
vious EKF, the developed method based on UKF-SPT allows estimating the transient
and steady-state regimes of an IMG, contrary to other existing approaches [25, 35, 36],
(ii) in contrast with [26, 27, 37, 38, 57], the design of this state estimation algorithm
is general concerning the network decomposition as well as compared with [37, 38] the
nonlinear dynamics associated with the generator are also included, (iii) the state es-

timation of all state variables arising from an IMG represented for a DA system (2.1) is carried out using fewer measurements (Subsection 2.2.2.4) concerning the conventional static estimators, which usually require redundancy on measurements, and (iv) the microgrid's nodal voltage phasors are considered as a part of the state variable to be estimated, which is sharp contrast with other estimation approaches [31–34, 39–47]. In all fo them, the measured generator's terminal voltage phasors are treated as known inputs or outputs to estimate the dynamic variables of generators.

3.3.1 Singular Perturbation Theory for Structure-Preserving Models

Within the time span of stability analysis, the time scales are associated with various speed responses of different devices such as generators, excitation systems, and network interconnections [58].

Contrary to the traditional singular perturbation theory (SPT) studies, which are focused on finding reduced slow subsystems [58, 59]. For estimator design purposes, a tailored model of an IMG structure based on a DA system (2.1) is obtained through the singular perturbation theory. The structure-preserving model (2.1) is remodeled as a pure ODE system; the new representation (3.17) recovers the same nonlinear phenomena that can be described by a conventional DA model (2.1), the standard model of an SPT problem is expressed as [58, 59]:

$$
\begin{aligned}
\dot{\boldsymbol{x}}(\boldsymbol{t}) &= \boldsymbol{f}(t, \boldsymbol{x}, \boldsymbol{z}, \epsilon) \\
\epsilon \dot{\boldsymbol{z}}(\boldsymbol{t}) &= \boldsymbol{g}(t, \boldsymbol{x}, \boldsymbol{z}, \epsilon)
\end{aligned}
\tag{3.17}
$$

where $\boldsymbol{x} \in \mathbb{R}^{n_d}$ is the vector of slow variables , $\boldsymbol{z} \in \mathbb{R}^{n_z}$ represents the vector of fast variables, and $\epsilon > 0$ is the small singular perturbation parameter, which is the ratio of the time scales of the slow and fast phenomena [58]. The SPT approach is asymptotic because as $\epsilon \to 0$, the results tend to be the exact results when $\epsilon = 0$.

The first task of time scale modeling is to identify ϵ, which could be due to small and large time constants ratios. The time scales can be analyzed by computing the system eigenvalues considering the parameters of generators and transmission lines to obtain the slow and fast variables.

Adopting this new representation makes it possible to design an estimator based on the UKF theory to recover all the state variables from an IMG represented as a DA system. The proposed approach allows generating a consistent set of sigma-points required to execute the prediction and correction step, avoiding the traditional DA model (2.1), due to the newly generated model is an entirely differential system.

To design the state estimation algorithm, the system (3.17) may be expressed as

$$
\begin{aligned}
\dot{\boldsymbol{x}}^{aug} &= \boldsymbol{F}(\boldsymbol{x}^{aug}, \epsilon, \boldsymbol{w}), \qquad \boldsymbol{x}^{aug} = [\boldsymbol{x}, \boldsymbol{z}]^{\top} \\
\boldsymbol{y} &= \boldsymbol{h}(\boldsymbol{x}^{aug}, \epsilon, \boldsymbol{v})
\end{aligned}
\tag{3.18}
$$

where $\boldsymbol{x}^{aug} \in \mathbb{R}^{n_d+n_z}$ is the augmented state variables, which comprises the dynamic variables; these can be, for instance, the internal variables of a power plant (say hydroelectric or wind turbine) such as the rotor angle, mechanical speed, and internal voltages, and the algebraic variables which are associated with network restrictions (bus voltage phasors), $\boldsymbol{F}$ is composed by $\boldsymbol{f}(\boldsymbol{x}, \boldsymbol{z}, \epsilon)$ represented by (2.2a)-(2.2c) and (2.6a)-(2.7), and $(1/\epsilon)\boldsymbol{g}(\boldsymbol{x}, \boldsymbol{z}, \epsilon)$ are the network restrictions, given by (2.11a) and (2.11b), $\boldsymbol{h} \in \mathbb{R}^m$ represents the set of measured outputs that are obtained at intervals of Δt, whose mathematical representation is given in Section 2.2.2.4, $\boldsymbol{w} \in \mathbb{R}^{n_d+n_z}$ and $\boldsymbol{v} \in \mathbb{R}^m$ are the process and measurement noises, respectively.

To derive the discrete-time UKF algorithm, the basic definition of the time derivative of the augmented state variable (3.18) must be considered [4],

$$\boldsymbol{x}^{aug}(k+1) = \boldsymbol{x}^{aug}(k) + \Delta t \times \boldsymbol{F}(\boldsymbol{x}^{aug}, \epsilon, \boldsymbol{w}) \tag{3.19}$$

which is appropriately rewritten in compact form:

$$\boldsymbol{x}_{k+1}^{aug} = \boldsymbol{F}(\boldsymbol{x}_k^{aug}, \epsilon, \boldsymbol{w}_k) \tag{3.20a}$$

$$\boldsymbol{y}_{k+1} = \boldsymbol{h}(\boldsymbol{x}_{k+1}^{aug}, \epsilon, \boldsymbol{v}_{k+1}) \tag{3.20b}$$

The proposed UKF uses the expressions (3.20a) and (3.20b) to predict and correct the state variables of an IMG expressed as a DA system. As it will be appreciated in the following section, the Kalman gain computation implies that the covariance matrix $\boldsymbol{Q}_k$ associated with the dynamic variables must be modified to generate a new covariance matrix $\boldsymbol{Q}_k^{aug}$, which comprises the augmented state variable (dynamic and algebraic variables).

The estimation problem of an IMG structure whose discrete mathematical representation is given by (3.20a) - (3.20b) turns to be a problem of observer design to estimate the augmented state variable $\boldsymbol{x}^{aug}$ in real-time despite the presence of system disturbances, using the same set of measurements (those used for EKF design). Again, as considered in the previous Section 3.2, the knowledge of generator and network parameters is assumed known, and nominal control input is considered to assure a correct transient behavior when the system is subject to different types of disturbances.

The proposed dynamic state estimation algorithm based on SPT includes the steps presented in the following section.

3.3.2 Proposed Method for Dynamic State Estimation Using the UKF for DAEs based on Singular Perturbation Theory (UKF-SPT)

The Unscented Transformation is a technique in which a group of deterministic samples is selected such that the weight of the mean and the covariance are equivalent to an aleatory variable through the nonlinear transformation. The UKF of an IMG adopting the SPT has the following steps:

- Set the value of ϵ that allows to recover the real behavior of the IMG as an ODE system and define a sampling period to obtain the discrete form of the singularly perturbed system (3.19) and represented in compact form as (3.20a).

- Set the weights of sigma-points, the adjustment of a transformation can be represented by three parameters: (i) α, can be modified between 10^{-4} and 1, (ii) β, is used to include information about the previous distribution, and (iii) κ is commonly established as zero. Using these three parameters, the new adjustment parameter λ, the weights associated with the mean W^m and with the covariance W^c, are obtained as:

$$\mu = \alpha^2(n_{aug} + \kappa) - n_{aug}$$
$$W_0^m = \mu/(n_{aug} + \mu)$$
$$W_0^c = \mu/(n_{aug} + \mu) + 1 - \alpha^2 + \beta$$
$$\boldsymbol{W}_i^m = \boldsymbol{W}_i^c = 1/[2(n_{aug} + \mu)], \quad i = 1, ..., 2n_{aug}, \quad n_{aug} = n_d + n_z$$

- Set the values related to the covariance matrices, $\boldsymbol{Q}_k^{aug}$ and $\boldsymbol{R}_k$. Also, initiate the state variables and the covariance matrix, $\boldsymbol{x}^{\hat{a}ug} = E[\boldsymbol{x}^{aug}]$ and $\boldsymbol{P}_0 = E[(\boldsymbol{x}^{aug} - \hat{\boldsymbol{x}}^{aug})(\boldsymbol{x}^{aug} - \hat{\boldsymbol{x}}^{aug})^\top]$, respectively.

- A set of $n_{aug} \times (2n_{aug} + 1)$ sigma-points associated with the augmented state variable must be generated:

$$\hat{\boldsymbol{X}}_{k|k,0}^{aug} = \hat{\boldsymbol{x}}_{k|k}^{aug}$$
$$\hat{\boldsymbol{X}}_{k|k,i}^{aug} = \hat{\boldsymbol{x}}_{k|k}^{aug} + \left(\sqrt{(n_{aug} + \mu)\boldsymbol{P}_{k|k}^{aug}}\right)_i \quad (3.21)$$
$$\hat{\boldsymbol{X}}_{k|k,i}^{aug} = \hat{\boldsymbol{x}}_{k|k}^{aug} - \left(\sqrt{(n_{aug} + \mu)\boldsymbol{P}_{k|k}^{aug}}\right)_{i-n_{aug}}$$

where $\left(\sqrt{(n_{aug} + \mu)\boldsymbol{P}_{k|k}^{aug}}\right)_i$ is the i-th column of the matrix square root, $\hat{\boldsymbol{x}}_{aug_{k|k}}$ is the estimated value of the augmented state variable and $\boldsymbol{P}_{k|k}^{aug}$ is the error covariance matrix.

- Each sigma-point of the augmented state variable is propagated through the singularly perturbed model (3.20a) to obtain $\hat{\boldsymbol{X}}_{k+1|k,i}^{aug}$:

$$\hat{\boldsymbol{X}}_{k+1|k}^{aug(i)} = \boldsymbol{F}(\hat{\boldsymbol{X}}_k^{aug(i)}, \epsilon, w_k) \quad (3.22)$$

- The estimation of the augmented state variable $\hat{\boldsymbol{x}}_{k+1|k}^{aug}$ and the covariance matrix

$\boldsymbol{P}_{k+1|k}^{aug}$ are given by

$$\hat{\boldsymbol{x}}_{k+1|k}^{aug} = \sum_{i=0}^{2n_{aug}} \boldsymbol{W}_i^m \hat{\boldsymbol{X}}_{aug_{k+1|k}}^{(i)} \tag{3.23a}$$

$$\boldsymbol{P}_{k+1|k}^{aug} = \sum_{i=0}^{2n_{aug}} \boldsymbol{W}_i^c (\hat{X}_{k+1|k}^{aug(i)} - \hat{\boldsymbol{x}}_{k+1|k}^{aug})(\hat{\boldsymbol{X}}_{k+1|k}^{aug(i)} - \hat{\boldsymbol{x}}_{k+1|k}^{aug})^\top + \boldsymbol{Q}_{k+1}^{aug} \tag{3.23b}$$

- Compute

$$\boldsymbol{Y}_{k+1|k}^{(i)} = \boldsymbol{h}(\hat{\boldsymbol{X}}_{k+1|k}^{aug(i)}) \tag{3.24}$$

- The Kalman gain for the augmented state variable is obtained by $\boldsymbol{K}_{k+1}^{aug} = \boldsymbol{P}_{k+1}^{xy}(\boldsymbol{P}_{k+1}^{yy})^{-1}$, where

$$\boldsymbol{P}_{k+1}^{yy} = \sum_{i=0}^{2n_{aug}} \boldsymbol{W}_i^c (\boldsymbol{Y}_{k+1|k}^{(i)} - \hat{\boldsymbol{y}}_{k+1|k})(\boldsymbol{Y}_{k+1|k}^{(i)} - \hat{\boldsymbol{y}}_{k+1|k})^\top + \boldsymbol{R}_{k+1} \tag{3.25a}$$

$$\boldsymbol{P}_{k+1}^{xy} = \sum_{i=0}^{2n_{aug}} \boldsymbol{W}_i^c (\hat{\boldsymbol{X}}_{k+1|k}^{aug(i)} - \hat{\boldsymbol{x}}_{k+1|k}^{aug})(\boldsymbol{Y}_{k+1|k}^{(i)} - \hat{\boldsymbol{y}}_{k+1|k})^\top \tag{3.25b}$$

- The estimated of the measured output and the update of the estimated augmented state are given by

$$\hat{\boldsymbol{y}}_{k+1|k} = \sum_{i=0}^{2n_{aug}} \boldsymbol{W}_i^m \boldsymbol{Y}_{k+1}^{(i)} \tag{3.26a}$$

$$\hat{\boldsymbol{x}}_{k+1|k+1}^{aug} = \hat{\boldsymbol{x}}_{k+1|k}^{aug} + \boldsymbol{K}_{k+1}^{aug}(\boldsymbol{y}_{k+1} - \boldsymbol{h}(\hat{\boldsymbol{x}}_{k+1|k}^{aug})) \tag{3.26b}$$

- From (3.26b) only the differential variables are considered $\hat{\boldsymbol{x}}_{k+1|k+1}$. In this way, given $\hat{\boldsymbol{x}}_{k+1|k+1}$ the algebraic variables $\hat{\boldsymbol{z}}_{k+1|k+1}$ are updated through the constraints

$$\boldsymbol{g}(\hat{\boldsymbol{x}}_{k+1|k+1}, \hat{\boldsymbol{z}}_{k+1|k+1}) = 0 \tag{3.27}$$

- Finally the covariance matrix is updated as:

$$\boldsymbol{P}_{k+1|k+1}^{aug} = (\boldsymbol{I} - \boldsymbol{K}_{k+1}^{aug}\boldsymbol{H}_{k+1}^{aug})\boldsymbol{P}_{k+1|k}^{aug} \tag{3.28}$$

3.3.2.1 Bad Data Analysis

The proposed UKF-SPT, like the previous state estimation algorithm based on EKF 3.2.2, also identifies the gross errors that affect the measurement outputs through a normalized innovation vector, which is computed as follows:

$$\gamma_{k+1,j} = \frac{|y_{k+1,j} - \hat{y}_{k+1,j}|}{\sqrt{\sum_{i=0}^{2n_{aug}} \boldsymbol{W}_i^c (\boldsymbol{Y}_{k+1|k,j}^{(i)} - \hat{y}_{k+1|k,j})^2 + r_{k,j}^2}} \leq \varUpsilon \tag{3.29}$$

where k indicates the k-th time step; the index j corresponds to the j-th measurement; $r_{k,j}$, represents the j-th diagonal element of $\boldsymbol{R}_k$. The innovation vector associated with each measurement must be within a range of values delimited by a threshold value of $\varUpsilon$. As stated in [18], a measurement must be discarded if it is greater than 1.5 p.u. Thus, when a gross error is detected, the $y_{k+1,j}$ is discarded and replaced by $y_{k,j}$ to update the estimated state variable.

Table 3.1 is added to clarify the main characteristics of the proposed UKF-SPT concerning some similar estimators for DA systems.

Technique	Characteristics
Proposed UKF-SPT	∘ Estimation without linearizing with a similar computational burden as of EKF. ∘ The creation of algebraic loops needed by sigma-points generation is significantly reduced adopting the SPT. ∘ High performance under very nonlinear systems and when the process and measurement noise is relatively big.
EKF for DA systems	∘ Suitable for nonlinear systems. ∘ The state estimation algorithm requires computing the Jacobian expressions. ∘ Its performance is not ideal in highly nonlinear systems.
UKF for DA systems reported in [48]	∘ Estimation without linearizing and suitable for the high nonlinear processes. ∘ Computational burden is very high because of the generation of consistent sigma-point (creation of algebraic loops).

Table 3.1: State estimation techniques [4]

3.3.3 Simulation Results

This section presents another test case adopting again the 7-bus IMG consisting of three wind generators and one hydro-generator (Fig. 3.5). This power grid was used to assess the EKF performance in the simulation results presented in Subsection 3.2.3.2. Firstly, in Subsection 3.3.3.1 to demonstrate the functioning of the proposed UKF-SPT, the algorithm is tested under load and wind variations assuming noisy measurements. For

comparative purposes, the conventional EKF for DA systems [48] is included. Secondly, in Subsection 3.3.3.2 the proposed estimator is tested when the 7-bus IMG is subject to a three-phase fault in the transmission line 5-6. Its performance is compared with the conventional EKF and UKF for DA systems [48].

3.3.3.1 Practical IMG and comparison against the conventional Extended Kalman Filter for DA systems

As previously mentioned in Subsection 3.2.3.2 there are 26 state variables arising from DA representation of 7-bus IMG; 12 are dynamic variables associated with the generators, and 14 are algebraic variables given by nodal voltage phasors. Again the set of ten measurements provided by a measurement device installed at bus one and whose measurement model is given by (2.12), which together with those measurements related to the active and reactive powers injected by each wind generator (2.9a) and (2.9a) allow the estimation of all state variables of this IMG. Only the electrical frequency, mechanical speeds of wind generators, and nodal voltage magnitudes are reported for study purposes.

The following covariance matrices are considered for the EKF: $\boldsymbol{Q}_{EKF,k} = diag([4 \times 10^{-5}, 4 \times 10^{-5}, 4 \times 10^{-5}, 4 \times 10^{-5}, 4 \times 10^{-5}, 4 \times 10^{-5}, 9 \times 10^{-6}, 9 \times 10^{-6}, 9 \times 10^{-6}, 9 \times 10^{-6}, 9 \times 10^{-6}, 9 \times 10^{-6}])$, $\boldsymbol{R}_{EKF,k} = 3 \times 10^{-6} \boldsymbol{I}_{10 \times 10}$ and the initial covariance matrix is set as $\boldsymbol{P}_{EKF,0}^{aug} = 4.5 \times 10^{-11} \boldsymbol{I}_{26 \times 26}$. On the other hand, for the developed UKF-SPT, we have that: $\boldsymbol{Q}_{UKF-SPT,k} = 4 \times 10^{-6} \boldsymbol{I}_{26 \times 26}$, $\boldsymbol{R}_{UKF-SPT,k} = 5 \times 10^{-4} \boldsymbol{I}_{10 \times 10}$ and the initial covariance matrix is set as $\boldsymbol{P}_{UKF-SPT,0} = 4.5 \times 10^{-6} \boldsymbol{I}_{26 \times 26}$. The performance of the two methods is assessed by tracking the system dynamics when the IMG is affected by wind and load variations, as shown in Fig. 3.9.
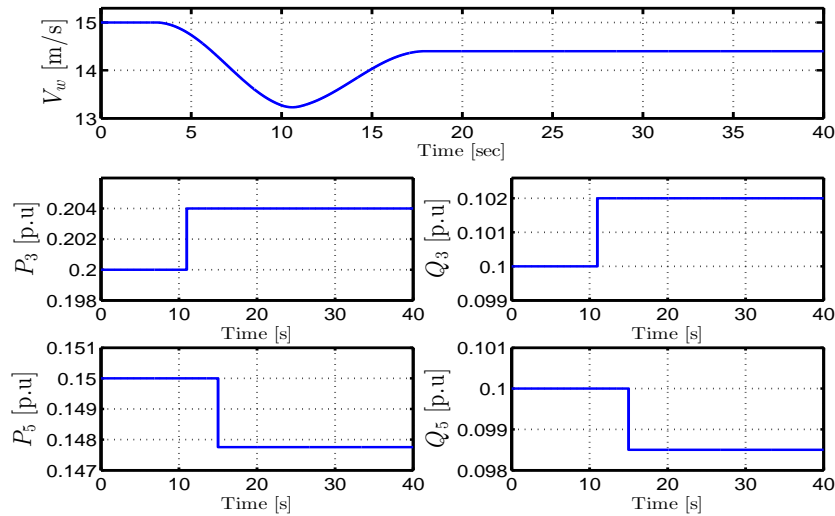
Figure 3.9: Wind speed and load variations.

The ten measured outputs are intentionally affected by Gaussian noise with a zero mean and variance of 3×10^{-7} while the Gaussian process noise is set to a variance of 1×10^{-9}. Furthermore, for this study case, only the measurements related to bus one (h_1, h_3, and h_4) are affected by gross errors during different time instants. The rest of the measurements are only corrupted by Gaussian noise. The measurement associated with the active power generated by the synchronous generator (h_1) is affected by gross errors at t= 1 [s], 3 [s], 20 [s] and 30 [s]. Similarly, the phase angle measurement (h_3) is affected at different time instants as shown in Fig. 3.10. On the other hand, the measurement of the bus voltage magnitude (h_4) is affected only at t= 10 [s] and 12 [s].
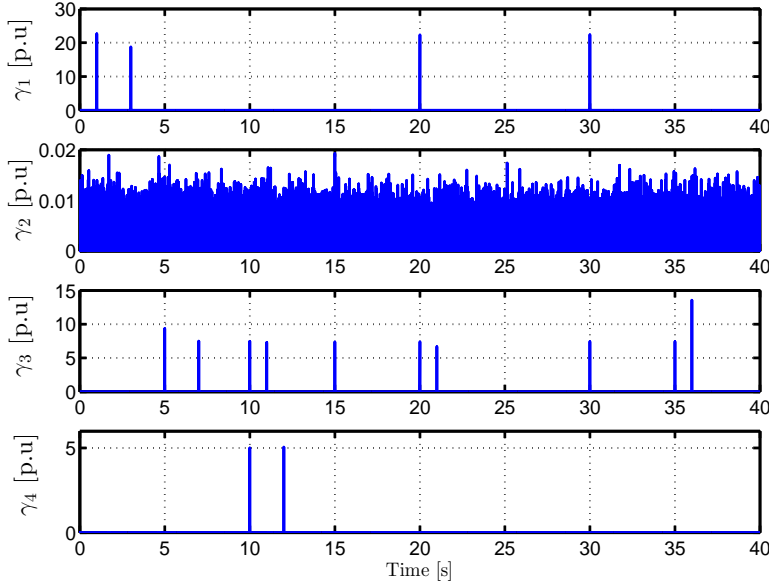
Figure 3.10: Dynamic of γ of each measurement.

The estimation of the nodal voltage magnitudes of the IMG is shown in Fig. 3.11 and 3.12. The estimators can reconstruct the dynamic voltage performance correctly in the face of rather extreme disturbances by assuming that they are known (the wind and load variations are assumed as known exogenous inputs for both estimators). As noticed the EKF performance is seriously affected by the noise, and these estimated values hardly can be used for monitoring or control purposes.

Figure 3.13 depicts the performances of the proposed UKF-SPT and the EKF estimating the IMG electrical frequency and the mechanical speed of the wind generators. The UKF-SPT, in comparison with the EKF, can capture the transient behavior related to these dynamic variables reducing considerably the the white Gaussian noise effect in the estimated signals.
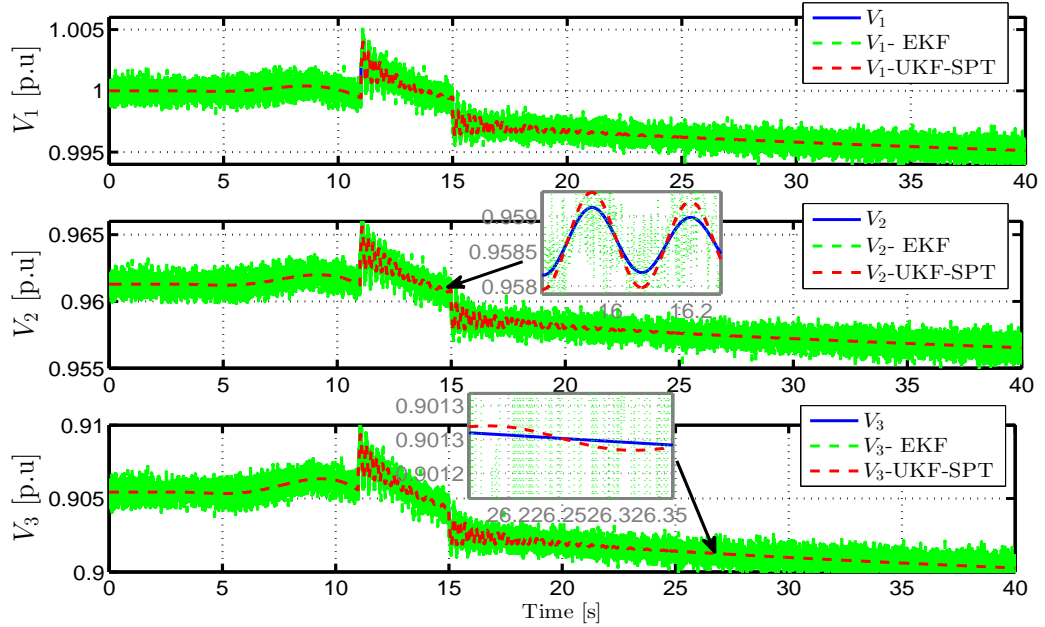
Figure 3.11: Nodal voltage magnitudes of the Microgrid
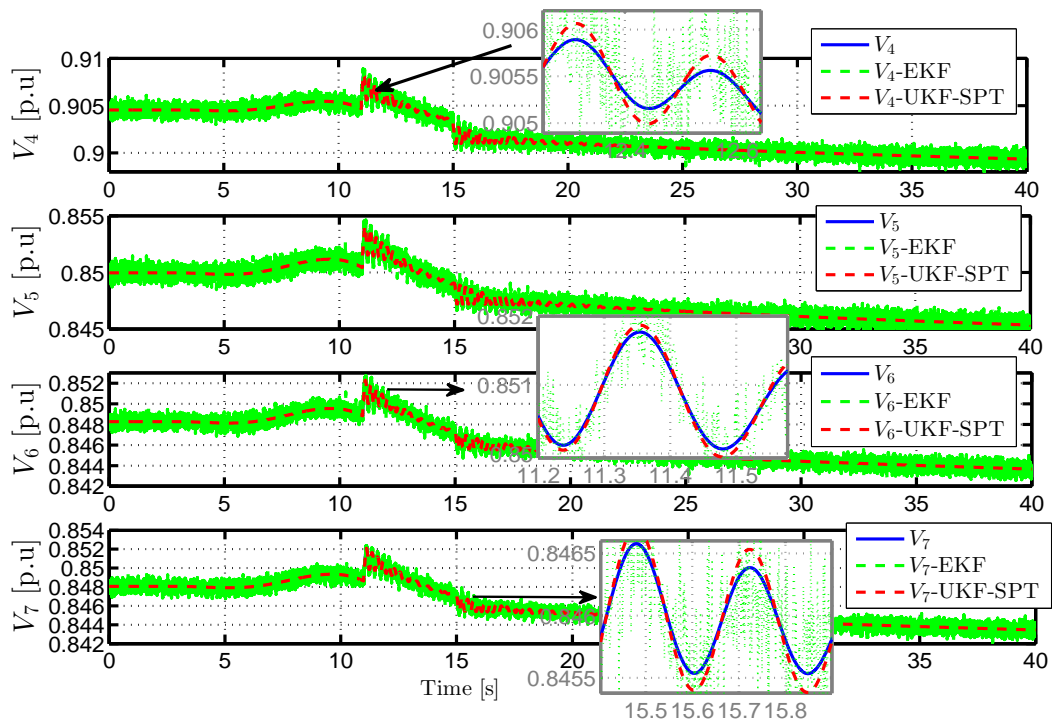
Figure 3.12: Nodal voltage magnitudes of the Microgrid
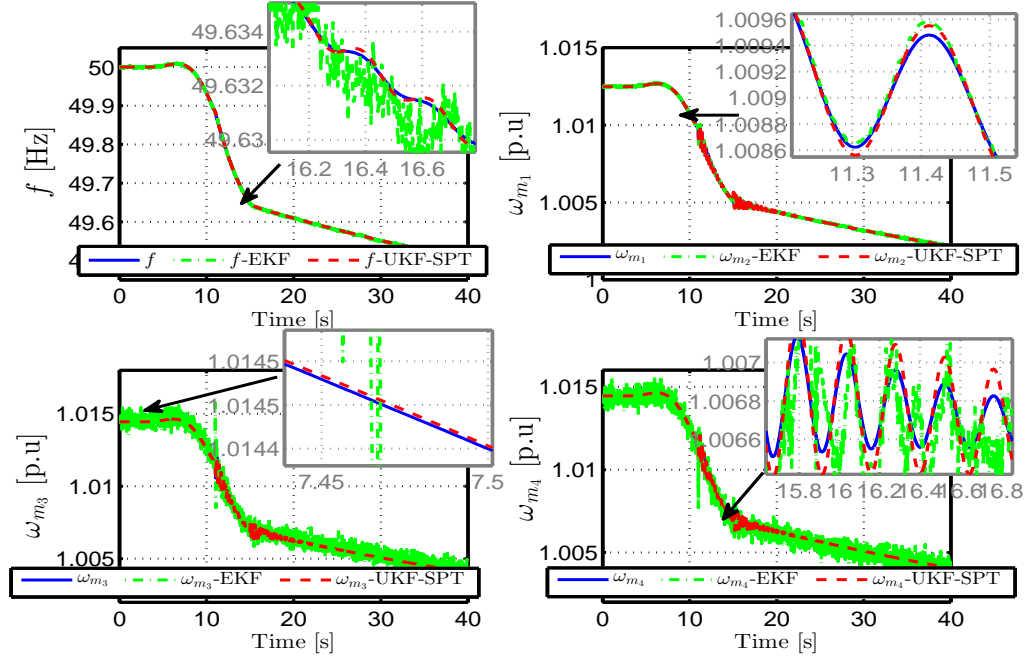
Figure 3.13: Comparison between the developed UKF-SPT and the conventional EKF.
Electrical frequency of the IMG and mechanical speeds of WG 1, 2 and 3.

Variables	Traditional EKF	Proposed UKF-SPT
f	2.3784×10^{-5}	9.4659×10^{-7}
ω_{m1}	2.8624×10^{-5}	2.4767×10^{-5}
ω_{m2}	1.4000×10^{-3}	3.0065×10^{-5}
ω_{m3}	1.4000×10^{-3}	3.0269×10^{-5}
θ_1	3.4164×10^{-4}	1.9774×10^{-4}
θ_2	3.2967×10^{-4}	2.0719×10^{-4}
θ_3	3.1652×10^{-4}	2.2323×10^{-4}
θ_4	3.0430×10^{-4}	2.3258×10^{-4}
θ_5	3.7539×10^{-4}	2.5227×10^{-4}
θ_6	1.1300×10^{-3}	2.7124×10^{-4}
θ_7	1.4000×10^{-3}	2.7310×10^{-4}
V_1	4.6606×10^{-4}	5.5691×10^{-5}
V_2	4.4455×10^{-4}	5.6981×10^{-5}
V_3	4.0848×10^{-4}	5.3204×10^{-5}
V_4	3.6940×10^{-4}	4.8919×10^{-5}
V_5	3.6381×10^{-4}	4.7837×10^{-5}
V_6	3.4401×10^{-4}	4.2621×10^{-5}
V_7	3.3975×10^{-4}	4.2237×10^{-5}

Table 3.2: RMSE in per-unit associated with estimators performance

Table 3.2 reports the RMSE associated with the estimation task, noticing that the RMSE obtained by the UKF-SPT is smaller than the one obtained by the EKF method for some variables estimation as the electrical frequency up to 80% smaller. The proposed estimation scheme base on the UKF-SPT suitably recovers the IMG state variables in a dynamic fashion and with a shallow margin of error.

3.3.3.2 IMG under three-phase fault

In this section, the proposed estimator is tested using the 7-bus IMG, which is affected by a three-phase fault applied to bus 5, at t = 0.5 [s]. The fault is cleared after 0.1 [s] (clearing time TCL). Figures 3.2 and 3.3 show the network's dynamic performance for selected variables, where it is observed that the IMG returns to the pre-fault conditions.

For this study case, the conventional UKF for DA systems [48] is also included for comparative purposes. For this, the three estimators are tested under the same conditions (the three-phase fault and process/measurement noises). The traditional EKF and the proposed UKF-SPT estimators employed the same covariance matrices associated with the process and measurement noises used in the previous study case (Subsection 3.3.3.1). On the other hand, for the conventional UKF, the following covariance matrices are considered: $\boldsymbol{Q}_{UKF,k} = diag([20 \times 10^{-5}, 20 \times 10^{-5}, 10 \times 10^{-5}, 40 \times 10^{-5}, 4 \times 10^{-5}, 40 \times 10^{-5}, 40 \times 10^{-5}, 40 \times 10^{-5}, 40 \times 10^{-5}, 40 \times 10^{-5}, 40 \times 10^{-5}, 40 \times 10^{-5}])$, $\boldsymbol{R}_{UKF,k} = 5 \times 10^{-5} \boldsymbol{I}_{10 \times 10}$ and the initial covariance matrix is set as $\boldsymbol{P}_{UKF,0} = 10 \times 10^{-9} \boldsymbol{I}_{12 \times 12}$. Also, the same set of ten measurements are used.

Principally, to show the prowess of the proposed UKF-SPT, the performance of the estimators is studied for the estimation of dynamic state variables of the synchronous generator connected to node one and the wind power generator at node four.
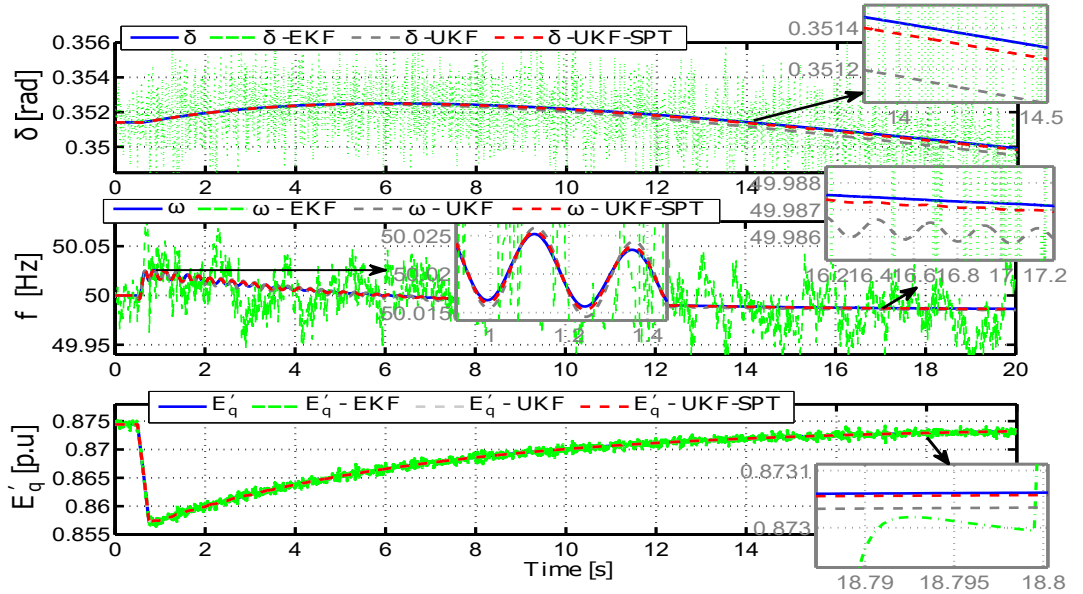
Figure 3.14: Load angle, electrical frequency and q-axis E.M.F of hydro generator.

As can be appreciated from Fig. 3.2 and 3.3, all estimators recover the transient and the steady-state regimes associated with the 7-bus IMG operation. It should be pointed out that the transient and the steady-state responses obtained with the developed UKF-SPT are better than those acquired by the other estimators. Furthermore, the UKF-SPT considerably reduces the noise effect in the estimated values.
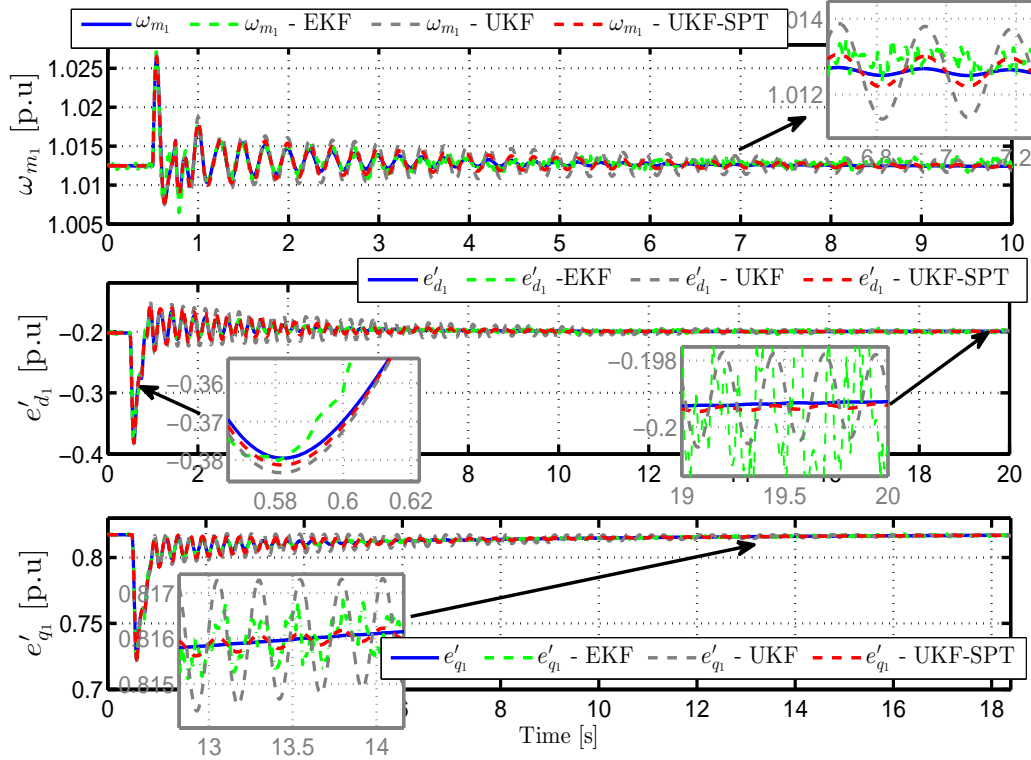
Figure 3.15: Mechanical speed of WG, d-axis E.M.F of WG and q-axis E.M.F of WG.

Furthermore, a comparative analysis about the execution times of three estimators is presented. The simulation results were obtained through a computer with Intel (R) Core (TM) i5-2.9GHz, 8 GB of RAM, 64-bit OS, with MATLAB / Simulink R2013-b platform to simulate the test case using an integration time step of 1 [ms]. Under these conditions, the execution times are reported in Table 3.3. Note that the computational time of the UKF-SPT is reduced by about 95 % concerning the conventional UKF for DA systems, showing that the algebraic loops considerably affect the execution time.

The difference among execution times lies in the fact that the proposed UKF-SPT adopts a completely differential representation of the IMG. Thus, the prediction step is carried out more efficiently, reducing the algebraic loops. In contrast, the conventional EKF and UKF for DA systems [48] resort to algebraic loops for both the prediction and correction steps, an aspect that directly reflects on increased execution times.

The minimum, average, and maximum computing times are obtained for ten IMG

test system simulations.

Algorithm	EKF	UKF	Proposed UKF-SPT
Execution minimum time [min]	≈ 7.250	≈ 95.0	≈ 4.150
Execution average time [min]	≈ 7.613	≈ 101.6	≈ 5.632
Execution maximum time [min]	≈ 8.166	≈ 106.0	≈ 5.866

Table 3.3: Execution times

3.4 Concluding Remarks

This chapter has put forward a novel and comprehensive state estimation methodology for the dynamic state estimation for IMG structures modeled as a set of DAEs consisting of two dynamic estimators based on Kalman Filter theory derived in Sections 3.2 and 3.3. As corroborated from simulation results, all the state variables (dynamic and algebraic) of an IMG can be estimated. This feature dramatically contrasts with other existing estimation approaches [31–34, 39–47] where the bus voltage phasors are considered as known inputs available through measurement device, as well as the new operation points of the IMG in the presence of different perturbations are obtained. Furthermore, the proposed estimators can capture the transient and steady-state behavior associated with the IMG operation employing fewer measurements than conventional static estimators. The developed dynamic state estimation algorithms may be straightforwardly implemented, this being an essential feature for evaluating the estimation schemes for IMGs consisting of several electrical variables to be estimated. Specifically, the proposed UKF-SPT estimator reduces the algebraic loops present in the prediction and correction steps compared with other UKF estimators for DA systems, thus, reducing the required computational load and the simulation time.

To clarify the main contributions of both proposed estimators for IMG structures (EKF and UKF-SPT) concerning the previous dynamic estimation approaches for electric power systems, Table 3.4 is added.

As mentioned above the two proposed estimators offer a solution for IMGs state estimation problem but there are some aspects that should be pointed out as: (i) these state estimation algorithms were designed based on a centralized approach (also known wide-area) requiring the global knowledge of the system and of a generalized set of measurements to reconstruct the state variables, (ii) the computational efficiency is not optimal; the number of equations involved by the estimators increases considerably according to the network dimension, as well as, the Riccati equations (those related to the correction step) grows quadratically according to the states to be estimated, this is directly reflecting on extra computational load, (iii) the tuning scheme, which is related to the selection of covariances matrices $(\boldsymbol{Q}_k, \boldsymbol{R}_k)$ is not transparent, these usually are set through heuristic methods, and (iv) the proposed estimators do not have a formal

convergence proof their functioning is just corroborated by numerical simulations.

These points are used to motivate the scope of the following chapter; the design of a dynamic estimator for MPSs taking as main objectives: (i) the computational efficiency, (ii) robust functioning against measurement noise and parametric uncertainty, (iii) the decentralization of dynamic variables estimation, and (iv) tuning criteria coupled with formal convergence analysis.

	Proposed Estimators for IMG structures	Other Existing Approaches [31–34, 39, 42–46]
Based on	EKF/UKF-SPT	EKF, UKF, Particle Filter (PF), Extended PF, H-infinity
Adopted Model	Differential Algebraic Equations (DAEs)	Ordinary Differential Equations (ODEs)
Applied to	Islanded Microgrids	Transmission systems, the reported approaches in [28, 37, 38] are applied to MGs in comparison to those ones [33, 39, 44] which are applied to a Single Machine Infinite-Bus Power System.
Generator units	Synchronous generators and wind generators	Synchronous generators and in [37, 38] different energy resources are considered (PV, wind generators), but they are represented as idealized voltage sources.
Estimated State Variables	Dynamic (generator units) and algebraic variables (bus voltage phasors)	Only dynamic variables (those which are related to generator units). Moreover, with respect to the approach [60] the dynamic variables together with phase angles θ_i are estimated but considering constant generator terminal voltages which reduce the ability to capture the full of the system.
Bus voltage phasors	Estimated by the proposed estimator	The algebraic variables (V_i, θ_i) are treated as known inputs obtained by a PMU device.
Approach	Centralized	Decentralized
Measurements	Fewer	More - a PMU at every generator terminal
Computational burden	More	Less and with respect to [43] the proposed Particle Filter (PF) demands an extra computational load due to high complexity difficult to implement.

Table 3.4: Comparison of different state estimation approaches

Decentralized Robust State Estimation of Multimachine Power Systems

Abstract: In this chapter, a decentralized state estimation algorithm of a class of Multimachine Power System is presented. Firstly, the MPS model presented in Section 2.3 is rewritten, adding a new state variable representing the nonlinear interaction among machines, unknown disturbances, and parametric uncertainty. Later a Luenberger-type nonlinear observer is designed to estimate every generation unit's state by considering only local information. A comparison with the traditional Extended Kalman Filter (centralized version) is carried out to show the proposed design's potential.

4.1 Introduction

Using voltage phasors, active and reactive powers, and frequency as measurements, different state estimation schemes based on the Extended Kalman Filter (EKF) have been proposed [31, 32, 34, 40–42, 61–63]. These reported estimators can recover transient and steady-state behavior, even in the presence of faults and disturbances (e.g., three-phase faults and sudden load changes). The EKF and its variations [4, 64, 65] are well known and have a constructive design showing a robust behavior against parameter errors and measurement noise. However, they require a large computational load associated with the number of equations to be solved and a heuristic tuning, not to mention the lack of convergence proofs. Most of these approaches [31, 34, 40, 41] are centralized (also known as wide-area estimation schemes). The main drawback is that the computational load gradually increases according to the system's dimension. They require collecting all the measurements and using them together with the whole system to estimate the state [66]. Also, there are decentralized (or local) approaches adopting only the local generator model and using local information to estimate the states [32, 33, 42, 61–63].

Another approach used over 20 years to recover the dynamic state variables raised

from a MPS model is the observers based on sliding modes (SM) theory. For example, in [67], the dynamic state variables of every machine are augmented considering an additional state, which accounts for the unmeasured bounded disturbances and the interconnection among generators. Based on the sliding modes perturbation observer (SMPO) technique, the resulting estimation scheme has a less computational load than the EKF. Its robust behavior and convergence are formally tested in the presence of model and parameter errors. However, it is necessary to include a perturbation estimator that complicates both the resulting scheme and the large set of non-parameterized gains tuning. In [68], a sliding mode observer is designed, the relative speed is estimated using load angle with electrical power as measurements. This estimation scheme does not have a systematic construction despite representing the interconnection terms and uncertainties by nonlinear functions. It requires additional information, local and neighboring, measurements to reconstruct the state. The reported SM design presents a complex structure, unclear tuning, and noise can considerably affect its behavior.

Along with the aforementioned estimation schemes, in scientific literature, Luenberger like observers can be found [69–71]. In [69, 70], the estimator design is based on the fully linearized representation of the MPS, ignoring the model errors. On the other hand, by adopting a linear representation of MPS, the state is reconstructed through a centralized approach [71]. Specifically, the observer gains are precalculated off-line around a particular equilibrium point.

These considerations motivate the scope of the present study: developing a state estimation design methodology that retains the advantages of EKF and SM estimators and overcomes their obstacles. The aims are: (i) to retain the low-dimensionality (low online computational load), disturbance rejection capability and formal assessment of robust convergence of the SM observer, and the robustness of the EKF concerning measurement noise, and (ii) draw robust functioning assurance conditions coupled with a conventional-like simple tuning scheme.

The problem is solved within a constructive geometric estimation framework by combining ideas from electrical engineering, SM and EKF estimation, MPS industrial control with conventional tuning, and small gain-based convergence assessment for two-subsystems interconnections. Through the unknown input-state extension with integral action, [72] of the geometric state estimation [73, 74], the dynamic states of generators are recovered with a non-high gain observer based on a state-unmeasured input observable decentralized model through the local information by using load angle as the individual measured output.

Firstly, a tailored model is built. The observability analysis shows that the augmented state can be reconstructed in a fast and robust way, even in the presence of measurement noise and parametric uncertainty. Secondly, a dynamic state estimator requiring fewer measurements and a precise and systematic industrial-like tuning is presented. Also, the computational load is significantly reduced, allowing on-line implementations. Finally, the estimator is connected and compared with previous related studies with NL EKF and SM observer designs. The proposed methodology is illustrated and tested with a representative benchmark example employed in previous

MPS studies [32, 40, 55, 68, 75–77], finding that the proposed estimator yields a better compromise between reconstruction speed, robustness to modeling and measurement errors, and on-line computational load than the compromises of the SMPO and EKF observers.

4.2 Preliminaries

The dynamic model of MPS (2.13) presented in Section 2.3 is taking as the starting point to design a decentralized estimator. The following theoretical assumptions are imposed:

Assumption 1. Only the load angle associated with each generator bus is measured.

Assumption 2. The adopted MPS model (2.13) - Section 2.3, considers loads of the constant impedance type, i.e., all zero injection nodes are removed considering only the generator nodes. Moreover, it is assumed that the generators are connected through a purely inductive network.

Assumption 3. For MPS model (2.13), the dynamic state variables of each generator are given by load angle, relative speed and electrical power variation, i.e., $\boldsymbol{x}_i := \left[\delta_i, \omega_i, P_i \right]^\top$, where $P_i = \Delta P_{e_i} = P_{e_i} - P_{m_i}$ by assuming a constant mechanical input power for every generator.

The following estimation objective is formulated:

Objective. *Estimate in a decentralized fashion the dynamic variables* $\boldsymbol{x}_i := \left[\delta_i, \omega_i, P_i \right]^\top$ *of each generator using the associated load angle as individual measured output and assuming that* $d_{\omega_i}, I_{q_i}, P_{m_i}$ *and* u_i *are known.*

The state estimation objective is achieved following a methodology which involves the steps below:

1. The state estimation problem of MPS is solved within a constructive framework, by combining notions and tools from electrical engineering, nonlinear estimation, and model design.

2. In Subsection 4.4.3 a tailored estimation model of MPS (2.13) is built, adding a new state variable one per machine, which stands for the nonlinear interaction among machines, unknown disturbances, and parametric uncertainties.

3. An observability analysis is carried out in Subsection 4.4.4, showing that the augmented state can be reconstructed in a fast and robust way, even in the presence of measurement noise and model errors. This observability (instant) property indicates that the dynamic variables of each generator $\boldsymbol{x}_i$ can be estimated in a distributed way.

4. Through the unknown input-state extension with integral action [72] of the geometric state estimation [73, 74] (Subsection 4.4.5). The dynamic state variables $\boldsymbol{x}_i$ of each generator are reconstructed in a decentralized way employing a state-unmeasured input observable decentralized model (Subsection 4.4.3) through local information and by using the associated load angle as the individual measured output (one measurement per machine).

5. The proposed GE estimator is coupled with conventional tuning (Subsection 4.4.6) and small gain-based convergence analysis for estimation error dynamics against measurement noise and parasitic dynamics (Subsection 4.4.7). Following the steps presented in this chapter, the proposed estimation methodology can be extrapolated to more complex grids (with the same assumptions presented in Section 4.2) considering more generators and interconnections.

6. The estimation methodology is put in perspective with previous (EKF and SMPO) approaches employed for MPSs, and it is illustrated and tested with a representative case example used in many estimation and control studies by power system community [32, 40, 55, 68, 75–77], including functioning comparison it is NL EKF counterpart.

In the next sections, the proposed methodology is explained in detail. Firstly, a short explanation of NL EKF and SMPO estimators is given to motivate a design of an improved estimation scheme that allows retaining the main features of both techniques. Furthermore, the steps involved in the formulation of the linear decentralized observable model are given, and details about the construction of the proposed estimation scheme are presented.

4.3 Motivation

As a preamble for estimator design, and for comparison purposes versus existing estimation methodologies, in this section are recalled: the NL EKF as one of the most employed and accepted model-based state estimation technique in MPS and sliding mode perturbation observer (SMPO) as a representative example of academic research.

4.3.1 Nonlinear Extended Kalman Filter and Sliding Mode Perturbation Observer

By assuming that the associated stochastic observability condition [78] of the stochastic version of the MPS model (2.15a) is met, it is denoted by

$$\dot{\boldsymbol{x}} = \boldsymbol{f}(\boldsymbol{x}, \boldsymbol{d}_x) + \boldsymbol{w}, \quad \boldsymbol{x}(0) = \boldsymbol{x}_0, \quad \boldsymbol{w} \sim N[\boldsymbol{0}, \boldsymbol{Q}], \quad \boldsymbol{y} = \boldsymbol{C}\boldsymbol{x} + \boldsymbol{v}, \quad \boldsymbol{v} \sim N[\boldsymbol{0}, \boldsymbol{R}] \quad (4.1a)$$

the related NL EKF is written as

$$\dot{\hat{\boldsymbol{x}}} = \boldsymbol{f}(\hat{\boldsymbol{x}}, \boldsymbol{d}_x) + \boldsymbol{g}_{ekf}(\boldsymbol{\Sigma}, \boldsymbol{R})(\boldsymbol{y} - \boldsymbol{C}\hat{\boldsymbol{x}}), \qquad \hat{\boldsymbol{x}}(0) = \hat{\boldsymbol{x}}_0 \tag{4.1b}$$

$$\dot{\boldsymbol{\Sigma}} = \boldsymbol{\Sigma}\boldsymbol{J}(\hat{\boldsymbol{x}}, \boldsymbol{d}_x) + \boldsymbol{J}^\top(\hat{\boldsymbol{x}}, \boldsymbol{d}_x)\boldsymbol{\Sigma} + \boldsymbol{Q} - \boldsymbol{\Sigma}\boldsymbol{C}^\top\boldsymbol{R}^{-1}\boldsymbol{C}\boldsymbol{\Sigma}, \qquad \boldsymbol{\Sigma}(0) = \boldsymbol{\Sigma}_0 \tag{4.1c}$$

where

$$n_x = 3\text{N}, \qquad n_\Sigma = n_x(n_x + 1)/2, \qquad n_{ekf} = n_\Sigma + n_x \tag{4.1d}$$

$$\boldsymbol{g}_{ekf}(\boldsymbol{\sigma}, \boldsymbol{R}) = \boldsymbol{\Sigma}\boldsymbol{C}^\top\boldsymbol{R}^{-1}, \quad \boldsymbol{J}(\hat{\boldsymbol{x}}, \boldsymbol{d}_x) = \partial_{\boldsymbol{x}}\boldsymbol{f}(\boldsymbol{x}, \boldsymbol{dx}) \tag{4.1e}$$

$$\boldsymbol{R} = bd(r_1, \dots, r_\text{N}), \quad \boldsymbol{Q} = \boldsymbol{Q}^\top = bd[\boldsymbol{q}_1, \dots, \boldsymbol{q}_\text{N}] \tag{4.1f}$$

$$\boldsymbol{q}_i = q_i\boldsymbol{I}_{3\times3}, \quad \dim\boldsymbol{\Sigma} = \dim\boldsymbol{Q} = n_x \times n_x \tag{4.1g}$$

$$\boldsymbol{\kappa}_{ekf} = (r^\top, \boldsymbol{q}^\top)^\top, \quad \dim\boldsymbol{\kappa}_{ekf} = n_k = 2\text{N} \tag{4.1h}$$

$\hat{\boldsymbol{x}}$ is the estimate of the state $\boldsymbol{x}$, $\boldsymbol{\Sigma}$ is the estimate error covariance matrix with n_Σ equations of the Ricatti matrix ODE, $\boldsymbol{Q}$ (or $\boldsymbol{R}$) is the model (or measurement) error covariance (symmetric positive definite) diagonal (or block diagonal) matrix with N adjustable parameter vector r (or $\boldsymbol{q}_i$), n_{ekf} is the number of estimator ODEs, and $\boldsymbol{\kappa}_{ekf}$ is the vector with the 2N adjustable parameters of the NL EKF, according to the expressions.

The advantages of the EKF are the simplicity of construction and its robust behavior in model parameters and measurement noise errors. Its disadvantages are (i) an on-line computational load that grows rapidly (quadratically) n_Σ with the number of $n_x = 3\text{N}$ of states, and (ii) the choice of the tuning pairs $(r_{i=1,\dots,\text{N}}, \boldsymbol{q}_{i=1,\dots,\text{N}})$, one per machine, r_i is set equal to the squared instrument standard deviation and $\boldsymbol{q}_{i=1,\dots,\text{N}}$ are found from functioning-based calibration/tuning based on experience and heuristics, without clear/transparent/explicit connection between the dependency of estimator convergence on the choice of the $\boldsymbol{q}_i$'s.

On the other hand and according to the SMPO technique [67, 79, 80], based on the model

$$\dot{\boldsymbol{x}}_i = \mathcal{A}_i\boldsymbol{x}_i + \boldsymbol{b}_d d_{\omega_i} + \boldsymbol{b}_u(u_i + \sigma_i), \qquad \boldsymbol{x}_i(0) = \boldsymbol{x}_{i_0} \tag{4.2a}$$

$$\dot{\sigma}_i = 0, \qquad \sigma_i(0) = \sigma_{i_0} \tag{4.2b}$$

with augmented fictitious state, one per machine, that accounts for the combined effect of unmeasured disturbances and state dependency on other machines, under the assumption that $\dot{\gamma}_i(\boldsymbol{x}, \boldsymbol{d}_\gamma)$ is bounded, the state estimation task can be done in a decentralized manner with the following observer driven by standard (constant gain $[\boldsymbol{\varrho}_i, \varrho_{\sigma_i}]$)

and sliding (on-off gain $[\boldsymbol{k}_i, k_{\sigma_i}]$ sign) measurement injections:

$$\dot{\hat{\boldsymbol{x}}}_i = \mathcal{A}_i\hat{\boldsymbol{x}}_i + \boldsymbol{b}_d d_{\omega_i} + \boldsymbol{b}_u(u_i + \hat{\sigma}_i) - \boldsymbol{\varrho}_i(y_i - \boldsymbol{c}_y\hat{\boldsymbol{x}}_i) - \boldsymbol{k}_i sgn(y_i - \boldsymbol{c}_y\hat{\boldsymbol{x}}_i), \quad \hat{\boldsymbol{x}}_i(0) = \hat{\boldsymbol{x}}_{i_0} \tag{4.3a}$$

$$\dot{\hat{\sigma}}_i = -\varrho_{\sigma_i}(y_i - \boldsymbol{c}_y\hat{\boldsymbol{x}}_i) - k_{\sigma_i} sgn(y_i - \boldsymbol{c}_y\hat{\boldsymbol{x}}_i), \quad \dim(\hat{\boldsymbol{x}}_i, \hat{\sigma}_i) = (3N, N) \qquad \hat{\sigma}_i(0) = \hat{\sigma}_{i_0} \tag{4.3b}$$

where the standard/asymptotic gain pair $(\boldsymbol{\varrho}_i, \varrho_{\sigma_i})$ is chosen with pole placement, and the gains pair $\boldsymbol{k}_i, k_{\sigma_i}$ of the sliding surface is tuned according to inequalities so that the error dynamic on the sliding mode is stable.

The preceding SM observer design (4.3) has: (*i*) a systematic construction, (*ii*) a difficult tuning with many (typically eight) per-machine adjustable parameters, and (*iii*) convergence criteria coupled with a tuning guideline based on upper bounds of estimation errors (including the convergence to the sliding surface). It must be pointed out that [67]: (i) as it stands, the SMPO observer (4.3) is highly susceptible to measurement noise, and (ii) consequently, the observer (4.3) must be further redesigned to cope with measurement noise. As far as we know, such redesign has not been executed in the reported study [67].

The preceding considerations motivate the present study on the improvement of the MPS state estimator designs. Concerning the EKF design, formal functioning assessment, robustness to persistent model parameter error, online computational load, and tuning systematicity must be attained. Furthermore, for SMPO observers, tuning simplicity and robustness for measurement noise must be retained.

4.4 State Estimator

In this section, the estimation problem is presented in formal fashion. Then, the linear decentralized observable model with unknown-reconstructible input is derived. A compact representation of this estimation model is obtained to carry out a formal observability analysis. It is taken as a reference to derive the proposed estimation scheme, including the conditions to ensure estimation error dynamics convergence against measurement and parametric uncertainties coupled with a practical tuning guideline.

4.4.1 Problem

The present study consists in designing the linear gains $(\boldsymbol{k}_i^{\boldsymbol{x}}, k_i^{\iota})$ (four per machine) of the model-based NL state estimator for the MPS system (2.14), of the form

$$\dot{\hat{\boldsymbol{x}}}_i = \boldsymbol{A}_i\hat{\boldsymbol{x}}_i + \boldsymbol{b}_d d_{\omega_i} + \boldsymbol{b}_u(u_i + \hat{\iota}_i) + \boldsymbol{k}_i^{\boldsymbol{x}}(\zeta_i^o, \varpi_i^o)(y_i - \boldsymbol{c}_y\hat{\boldsymbol{x}}_i), \quad \hat{\boldsymbol{x}}_i(0) = \hat{\boldsymbol{x}}_{i0} \tag{4.4a}$$

$$\dot{\hat{\iota}}_i = k_i^{\iota}(\zeta_i^o, \varpi_i^o)(y_i - \boldsymbol{c}_y\hat{\boldsymbol{x}}_i), \qquad \hat{\iota}_i(0) = \iota_{i_0}, \qquad i = 1, \ldots, N \tag{4.4b}$$

with constant-gain measurement injection correction to preclude functioning fragility concerning measurement noise and with a decentralized structure (including $\boldsymbol{A}_i$ which is a suitable variant of $\mathcal{A}_i$ of SMPO (to be precised)) intended to draw a tuning scheme as conventional as possible, in terms of the per-machine adjustable damping-frequency pair (ζ_i^o, ϖ_i^o): (i) associated with the state convergence error of the i-th machine, and (ii) with transparent connection with the natural damping-frequency pair of the i-th machine.

Driven by the measured input-output pair signals $(y_i, \boldsymbol{d}_i)(\mathrm{t})$ of the actual MPS (2.14), the dynamic data processor must produce a robustly convergent state estimates $\hat{\boldsymbol{\chi}}_i(t)$, i.e.,

$$\hat{\boldsymbol{\chi}}_{i_0} \approx \boldsymbol{\chi}_{i0} \quad \Longrightarrow \quad \hat{\boldsymbol{\chi}}_i(t) \longrightarrow_r \boldsymbol{\chi}_i(t) = \boldsymbol{\tau}_i[t, \boldsymbol{\chi}_{i_0}, \boldsymbol{d}_i(\cdot)] \in X, \qquad y_i = \boldsymbol{\kappa}\boldsymbol{\chi}_i(t) \qquad (4.5)$$

where

$$\boldsymbol{\chi}_i = [\boldsymbol{x}_i, \iota_i]^\top, \quad \boldsymbol{\kappa} = [1, 0, 0, 0], \quad \boldsymbol{d}_i = [d_{\omega_i}, u_i]^\top, \quad \dim(\hat{\boldsymbol{\chi}}_i) = 4$$

The present dissertation is focused on designing a methodology with:

1. Systematic construction.

2. A robust convergence criterion coupled with simple gain tuning.

3. Identification of the underlying solubility (observability) property.

4. Robust functioning in the sense of an adequate compromise between reconstruction speed, robustness concerning model error and noise, and online computational load.

In this way, motivated by a geometric estimator (GE) based on a state-unmeasured input observable decentralized model, the augmented state is reconstructed by the unknown input-state extension with integral action [72] of the geometric state estimation [73, 74]. The GE drops the SM-type discontinuous injection functions to eliminate unduly sensitivity to noise and through conventional Luenberger-like injection, effectively and more simply with more application-oriented tuning (tested in a large industrial scale multi-component distillation column, with experimental data [81]) what the SMPO (4.3) does.

4.4.2 MPS Dynamics

For the observer model design (in Subsection 4.4.3) and gain tuning simplicity purposes (in Subsection 4.4.6), the expression $\gamma_i(\boldsymbol{x}, \boldsymbol{d}_\gamma)$ (2.13i) is expanded in Taylor series (TS) expansion about the nominal state-input pair $(\bar{\boldsymbol{x}}, \bar{\boldsymbol{d}}_\gamma)$

$$\gamma_i(\boldsymbol{x}, \boldsymbol{d}_\gamma) = \boldsymbol{l}_i(\boldsymbol{x} - \bar{\boldsymbol{x}}) + \boldsymbol{o}_i(\boldsymbol{x}, \boldsymbol{d}_\gamma) \qquad (4.6a)$$

$$\boldsymbol{l}_i = [\partial_{\boldsymbol{x}} \gamma_i(\boldsymbol{x}, \boldsymbol{d}_\gamma)]_{(\boldsymbol{x}, \boldsymbol{d}_\gamma) = (\bar{\boldsymbol{x}}, \bar{\boldsymbol{d}}_\gamma)} = [\alpha_i, -q_i, 0], \quad \boldsymbol{o}_i(\bar{\boldsymbol{x}}, \bar{\boldsymbol{d}}_\gamma) = 0 \qquad (4.6b)$$

with linear component $\boldsymbol{l}_i(\boldsymbol{x} - \bar{\boldsymbol{x}})$ and nonlinear one $\boldsymbol{o}_i(\boldsymbol{x}, \boldsymbol{d}_\gamma)$ Lipschitz bounded as

$$|\boldsymbol{o}_i(\boldsymbol{x}, \boldsymbol{d}_\gamma)| \leq L_x^{o_i}(\boldsymbol{x}, \boldsymbol{d}_\gamma)|\boldsymbol{x} - \bar{\boldsymbol{x}}| + L_w^{o_i}(\boldsymbol{x}, \boldsymbol{d}_\gamma)|\boldsymbol{d}_\gamma - \bar{\boldsymbol{d}}_\gamma| \leq l_x^{o_i}|\boldsymbol{x} - \bar{\boldsymbol{x}}| + l_{\boldsymbol{d}_\gamma}^{o_i}|\boldsymbol{d}_\gamma - \bar{\boldsymbol{d}}_\gamma| \quad \text{(4.7a)}$$

$$L_x^{o_i}(\bar{\boldsymbol{x}}, \bar{\boldsymbol{d}}_\gamma) = 0 \leq L_x^{o_i}(\boldsymbol{x}, \boldsymbol{d}_\gamma) l_x^{o_i} := \max_{(\boldsymbol{x}, \boldsymbol{d}_\gamma) \in X \times D_\gamma} L_x^{o_i}(\boldsymbol{x}, \boldsymbol{d}_\gamma) \quad \text{(4.7b)}$$

$$L_{\boldsymbol{d}_\gamma}^{o_i}(\bar{\boldsymbol{x}}, \bar{\boldsymbol{d}}_\gamma) = 0 \leq L_{\boldsymbol{d}_\gamma}^{o_i}(\boldsymbol{x}, \boldsymbol{d}_\gamma) l_{\boldsymbol{d}_\gamma}^{o_i} := \max_{(\boldsymbol{x}, \boldsymbol{d}_\gamma) \in X \times D_\gamma} L_{\boldsymbol{d}_\gamma}^{o_i}(\boldsymbol{x}, \boldsymbol{d}_\gamma) \quad \text{(4.7c)}$$

and express the MPS (2.14) in per-machine ι_i-parametric form

$$\dot{\boldsymbol{x}}_i = \boldsymbol{A}_i \boldsymbol{x}_i + \boldsymbol{b}_d d_{\omega_i} + \boldsymbol{b}_u(u_i + \iota_i), \qquad \hat{x}_i(0) = \hat{x}_{i0} \quad \text{(4.8a)}$$

$$y_i = \boldsymbol{c}_y \boldsymbol{x}_i, \qquad \iota_i = g_i(\boldsymbol{x}, \boldsymbol{d}_\gamma), \quad i = 1, \dots, \text{N} \quad \text{(4.8b)}$$

where

$$g_i(\boldsymbol{x}, \boldsymbol{d}_\gamma) = \boldsymbol{o}_i(\boldsymbol{x}, \boldsymbol{d}_\gamma) - \boldsymbol{l}_i \bar{\boldsymbol{x}}, \quad g_i(\bar{\boldsymbol{x}}, \bar{\boldsymbol{d}}_\gamma) = \boldsymbol{l}_i \bar{\boldsymbol{x}}$$

$$\alpha_i = \bar{E}'_{q_i} \sum_{j=1}^{\text{N}} B_{ij} \left[\bar{E}'_{q_j} \cos(\bar{\delta}_i - \bar{\delta}_j) + \bar{E}'_{q_j} \sin(\bar{\delta}_i - \bar{\delta}_j) \bar{\omega}_j \right], \quad q_i = \bar{Q}_{e_i}$$

$$\boldsymbol{A}_i = \begin{bmatrix} 0 & 1 & 0 \\ 0 & -a_i & -b_i \\ \alpha_i & -q_i & -c_i \end{bmatrix}, \quad |e^{\boldsymbol{A}_i t}| \leq a_i e^{-\lambda_i t}, \quad \lambda_i = \zeta_i^m w_i^m$$

$$\lambda_i = \min(\zeta_i^m \varpi_i^m, \varpi_i^e) \approx \begin{cases} \lambda_{1,2}^i = -\zeta_i^m \varpi_i^m \pm \left[\varpi_i^m \sqrt{1 - \zeta_i^{m2}} \right] j \\ \lambda_3^i = -\varpi_i^e \end{cases} \quad \text{(4.9)}$$

and $\lambda_{1,2}^i$ and λ_3^i are the three eigenvalues of $\boldsymbol{A}_i$ in (4.8) which can be uniquely solved as a function of i-th machine parameters:

$$(\zeta_i^m, \varpi_i^m, \varpi_i^e) = \mathcal{F}(a_i, b_i, \alpha_i, q_i, c_i)$$

From the application of standard (Lyapunov's converse theorem [82], and Gronwall's generalized lemma [82, 83]), the i-th machine state motion-output signal pair is EU bounded as follows

$$|\boldsymbol{x}_i(t) - \bar{\boldsymbol{x}}_i| = |y_i(t) - \bar{y}_i| \leq a_i e^{-l_{x_i} t} \epsilon_{i_0} + (a_i/l_{x_i}) \epsilon_{\Theta_i}$$
$$\leq a_i \epsilon_{\boldsymbol{x}_{i_0}} + (a_i/l_{x_i}) \epsilon_{\Theta_i} := \epsilon_{\boldsymbol{x}_i}, \quad a_i, l_{x_i} > 0 \tag{4.10}$$
$$|\dot{\boldsymbol{x}}_i(t)| \leq \lambda_i^+ \epsilon_{\boldsymbol{x}_i} + (a_i/l_{x_i})^+ \epsilon_{\Theta_i} := \epsilon_{\dot{\boldsymbol{x}}_i} \tag{4.11}$$

where

$$0 < a_i < a_x, \ l_{x_i} = \lambda_i - a_i l_{\boldsymbol{x}_i}^{\Theta_i} > \lambda_x, \quad \lambda_i = \zeta_i^m \varpi_i^m, \quad \lambda_i^+ = \varpi_i^e$$

$$\Theta_i = \boldsymbol{b}_d d_{\omega_i} + \boldsymbol{b}_u [u_i + g_i(\boldsymbol{x}, \boldsymbol{d}_\gamma)], \quad |\Theta_i|(t) \leq \epsilon_{\Theta_i}$$
$$\epsilon_{\Theta_i} = l_{d_{\omega_i}}^{\Theta_i} \epsilon_{d_{\omega_i}} + l_{u_i}^{\Theta_i} \epsilon_{u_i} + l_{\boldsymbol{x}}^{\Theta_i} \epsilon_{\boldsymbol{x}} + l_{\boldsymbol{d}_\gamma}^{\Theta_i} \epsilon_{\boldsymbol{d}_\gamma}$$

The MPS representation (4.8) retains the linear part of $\gamma_i(\boldsymbol{x}, \boldsymbol{d}_\gamma)$ incorporating α_i and q_i in $\mathcal{A}_i$ of SMPO approach allowing to have a better description of the i-th machine 3rd-order dynamics regarded as individual.

4.4.3 Estimation Model

It is assumed that the signal ι_i is in a slow-varying regime (SVR) concerning the exponential convergence speed ϖ_i^o of the observer (to be designed), i.e.,

$$\dot{\iota}_i = \dot{g}_i(\boldsymbol{x}, \boldsymbol{d}_\gamma) = F_i(\boldsymbol{x}, \boldsymbol{d}_\gamma, \dot{\boldsymbol{d}}_\gamma) \approx_{svr} 0 \qquad |\dot{\iota}_i/\iota_i| := \lambda_i << \varpi_i^o, \quad i = 1, \dots, \mathrm{N} \tag{4.12}$$

understanding that the pertinence of this assumption will be validated a posteriori when assessing the estimation error dynamics of the proposed methodology. From the enforcement assumption (4.12) on the MPS model (4.8) with the omission of the nonlinear static map, the linear decentralized estimation model follows:

$$\dot{\boldsymbol{x}}_i = \boldsymbol{A}_i \boldsymbol{x}_i + \boldsymbol{b}_d d_{\omega_i} + \boldsymbol{b}_u(u_i + \iota_i), \quad \boldsymbol{x}_i(0) = \boldsymbol{x}_{i0}, \qquad y_i = \boldsymbol{c}_y \boldsymbol{x}_i \tag{4.13a}$$
$$\dot{\iota}_i \approx 0, \quad \iota_i(0) = \iota_{i0}, \quad i = 1, \dots, \mathrm{N} \tag{4.13b}$$

where ι_i is a an unknown exogenous input signal.

In compact notation, the augmented linear decentralized system (4.13) is written as:

$$\dot{\boldsymbol{\chi}}_i = \boldsymbol{\mathcal{A}}_a \boldsymbol{\chi}_i + \boldsymbol{\beta}_d d_{\omega_i} + \boldsymbol{\beta}_u u_i, \qquad i = 1, \dots, \mathrm{N} \tag{4.14a}$$
$$y_i = \boldsymbol{\kappa} \boldsymbol{\chi}_i \tag{4.14b}$$

where

$$\boldsymbol{\mathcal{A}}_a = \begin{bmatrix} 0 & 1 & 0 & 0 \\ 0 & -a_i & -b_i & 0 \\ \alpha_i & -q_i & -c_i & 1 \\ 0 & 0 & 0 & 0 \end{bmatrix}, \quad \boldsymbol{\beta}_d = \begin{bmatrix} \boldsymbol{b}_d \\ 0 \end{bmatrix}, \quad \boldsymbol{\beta}_u = \begin{bmatrix} \boldsymbol{b}_u \\ 0 \end{bmatrix}, \quad \boldsymbol{\kappa} = [1, 0, 0, 0]$$

4.4.4 Observability

Here, the candidate model's robust observability is characterized and expressed as solvability of an instantaneous observability problem, which in turn provides a coordinate change to the model form where estimator convergence coupled with a simple and application-oriented pole placement-based tuning can be executed.

The observability matrix of the state-augmented estimation model (4.14) is given by

$$\boldsymbol{O}_i = \begin{bmatrix} \boldsymbol{\kappa} \\ \boldsymbol{\kappa}\boldsymbol{\mathcal{A}}_a \\ \boldsymbol{\kappa}\boldsymbol{\mathcal{A}}_a^2 \\ \boldsymbol{\kappa}\boldsymbol{\mathcal{A}}_a^3 \end{bmatrix} = \begin{bmatrix} 1 & 0 & 0 & 0 \\ 0 & 1 & 0 & 0 \\ 0 & -a_i & -b_i & 0 \\ -b_i\alpha_i & a_i^2 + b_i q_i & b_i(a_i + c_i) & -b_i \end{bmatrix} \tag{4.15}$$

$$rank\ \boldsymbol{O}_i = 4 \quad det(\boldsymbol{O}_i) \neq_r 0 \quad \Longleftrightarrow \quad b_i = D_i/M_i \neq_r 0, \qquad i = 1, \dots N \tag{4.16}$$

meaning that the matrix pair $(\boldsymbol{\mathcal{A}}_a, \boldsymbol{\kappa})$ is robustly observable because the coefficient b_i which denotes a parameter associated with the inertia constant (M_i) is robustly strictly positive $b_i >_r 0$.

Let us now consider the problem of uniquely-robustly and instantaneously determining at each time t the augmented state $\boldsymbol{\chi}_i(t)$ of the estimation model (4.13) on the basis of the measured output (y_i) and input $(u_i$ and $d_{\omega_i})$ signals as well as their time derivatives (up to adequate order) at time t.

For this aim, perform successive time derivations of the output map of the estimation model (4.14) to draw the four algebraic equation set [84]

$$\boldsymbol{\psi}_i(t) = \boldsymbol{O}_i\boldsymbol{\chi}_i + \boldsymbol{\varrho}_i(t), \quad i = 1, \dots N, \quad \boldsymbol{O}_i : (4.15) \tag{4.17}$$

where

$$\boldsymbol{\psi}_i = \begin{bmatrix} y_i \\ \dot{y}_i \\ \ddot{y}_i \\ \dddot{y}_i \end{bmatrix}, \quad \boldsymbol{\varrho}_i(t) = \boldsymbol{T}_i\boldsymbol{v}_i, \quad \boldsymbol{T}_i = \begin{bmatrix} 0 & 0 & 0 \\ 0 & 0 & 0 \\ 0 & \boldsymbol{\kappa}\boldsymbol{\mathcal{A}}_a\boldsymbol{\beta}_d & 0 \\ \boldsymbol{\kappa}\boldsymbol{\mathcal{A}}_a^2\boldsymbol{\beta}_u & \boldsymbol{\kappa}\boldsymbol{\mathcal{A}}_a^2\boldsymbol{\beta}_d & \boldsymbol{\kappa}\boldsymbol{\mathcal{A}}_a\boldsymbol{\beta}_d \end{bmatrix}, \quad \boldsymbol{v}_i = [u_i, d_{\omega_i}, \dot{d}_{\omega_i}]^\top$$

$\boldsymbol{O}_i$ is the i-th Kalman observability matrix and $\boldsymbol{T}_i$ is the i-th Toeplitz transmission matrix [84] with Markov parameters with respect to $\boldsymbol{v}_i$.

By the observability property (4.16), the preceding algebraic equation has a robust-unique solution

$$\boldsymbol{\chi}_i(t) = \boldsymbol{O}_i^{-1}[\boldsymbol{\psi}_i(t) - \boldsymbol{\varrho}_i(t)] := \boldsymbol{s}_i[\boldsymbol{\psi}_i(t), \boldsymbol{v}_i(t)], \quad i = 1, \ldots, \mathrm{N}, \quad \boldsymbol{O}_i : (4.15) \qquad (4.18)$$

establishing that the linear-decentralized observer model (4.13), with the unmeasured input ι_i as augmented state, is instantaneously observable in the sense that [85, 86]: the state $\boldsymbol{\chi}_i$ at time t is robustly-uniquely determined by the measured output-signal pair and its derivatives (up to order one) at time t. Eq (4.17) is an auxiliary "improper" observer, in the sense that it requires signal derivatives that establish the attainable behavior attainable with any proper observer.

According to the estimation model (4.14): the observability of this augmented state implies the reconstructibility through a suitable dynamic observer (arbitrarily fast, up to model error and noise levels), to be designed in the next subsection, of the unknown augmented state $\iota_i(t)$ of the estimation model (4.13). This key robust observability property in the light of the standard model (2.14) and its realization in ι-parametric form (4.8): (i) means that the (numerical) value for the image signal $\iota_i(t)$ of the state-vector-pair $(\boldsymbol{x}_i, \boldsymbol{d}_i)(t)$ under the nonlinear algebraic map g_i associated with the standard model (2.14) expressed in ι-parametric form (4.8) can be reconstructed, (ii) explains/is in agreement the functioning of the SMPO (4.3) observer as consequence of the Kalman observability-based property (4.15) of the its augmented state model (4.14), where our/the unknown-recosntructible ι_i is called the "fictitious state", and (iii) explains the functioning of the NL EKF because the R observability of the augmented linear system (4.14) implies the fulfillment of the local time-varying stochastic (weighted Grammian) observability condition which is behind of the NL EKF [78], because the Kalman observability of the four-state per machine augmented decentralized linear model (4.14) implies the stochastic observability of the set of three-state per machine nondecentralized standard nonlinear model (4.8).

4.4.5 Nominally Convergent Estimator

Recall the structure of the auxiliary observer (4.17), set the robustly invertible time-varying coordinate change υ

$$\boldsymbol{z}_i(t) = \boldsymbol{O}_i \boldsymbol{\chi}_i(t) + \boldsymbol{\varrho}_i(t), \qquad i = 1, \ldots, \mathrm{N} \qquad (4.19)$$

and apply it to (4.14) get the observer model (4.20) in z-coordinate

$$\dot{\boldsymbol{z}}_i = \boldsymbol{\Gamma}_i \boldsymbol{z}_i + \boldsymbol{\beta}\phi_i(t), \quad \boldsymbol{z}_i(0) = \boldsymbol{z}_{i_0} \quad y_i = \boldsymbol{\kappa}\boldsymbol{z}_i, \quad i = 1, ..., \mathrm{N} \qquad (4.20)$$

where

$$\boldsymbol{\Gamma}_i = \begin{bmatrix} 0 & 1 & 0 & 0 \\ 0 & 0 & 1 & 0 \\ 0 & 0 & 0 & 1 \\ -\gamma_1^i & -\gamma_2^i & -\gamma_3^i & -\gamma_4^i \end{bmatrix}, \quad (\gamma_1^i, \gamma_2^i, \gamma_3^i, \gamma_4^i) = (0, b_i\alpha_i, a_ic_i - b_iq_i, a_i + c_i)$$

$$\phi_i(t) = \boldsymbol{\kappa}\boldsymbol{\mathcal{A}}_a^2\boldsymbol{\beta}_d\dot{d}_{\omega_i} + \boldsymbol{\kappa}\boldsymbol{\mathcal{A}}_a^2\boldsymbol{\beta}_u\dot{u}_i + \boldsymbol{\kappa}\boldsymbol{\mathcal{A}}_a\boldsymbol{\beta}_d\ddot{d}_{\omega_i} = c_i\dot{d}_{\omega_i} - b_i\dot{u}_i + \ddot{d}_{\omega_i}$$

$$\boldsymbol{\beta} = [0, 0, 0, 1]^\top, \qquad \boldsymbol{\kappa} = [1, 0, 0, 0]$$

and, for the moment, the exogenous input $\phi_i(t)$ of (4.20) is assumed to be known, in the understanding that -as we shall see later- the improperness (dependency of measured signal derivatives) in the observer disappears when it is written in original coordinates.

Based on the candidate model (4.20) set the linear-decentralized improper observer in z-coordinates

$$\dot{\hat{\boldsymbol{z}}}_i = \boldsymbol{\Gamma}_i\hat{\boldsymbol{z}}_i + \boldsymbol{\beta}\phi_i(t) + \boldsymbol{k}_i(y_i - \boldsymbol{\kappa}\hat{\boldsymbol{z}}_i), \quad \hat{\boldsymbol{z}}_i(0) = \hat{\boldsymbol{z}}_{i_0}, \quad i = 1, ..., \mathrm{N} \qquad (4.21)$$

with adjustable gain

$$\boldsymbol{k}_i(\zeta_i^o, \varpi_i^o) = [k_1^i, k_2^i, k_3^i, k_4^i]^\top = [4\zeta_i^o\varpi_i^o, (4\zeta_i^{o2} + 2)\varpi_i^{o2}, 4\zeta_i^o\varpi_i^{o3}, \varpi_i^{o4}]^\top \qquad (4.22)$$

To assess nominal convergence with respect to actual MPS (4.13), let us express the actual MPS in z-coordinate

$$\begin{aligned} \dot{\boldsymbol{z}}_i &= \boldsymbol{\Gamma}_i\boldsymbol{z}_i + \boldsymbol{\beta}\{\phi_i(t) - b_iF_i(\boldsymbol{z}, \boldsymbol{d}_\gamma, \dot{\boldsymbol{d}}_\gamma)\}, \quad \boldsymbol{z}_i(0) = \boldsymbol{z}_{i_0} \\ y_i &= \boldsymbol{\kappa}\boldsymbol{z}_i, \qquad i = 1, ..., \mathrm{N} \end{aligned} \qquad (4.23)$$

where

$$F_i(\boldsymbol{z}, \boldsymbol{d}_\gamma, \dot{\boldsymbol{d}}_\gamma) = \{[\partial_{\boldsymbol{x}}\boldsymbol{o}_i(\boldsymbol{x}, \boldsymbol{d}_\gamma)]\boldsymbol{f}(\boldsymbol{x}, \boldsymbol{d}_x) + [\partial_{\boldsymbol{d}_\gamma}\boldsymbol{o}_i(\boldsymbol{x}, \boldsymbol{d}_\gamma)]\dot{\boldsymbol{d}}_\gamma\}_{\boldsymbol{x} = \boldsymbol{O}\boldsymbol{z} + \boldsymbol{M}\boldsymbol{\varrho}}$$

and substract the preceding i-th machine model (4.23) from observer (4.21) to draw the estimation error dynamics

$$\dot{\tilde{\boldsymbol{z}}}_i = \boldsymbol{E}_i\tilde{\boldsymbol{z}}_i + \boldsymbol{\beta}\theta_i(t), \qquad \tilde{\boldsymbol{z}}_i(0) = \tilde{\boldsymbol{z}}_{i_0}, \qquad i = 1, ..., \mathrm{N} \qquad (4.24)$$

where

$$\boldsymbol{E}_i = \boldsymbol{\Gamma}_i - \boldsymbol{k}_o^i\boldsymbol{\kappa}, \qquad |e^{-\boldsymbol{E}_i t}| \le a_i e^{-\lambda_i^o t} \qquad (4.25\mathrm{a})$$

$$\theta_i(t) = F_i(\boldsymbol{z}, \boldsymbol{d}_\gamma, \dot{\boldsymbol{d}}_\gamma), \quad |\theta_i|(t) \le \epsilon_{\theta_i} = l_{\boldsymbol{z}}^{F_i}\epsilon_{\boldsymbol{z}} + l_{\boldsymbol{d}_\gamma}^{F_i}\epsilon_{\boldsymbol{d}_\gamma} + l_{\dot{\boldsymbol{d}}_\gamma}^{F_i}\epsilon_{\dot{\boldsymbol{d}}_\gamma} \qquad (4.25\mathrm{b})$$

with state error motions EU bounded as

$$|\tilde{\boldsymbol{z}}_i(t)| \leq a_i^o e^{-\lambda_i^o t}|\tilde{\boldsymbol{z}}_{i_0}| + (a_i^o/\lambda_i^o)\epsilon_{\theta_i}, \qquad i = 1, ..., \mathrm{N} \tag{4.26}$$

The application to (4.14) of the inverse coordinate change

$$\hat{\boldsymbol{\chi}}_i(t) = \boldsymbol{O}_i^{-1}(\hat{\boldsymbol{z}}_i(t) - \boldsymbol{\varrho}_i(t)), \qquad i = 1, ..., \mathrm{N} \tag{4.27}$$

yields the robustly convergent observer in $\boldsymbol{\chi}_i$-coordinate

$$\dot{\hat{\boldsymbol{\chi}}}_i = \boldsymbol{f}_i(\hat{\boldsymbol{\chi}}_i, \boldsymbol{d}_i) + \boldsymbol{k}_i^o(\zeta_i^o, \varpi_i^o)(y_i - \kappa\hat{\boldsymbol{\chi}}_i), \qquad i = 1, ..., \mathrm{N} \tag{4.28}$$

where

$$\boldsymbol{k}_i^o(\zeta_i^o, \varpi_i^o) = \boldsymbol{O}_i^{-1}\boldsymbol{k}_i(\zeta_i^o, \varpi_i^o) = (k_i^\delta, k_i^\omega, k_i^P, k_i^\iota)^\top(\zeta_i^o, \varpi_i^o)$$
$$k_i^\delta(\zeta_i^o, \varpi_i^o) = 4\zeta_i^o\varpi_i^o, \qquad k_i^\omega(\zeta_i^o, \varpi_i^o) = (4\zeta_i^{o2} + 2)\varpi_i^{o2}$$
$$k_i^P(\zeta_i^o, \varpi_i^o) = -(a_i/b_i)(4\zeta_i^{o2} + 2)\varpi_i^{o2} - (1/b_i)4\zeta_i^o\varpi_i^{o3}$$
$$k_i^\iota(\zeta_i^o, \varpi_i^o) = -\alpha_i 4\zeta_i^o\varpi_i^o + (q_i - ((c_i a_i)/b_i))(4\zeta_i^{o2} + 2)\varpi_i^{o2} - ((c_i + a_i)/b_i)4\zeta_i^o\varpi_i^{o3} - (1/b_i)\varpi_i^{o4}$$

The robustly convergent estimation error of the MPS estimator (4.28) is EU bounded as:

$$|\tilde{\boldsymbol{\chi}}_i(t)| \leq a_i^\chi e^{-\lambda_i^o t}|\tilde{\boldsymbol{\chi}}_{i_0}| + (a_i^\chi/\lambda_i^o)\epsilon_{\theta_i} \tag{4.29}$$

The linear-decentralized observer (4.28) in $(\boldsymbol{x}_i, \iota_i)$ coordinates is given by

$$\dot{\hat{\boldsymbol{x}}}_i = \boldsymbol{A}_i\hat{\boldsymbol{x}}_i + \boldsymbol{b}_d d_{\omega_i} + \boldsymbol{b}_u(u_i + \hat{\iota}_i) + \boldsymbol{k}_i^x(\zeta_i^o, \varpi_i^o)(y_i - \boldsymbol{c}_y\hat{\boldsymbol{x}}_i), \quad \hat{\boldsymbol{x}}_i(0) = \hat{\boldsymbol{x}}_{i0} \tag{4.30a}$$
$$\dot{\hat{\iota}}_i = k_i^\iota(\zeta_i^o, \varpi_i^o)(y_i - \boldsymbol{c}_y\hat{\boldsymbol{x}}_i), \quad \hat{\iota}_i(0) = \iota_{i_0}, \quad i = 1, \dots, \mathrm{N} \tag{4.30b}$$

where
$$\boldsymbol{k}_i^x(\zeta_i^o, \varpi_i^o) = (k_i^\delta, k_i^\omega, k_i^P)^\top(\zeta_i^o, \varpi_i^o), \qquad k_i^\iota = k_i^\iota(\zeta_i^o, \varpi_i^o)$$

The GE estimator (4.28) allows reconstructing the dynamic variables (load angle, relative speed, and electrical power variation) together with the fictitious state of every generator in a decentralized way using the load angle as individual measurement output.

Its detailed form is written as follows:

$$\dot{\hat{\delta}}_i = \hat{\omega}_i + k_i^\delta(\zeta_i^o, \varpi_i^o)(y_i - \hat{\delta}_i), \qquad \hat{\delta}_i(0) = \hat{\delta}_{i_0}, \qquad y_i = \delta_i \tag{4.31a}$$

$$\dot{\hat{\omega}}_i = -a_i\hat{\omega}_i - b_i\hat{P}_i + d_{\omega_i} + k_i^\omega(\zeta_i^o, \varpi_i^o)(y_i - \hat{\delta}_i), \qquad \hat{\omega}_i(0) = \omega_{i_0} \tag{4.31b}$$

$$\dot{\hat{P}}_i = \alpha_i\hat{\delta}_i - q_i\hat{\omega}_i - c_i\hat{P}_i + u_i + \hat{\iota}_i + k_i^P(\zeta_i^o, \varpi_i^o)(y_i - \hat{\delta}_i), \qquad \hat{P}_i(0) = \hat{P}_{i_0} \tag{4.31c}$$

$$\dot{\hat{\iota}}_i = k_i^\iota(\zeta_i^o, \varpi_i^o)(y_i - \hat{\delta}_i), \qquad \hat{\iota}_i(0) = \hat{\iota}_{i_0}, \qquad i = 1, ..., \text{N} \tag{4.31d}$$

The proposed decentralized estimator (4.30) derived following the methodology presented in Section (4.4) allows estimating the dynamic variables (load angle, relative speed, and electrical power variation) of each generator in a decentralized fashion using local information and the load angle as individual measured output. Furthermore, by including a formal convergence analysis of estimation error dynamics (Subsection 4.4.7) in the presence of measurement noise and parasitic dynamics. The proposed methodology can be applied in different power networks (with the same assumptions of Section 4.2), considering more generator units and network connections under distinct scenarios (variations in the mechanical input power, load changes, model errors, unknown disturbances) and the convergence of estimation error is still guaranteed.

4.4.6 Tuning Scheme

The tuning guideline is derived according to the pole placement approach. For this, the natural decentralized characteristic polynomial of $\boldsymbol{A}_i$ is obtained

$$p_i(\lambda) = \lambda^3 + a_1^i\lambda^2 + a_2^i\lambda + a_3^i = (\lambda - \lambda_1^i)(\lambda - \lambda_2^i)(\lambda - \lambda_3^i) = 0$$
$$\lambda_{1,2}^i = -\zeta_i^m\varpi_i^m \pm \left[\varpi_i^m\sqrt{1 - \zeta_i^{m2}}\right]j, \quad \lambda_3^i = -\varpi_i^e \tag{4.32}$$

The characteristic polynomial of $\boldsymbol{E}_i$ (4.25a) is

$$p_i(\lambda) = \lambda^4 + a_1^i\lambda^3 + a_2^i\lambda^2 + a_3^i\lambda + a_4^i = (\lambda - \lambda_1^i)(\lambda - \lambda_2^i)(\lambda - \lambda_3^i)(\lambda - \lambda_4^i) = 0 \tag{4.33}$$

in terms of gains $\boldsymbol{k}_i$ and entries of $\boldsymbol{\Gamma}_i$ is given by

$$p_i(\lambda) = \lambda^4 + (\gamma_4^i + k_1^i)\lambda^3 + (\gamma_3^i + \gamma_4^i k_1^i + k_2^i)\lambda^2 + (\gamma_3^i k_1^i + \gamma_4^i k_2^i + \gamma_2^i + k_3^i)\lambda + (\gamma_2^i k_1^i + \gamma_3^i k_2^i + \gamma_4^i k_3^i + \gamma_1^i + k_4^i) \tag{4.34}$$

Motivated by optimal LQR and EKF as well as GE [87], two complex-conjugate pole pairs give the prescribed pole pattern associated with (4.34) with damping frequency pair

$$\nu_{1,2}^i = -\zeta_i^o\varpi_i^o \pm \left[\varpi_i^o\sqrt{1 - \zeta_i^{o2}}\right]j, \qquad \nu_{3,4}^i = -\zeta_i^o\varpi_i^o \pm \left[\varpi_i^o\sqrt{1 - \zeta_i^{o2}}\right]j \tag{4.35}$$

where

$$\zeta_i^o = n_i^\zeta \zeta_i^m, \qquad \varpi_i^o = n_i^\varpi \varpi_i^m$$

$$n_i^\zeta = n_\zeta \in [1, 6] := \mathcal{J}_\zeta, \qquad n_i^\varpi = n_\varpi \in [10, 50] := \mathcal{J}_\varpi$$

in order to: (i) exploit the natural characteristics of MPS to obtain a better functioning in terms of an adequate compromise between speed reconstruction and tolerance to measurement noise (in the next Subsection), and (ii) have a conventional-like simple, transparent, and easy to apply tuning procedure based on two-parameter tuning.

This tuning procedure is compared favorably concerning: (i) the tuning of NL EKF, which does not have a clear physical meaning, and (ii) the SMPO estimation scheme (4.3) based on the selection of 8 tuning parameters, which are connected via existence-like pole placement theoretical argument for asymptotic injection part and not clear meaning for the nonlinear sliding/saturation part.

4.4.7 Robust Convergence (in the presence of noise and parasitic dynamics)

To ensure robust convergence and a tuning procedure against measurement noise and parametric uncertainty. The actual dynamics of MPS in z-coordinates are considered

$$\dot{\pi} = \varrho(\boldsymbol{z}, \boldsymbol{d}_x; \pi, \upsilon), \qquad \pi(0) = \pi_0 \tag{4.36a}$$

$$\dot{\boldsymbol{z}}_i = \boldsymbol{\Gamma}_i \boldsymbol{z}_i + \boldsymbol{\beta}\{\phi_i(t) - b_i F_i(\boldsymbol{z}, \boldsymbol{d}_\gamma, \dot{\boldsymbol{d}}_\gamma)\}, \quad y_i = \boldsymbol{\kappa} \boldsymbol{z}_i + e_{y_i}(\pi) \qquad \boldsymbol{z}_i(0) = \boldsymbol{z}_{i_0} \tag{4.36b}$$

Subtract (4.21) from (4.36) and obtain the estimation error dynamics:

$$\dot{\pi} = \varrho(\boldsymbol{z}, \boldsymbol{d}_x; \pi, \upsilon), \qquad \pi(0) = \pi_0 \tag{4.37a}$$

$$\dot{\tilde{\boldsymbol{z}}}_i = \mathsf{A}_i \tilde{\boldsymbol{z}}_i + \boldsymbol{\varepsilon}_i(\boldsymbol{z}, \boldsymbol{v}_i, \dot{\boldsymbol{v}}_i, \boldsymbol{d}_\gamma, \dot{\boldsymbol{d}}_\gamma; \tilde{\boldsymbol{z}}, \tilde{\boldsymbol{v}}_i, \dot{\tilde{\boldsymbol{v}}}_i, \tilde{\boldsymbol{d}}_\gamma, \dot{\tilde{\boldsymbol{d}}}_\gamma, \tilde{\boldsymbol{p}}_i, \pi), \qquad \tilde{\boldsymbol{z}}(0) = \tilde{\boldsymbol{z}}_{i_0} \tag{4.37b}$$

where

$$\tilde{\boldsymbol{z}}_i = \hat{\boldsymbol{z}}_i - \boldsymbol{z}_i, \quad \boldsymbol{z}_i = \begin{bmatrix} z_{1i}, z_{2i}, z_{3i}, z_{4i} \end{bmatrix}^\top, \quad \mathsf{A}_i = \begin{bmatrix} -4\zeta_i^o \varpi_i^o & 1 & 0 & 0 \\ -(4\zeta_i^{o2} + 2)\varpi_i^{o2} & 0 & 1 & 0 \\ -4\zeta_i^o \varpi_i^{o3} & 0 & 0 & 1 \\ -\varpi_i^{o4} & -\gamma_2^i & -\gamma_3^i & -\gamma_4^i \end{bmatrix} \tag{4.38a}$$

$$|e^{\mathsf{A}_i t}| \le a_{e_i} e^{-\lambda_{s_i} t}, \quad \lambda_{s_i} = \zeta_i^o \varpi_i^o, \qquad \{\boldsymbol{\varepsilon}_i\} : (A.0.3a) \tag{4.38b}$$

System (4.37) is made by two subsystems interconnected via Lipschitz bounded map (ε_i).

From the application of Lyapunov's converse theorem, the estimation errors of

(4.37b) are bounded as

$$|\tilde{\mathbf{z}}_i| \leq a_{e_i}|\tilde{\mathbf{z}}_{i_0}|e^{-\zeta_i^o\varpi_i^o(t-t_0)} + a_{e_i}\int_{t_0}^t e^{-\zeta_i^o\varpi_i^o}|\boldsymbol{\varepsilon}_i(\boldsymbol{z},\boldsymbol{v}_i,\dot{\boldsymbol{v}}_i,\boldsymbol{d}_\gamma,\dot{\boldsymbol{d}}_\gamma;\tilde{\boldsymbol{z}},\tilde{\boldsymbol{v}}_i,\dot{\tilde{\boldsymbol{v}}}_i,\tilde{\boldsymbol{d}}_\gamma,\dot{\tilde{\boldsymbol{d}}}_\gamma,\tilde{\boldsymbol{p}}_i,\pi)|d\tau \tag{4.39}$$

considering, $|\tilde{\mathbf{p}}_i| \leq \varepsilon_{\mathbf{p}_i}$ yields,

$$\begin{aligned}
|\tilde{\mathbf{z}}_i| \leq &a_{e_i}|\tilde{\mathbf{z}}_{i_0}|e^{-\zeta_i^o\varpi_i^o(t-t_0)} + a_{e_i}l_i^{\varepsilon_i}\int_{t_0}^t e^{-\zeta_i^o\varpi_i^o(t-\tau)}|\tilde{\mathbf{z}}_i| \\
&+ a_{e_i}\int_{t_0}^t e^{-\zeta_i^o\varpi_i^o(t-\tau)}[l_{\mathbf{z}}^{\varepsilon_i}|\tilde{\mathbf{z}}| + l_\pi^{\varepsilon_i}|\pi| + l_{\boldsymbol{v}_i}^{\varepsilon_i}|\tilde{\boldsymbol{v}}_i| + l_{\dot{\boldsymbol{v}}_i}^{\varepsilon_i}|\dot{\tilde{\boldsymbol{v}}}_i| + l_{\boldsymbol{d}_\gamma}^{\varepsilon_i}|\tilde{\boldsymbol{d}}_\gamma| + l_{\dot{\boldsymbol{d}}_\gamma}^{\varepsilon_i}|\dot{\tilde{\boldsymbol{d}}}_\gamma| + l_{\boldsymbol{p}_i}^{\varepsilon_i}\varepsilon_{\boldsymbol{p}_i}]d\tau
\end{aligned} \tag{4.40}$$

where $l_a^{\varepsilon_i}$ is the Lipschitz constant of $\boldsymbol{\varepsilon}_i$ with respect to its argument a.

The application to this inequality of Gronwall's generalized lemma followed by integration by parts, and obtain the associated decay factor l_{ψ_i}, the estimation errors (4.40) are rewritten as:

$$\begin{aligned}
|\tilde{\mathbf{z}}_i| \leq a_{e_i}|\tilde{\mathbf{z}}_{i_0}|e^{-l_i(t-t_0)} + \frac{a_{e_i}l_{\mathbf{z}}^{\varepsilon_i}}{l_i}|\tilde{\boldsymbol{z}}| + \frac{a_{e_i}l_\pi^{\varepsilon_i}}{l_i}|\pi| + \frac{a_{e_i}l_{\boldsymbol{v}_i}^{\varepsilon_i}}{l_i}|\tilde{\boldsymbol{v}}_i| + \frac{a_{e_i}l_{\dot{\boldsymbol{v}}_i}^{\varepsilon_i}}{l_i}|\dot{\tilde{\boldsymbol{v}}}_i| + \frac{a_{e_i}l_{\boldsymbol{d}_\gamma}^{\varepsilon_i}}{l_i}|\tilde{\boldsymbol{d}}_\gamma| \\
+ \frac{a_{e_i}l_{\dot{\boldsymbol{d}}_\gamma}^{\varepsilon_i}}{l_i}|\dot{\tilde{\boldsymbol{d}}}_\gamma| + \frac{a_{e_i}l_{\boldsymbol{p}_i}^{\varepsilon_i}}{l_i}\varepsilon_{\boldsymbol{p}_i}
\end{aligned} \tag{4.41}$$

where

$$l_i = \zeta_i^o\varpi_i^o - a_{e_i}l_{\mathbf{z}_i}^{\varepsilon_i} \tag{4.42}$$

The norm of parasitic and estimation errors dynamics associated with the i-th (4.37) generator are replaced by its upper bound $(|\pi_i|,|\tilde{\boldsymbol{z}}_i|)(t) \leq (\sigma_{\pi_i},\sigma_{z_i})(t)$ [72, 87]:

$$\dot{\sigma}_\pi(t) = -l_\pi^\varrho\sigma_\pi + a_\pi l_\upsilon^\varrho\epsilon_\upsilon(t), \qquad \sigma_\pi(0) = \sigma_{\pi_0} \tag{4.43a}$$

$$\dot{\sigma}_{z_i}(t) = -l_i\sigma_{z_i} + a_{e_i}l_\pi^{\varepsilon_i}\sigma_\pi + a_{e_i}[l_{\mathbf{z}}^{\varepsilon_i}\epsilon_{\mathbf{z}}(t) + l_{\boldsymbol{d}_\gamma}^{\varepsilon_i}\epsilon_{\boldsymbol{d}_\gamma}(t) + l_{\dot{\boldsymbol{d}}_\gamma}^{\varepsilon_i}\epsilon_{\dot{\boldsymbol{d}}_\gamma}(t) + l_{\boldsymbol{v}_i}^{\varepsilon_i}\epsilon_{\boldsymbol{v}_i}(t) + l_{\dot{\boldsymbol{v}}_i}^{\varepsilon_i}\epsilon_{\dot{\boldsymbol{v}}_i}(t)$$

$$+ l_{\boldsymbol{p}_i}^{\varepsilon_i}\epsilon_{\boldsymbol{p}_i}], \quad \sigma_{z_i}(0) = \sigma_{z_{i_0}} \tag{4.43b}$$

where

$$l_\pi^\varrho > 0, \qquad l_i = \zeta_i^o\varpi_i^o - a_{e_i}l_{\mathbf{z}_i}^{\varepsilon_i} > 0 \tag{4.44}$$

(4.44) reflects the individual R stability of the parasitic (4.37a), and estimation error dynamics (4.37b) of the i-th generator. In vector form, the preceding bounding linear

system (4.43) is written as:

$$\dot{\boldsymbol{\sigma}}_a(t) = \mathcal{A}_a \boldsymbol{\sigma}_a + \boldsymbol{d}_{\sigma_a}(t), \qquad \sigma_a(0) = \sigma_{a_0} \tag{4.45}$$

where

$$\sigma_a = [\sigma_\pi, \sigma_{z_i}]^\top, \qquad \mathcal{A}_a = \begin{bmatrix} -l_\pi^\varrho & 0 \\ a_{e_i} l_\pi^{\varepsilon_i} & -l_i \end{bmatrix} \tag{4.46a}$$

$$\boldsymbol{d}_a(t) = \begin{bmatrix} a_\pi l_\upsilon^\varrho \epsilon_\upsilon(t) \\ a_{e_i}(l_{\boldsymbol{z}}^{\varepsilon_i} \epsilon_{\boldsymbol{z}}(t) + l_{\boldsymbol{d}_\gamma}^{\varepsilon_i} \epsilon_{\boldsymbol{d}_\gamma}(t) + l_{\dot{\boldsymbol{d}}_\gamma}^{\varepsilon_i} \epsilon_{\dot{\boldsymbol{d}}_\gamma}(t) + l_{\boldsymbol{v}_i}^{\varepsilon_i} \epsilon_{\boldsymbol{v}_i}(t) + l_{\dot{\boldsymbol{v}}_i}^{\varepsilon_i} \epsilon_{\dot{\boldsymbol{v}}_i}(t) + l_{\boldsymbol{p}_i}^{\varepsilon_i} \epsilon_{\boldsymbol{p}_i}) \end{bmatrix} \tag{4.46b}$$

based on the small gain theorem [83] conditions for the robust functioning of the system (4.45) and by Hurwitz Criterion: the system (4.45) is by construction RE stable according to

$$\begin{aligned} det(\mathcal{A}_a) &> 0 \\ l_\pi^\varrho l_i &> 0, \quad \Rightarrow \quad |e^{\mathcal{A}_a t}| \le a e^{-l_i t}, \quad l_i >_r 0 \end{aligned} \tag{4.47}$$

system (4.45) is RE stable if ϖ_i^o is set so that

$$\zeta_i^o \varpi_i^o > \lambda_{d_i}(\varpi_i^o, \varpi_i^{o2}) \tag{4.48}$$

where

$$\lambda_{d_i}(\varpi_i^o, \varpi_i^{o2}) := a_{e_i} l_{\boldsymbol{z}_i}^{\varepsilon_i}(\varpi_i^o, \varpi_i^{o2}) \tag{4.49}$$

Proposition 1. The GE error dynamics (4.37) are RE stable if the stabilizing term λ_{s_i} dominates the potentially destabilizing one λ_{d_i}, this is (see Fig. 4.1)[88]

$$\lambda_{s_i}(\varpi_i^o, \zeta_i^o) - \lambda_{d_i}(\varpi_i^o, \varpi_i^{o2}) := \lambda(\varpi_i^o, \varpi_i^{o2}) > 0 \tag{4.50}$$

where

$$\lambda_{s_i}(\zeta_i^o, \varpi_i^o) = \zeta_i^o \varpi_i^o \tag{4.51a}$$

$$\lambda_{d_i}(\varpi_i^o, \varpi_i^{o2}) = a_{e_i} l_{\boldsymbol{z}_i}^{\varepsilon_i}(\varpi_i^o, \varpi_i^{o2}) \tag{4.51b}$$

$l_{\boldsymbol{z}_i}^{\varepsilon_i}$ is a nonlocal Lipschitz constant and a_{e_i} is an strictly positive constant.

Condition (4.50) states that the linear-in-ϖ_i^o stabilizing term λ_{s_i} dominates the potentially destabilizing term λ_{s_i} (that grows linearly and quadratically with ϖ_i^o).

In the next proposition, the preceding convergence condition is stated in terms of low (ϖ_i^{o-}) and high (ϖ_i^{o+}) gain limits:

(*i*) Eq. (4.50) has two strictly positive and sufficiently separated roots ($\varpi_i^{o-}, \varpi_i^{o+}$)

for ϖ_i^o

$$\varpi_{L_i}^o = \varpi_i^{o-}(\varpi_i^o, \varpi_i^{o2}) \qquad \varpi_{H_i} = \varpi_i^{o+}(\varpi_i^o, \varpi_i^{o2}), \qquad 0 < \varpi_{L_i}^o < \varpi_{H_i}^o \qquad (4.52)$$

(ii) **Proposition 2.** The system (4.36) is RE stable if ϖ_i^o is set sufficiently above (or below) its lower (or upper) limit ϖ_i^{o-} (or ϖ_i^{o+}), according to the expressions:

$$\varpi_i^{o-}(\varpi_i^o, \varpi_i^{o2}) < \varpi_i^o < \varpi_i^{o+}(\varpi_i^o, \varpi_i^{o2}) \qquad (4.53)$$

In industrial practice, the upper bound ϖ_i^{o+} (4.53) is called ultimate gain (where inadmissible oscillatory behavior by error-noise propagation starts with ϖ_i^o increase) [89].
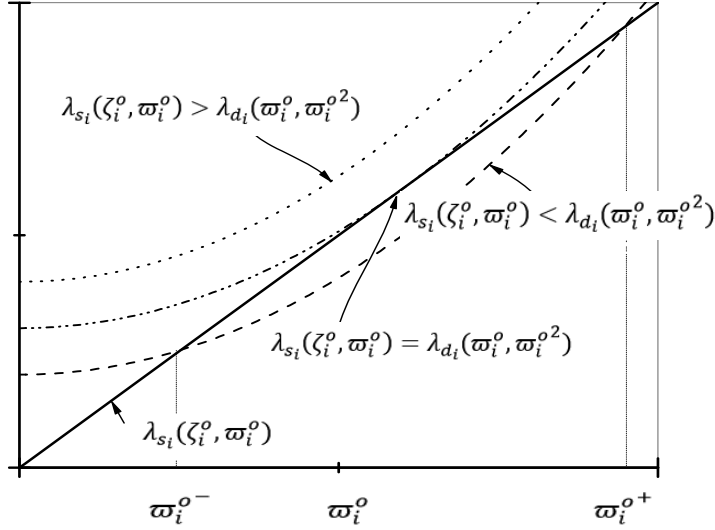
Figure 4.1: (a) GE condition (4.50) fulfillment (—-), non-fulfillment (....), and threshold case (–..–..)

4.4.8 Tuning Procedure (in the light of R convergence with noise and upper limit identification)

From **Proposition 2** in the light of the prescribed linear, non-interactive, pole assignable ($LNPA$) output error dynamical feature, the next conventional-like linear-filter tuning guidelines follows [88]:

1. Estimate the output natural frequency λ_i of each machine, and set the output error responses from 10 to 50 times faster than the dominant dynamics: $\varpi_i^o = n_\varpi \lambda_i$ with $n_\varpi \approx 10 - 50 \in \mathcal{J}_\varpi$.

2. Gradually increase n_w until the response becomes oscillatory at the ultimate value n_w^+, back off and set $n_w = n_w^+/(2\text{--}3)$ and set the damping factor $\zeta_i^o = n_i^\zeta \zeta_i^m$ with $n_\zeta \in [1,6] := \mathcal{J}_\zeta$.

3. Start with

$$n_\zeta = 4 \in \mathcal{J}_\zeta, \quad n_\varpi = 10 \in \mathcal{J}_\varpi$$

4.4.9 GE-EKF equivalence

For this, the EKF approach suggests the following decentralized stochastic model of MPS with augmented state

$$\dot{\boldsymbol{\chi}}_i = \boldsymbol{f}_i(\boldsymbol{\chi}_i, \boldsymbol{d}_i(t)) + \boldsymbol{B}_i(\boldsymbol{\chi}_i, t)\boldsymbol{\mu}_i(t), \quad \boldsymbol{\chi}_i(0) = \boldsymbol{\chi}_{i0} \tag{4.54a}$$

$$\dot{\boldsymbol{\mu}}_i = \boldsymbol{w}_i(t), \quad \boldsymbol{\mu}_i(0) = \boldsymbol{\mu}_{i_0} \quad y_i = \boldsymbol{\kappa}\boldsymbol{\chi}_i + v_i \tag{4.54b}$$

where

$$\boldsymbol{f}_i(\boldsymbol{\chi}_i, \boldsymbol{d}_i(t)) = \boldsymbol{\mathcal{A}}_a\boldsymbol{\chi}_i + \boldsymbol{\beta}_d d_{\omega_i} + \boldsymbol{\beta}_u u_i, \quad \boldsymbol{d}_i = \begin{bmatrix} d_{\omega_i} \\ u_i \end{bmatrix}$$

with

$$\boldsymbol{w}_i \sim N[\boldsymbol{0}, \boldsymbol{q}_i], \quad v_i \sim N[0, r_i], \quad \boldsymbol{\chi}_{i_0} \sim N[\hat{\boldsymbol{\chi}}_{i_0}, \boldsymbol{P}_{\chi 0}] \tag{4.55a}$$

$$\mu_{i_0} \sim N[\hat{\mu}_{i_0}, \boldsymbol{P}_{\mu_0}], \quad \{\boldsymbol{B}_i, \boldsymbol{q}_i, r_i, \boldsymbol{P}_{i_0}\} := \boldsymbol{M}_i \tag{4.55b}$$

the i-th augmented state, one per machine, $\boldsymbol{\mu}_i$ is an integrated white noise (Wiener process), $\boldsymbol{B}_i$ is an adjustable (to be chosen appropriately) nonlinear gain matrix that sets the model noise injection mechanism, $\boldsymbol{w}_i$ (or v_i) is a zero-mean Gaussian white noise with constant intensity matrix $\boldsymbol{q}_i$ (or r_i), and $\boldsymbol{\chi}_{i_0}$ (or μ_{i_0}) is a random vector with mean $\hat{\boldsymbol{\chi}}_{i_0}$ (or $\hat{\mu}_{i_0}$) and error covariance matrix $\boldsymbol{P}_{\chi 0}$ (or $\boldsymbol{P}_{\mu_0}$). Differently from the EKF approach (with constant matrix $\boldsymbol{B}_i$ equal to the identity) employed in the majority of MPS estimation studies [3, 32, 34, 42], here the fictitious state of the SMPO observer design is incorporated and the noise coefficient matrix is a design degree of freedom. In compact form, the stochastic model (4.54) is written as:

$$\dot{\boldsymbol{x}}_a = \boldsymbol{f}_a(\boldsymbol{x}_a, t) + \boldsymbol{B}_a(\boldsymbol{x}_a, t)\boldsymbol{w}_i(t), \quad \boldsymbol{x}_a(0) = \boldsymbol{x}_{a_0}$$
$$y_i = \boldsymbol{\kappa}\boldsymbol{x}_a + v_i \tag{4.56}$$

where

$$\boldsymbol{f}_a(\boldsymbol{x}_a, t) = \begin{bmatrix} \boldsymbol{f}_i(\boldsymbol{\chi}_i, \boldsymbol{d}_i) + \boldsymbol{B}_i(\boldsymbol{\chi}_i, t)\mu_i \\ 0 \end{bmatrix}, \quad \boldsymbol{x}_a = [\boldsymbol{\chi}_i, \mu_i]^\top, \quad \boldsymbol{B}_a = \begin{bmatrix} 0 \\ \boldsymbol{I} \end{bmatrix} \tag{4.57}$$

Assuming the augmented model motion $\boldsymbol{x}_a(t)$ is stochastically observable (with

respect to y_i) [78], the associated EKF is given by

$$\dot{\hat{x}}_a = f_a(\hat{x}_a, t) + g_{ekf}(P_i, r_i)(y_i - \kappa\hat{x}_a), \quad g_{ekf} = P_i\kappa^\top r_i^{-1}$$
$$\hat{x}_a(0) = \hat{x}_{a_0} \tag{4.58a}$$
$$\dot{P}_i = P_i J_a(\hat{x}_a, t) + J_a^\top(\hat{x}_a, t)P_i + B_a q_i B_a^\top - P_i\kappa_a^\top r_i^{-1}\kappa P_i,$$
$$P_i(0) = P_{i_0} \tag{4.58b}$$

where

$$J_a(\hat{x}_a, t) = \partial_{x_a} f_a(x_a, t) = \begin{bmatrix} \partial_{\chi_i} f_i(\chi_i, d_i) & B_i(\chi_i, t) \\ 0 & 0 \end{bmatrix} \tag{4.59}$$

dim $x_a = 4$, dim g_{ekf}=4×1; dim $y_i = 1$; dim $\kappa = 1 \times 4$; dim $P_i = $ dim $J_a(\hat{x}_a, t) = 4 \times 4$

The conditions for the equivalence between the GE (4.28) and the EKF (4.58) are given in terms of the choices of: (i) the pole placement-based tuning scheme of the GE (4.28) and (ii) the tuning matrix quartet M_i (4.55b) of the EKF (4.58).

Lemma 1. The GE (4.28) and the EKF (4.58) yield the same state estimate if and only if:

(i) The gain vector k_i^o of the GE (4.28) is set with a Butterworth pole configuration [88], and the ith 5-th output error derivative $(\hat{y}_i - y_i)^{(5)}$ is modeled as a zero-mean uncorrelated white noise w_i with intensity q_i, according to the expressions

$$(\hat{y}_i - y_i)^{(5)} = w_i \sim N[\mathbf{0}, q_i], \quad i = 1, \dots, N \tag{4.60}$$

(ii) For GE-EKF connection purposes, the flattening nonlinear coordinate change related to the robust observability property takes the EKF dynamic Riccati equation (RE) (4.58b) into the static RE (4.61)

$$\Gamma_i\Sigma_i + \Sigma_i\Gamma_i^\top + \pi_i q_i\pi_i^\top - \Sigma_i\Delta_i^\top r_i^{-1}\Delta_i\Sigma_i = 0 \tag{4.61}$$

where
$$\Gamma_i = \begin{bmatrix} 0 & 1 & 0 & 0 \\ 0 & 0 & 1 & 0 \\ 0 & 0 & 0 & 1 \\ 0 & 0 & 0 & 0 \end{bmatrix}, \quad \pi_i = \begin{bmatrix} 0 \\ 0 \\ 0 \\ 1 \end{bmatrix} \quad \Delta_i = [1, 0, 0, 0]$$

Σ_i is the solution of the static matrix Riccati equation (RE) and the matrix quartet M_i (4.55b) of the EKF (4.58) is set as follow

$$B_i = [O_i^{-1}]\pi_y, \quad q_i = q_i I_{4\times4}, \quad q_i = (\varpi_i^o)^{10} r_i \tag{4.62a}$$

$$\boldsymbol{\pi}_y = [0, 0, 0, 1]^\top, \quad \boldsymbol{P}_{i_0} = [\boldsymbol{O}_i^{-1}][\boldsymbol{\Sigma}_i][\boldsymbol{O}_i^{-1}]^\top \tag{4.62b}$$

The EKF (4.58) and (4.62) with dynamic Riccati equations (REs) is identical to the GE (4.28) without REs. Particularly, the solution of the static RE (4.61) via Butterworth pole-placement yields the optimal stationary gain $\mathbf{k}_i$ (4.63) which in original coordinates sets the gain $\boldsymbol{g}_{ekf}$ of EKF (4.58) and (4.62) [87].

$$\mathbf{k}_i = \boldsymbol{\Sigma}_i \boldsymbol{\Delta}_i^\top r_i^{-1} \tag{4.63}$$

4.4.10 Epilogue

According to theoretical ideas and developments and the robust functioning assessment of the proposed methodology, in terms of a suitable compromise between construction-tuning simplicity and systematicity, robustness (reliability), reconstruction speed, and on-line computational load. The NL GE estimator: (i) retains the acceptance and robust functioning in the presence of model parameter and measurement noise errors of the NL EKF and resolves the heavy on-line computational load and problematic heuristic tuning coupled with formal convergence analysis on RE-IS sense based on small gain theorem for coupled nonlinear systems and identification of NL observability property, and (ii) retains the robustness of SMPO against to the combined effect of unmeasured disturbances and state dependency on other machines as well as its comparatively low computational load, and the integral action achieves effectively and in a more straightforward manner (fewer tuning parameters) than the one of the SM with perturbation estimation scheme (4.3).

In Subsection 4.4.9, the proposed GE (4.28) for MPS was formally connected with the standard NL EKF approach employed in previous MPS estimation studies.

4.5 Simulation Results

In this section, the simulation results corroborate and illustrate the theoretical developments of Sections 4.3 and 4.4 with realistic testing using the popular Western System Coordinating Council (WSCC) [12] previously used in MPSs studies [32, 40, 55, 68, 75–77], which is shown in Fig.4.2.

Parameters	Generator 1	Generator 2	Generator 3
D_i [p.u.], T'_{d_i} [s]	6, 8.96	5, 6	2, 5.89
M_i [s]	2×23.1	2×6.1	2×3.01
x'_{d_i} [p.u.] , x_{d_i} [p.u.]	0.0608, 0.146	0.1198, 0.8958	0.1813, 1.3125
Field voltage E_{f_i} [p.u.]	1.056	1.789	1.403
Mechanical input power P_{m_i} [p.u.]	0.716	1.63	0.85

Table 4.1: Machine data

The system's nominal parameters and the operations used for the sample problem investigated are listed in Table 4.1. For evaluation purposes, the MPS from Fig. 4.2, the loads are assumed to be of the constant impedance type. Thus, the generators are connected through a reduced network which is also assumed as purely inductive and whose admittance matrix is computed from line parameters showed in Fig. 4.2.

The comparison between the proposed (4.28) and SMPO (4.3) observers has been already discussed in the theoretical developments: (i) the tuning of the proposed observer -underlain by robust convergence conditions- is considerably simpler, and (ii) in the presence of measurement noise, the SMPO observer (4.3) undergoes inadmissible behavior degradation -of chattering type- by measurement noise. Thus, the behavior of the proposed GE (4.21) in the present of realistic measurement noise will be compared with the standard-centralized NL EKF (4.1b)-(4.1c).
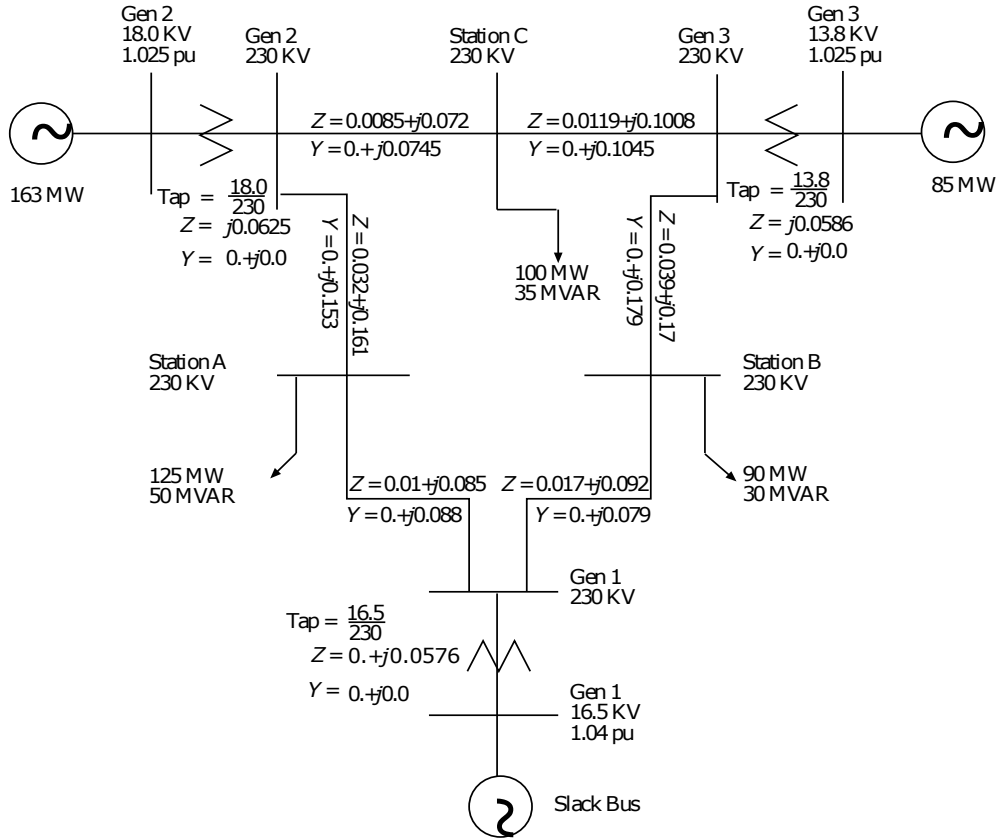
Figure 4.2: WSCC 3-machine, 9-bus system [12]

4.5.1 Tuning

For MPS of Fig. 4.2, the three GE estimators (one per generator unit) follow:

$$\lambda_1 = 1/15seg^{-1}, \qquad \lambda_2 = 1/20seg^{-1}, \qquad \lambda_3 = 1/20seg^{-1}$$

where $\lambda_{1,2,3}$ are the dominant frequencies associated with each machine. The adjustable vector $\boldsymbol{k}_i$ (4.22) of the proposed GE (4.21) is set according to the tuning procedure of Subsection 4.4.8. For each GE estimator there are two complex-conjugate pole pairs (4.35) with damping frequency pair: ϖ_i^o is set with $n_\varpi \approx 10$ times faster than the dominant frequency λ_i and the damping factor ζ_i^o is set as $n_\zeta \approx 4$ with respect to the natural damping factor of MPS dynamics.

For the centralized version of the traditional EKF (4.1b)-(4.1c), the covariance matrices $\boldsymbol{Q}, \boldsymbol{R}$ are

$$\boldsymbol{R} = bd(r_1, r_2, r_3), \quad r_1 = 1 \times 10^{-4}, \quad r_2 = 1 \times 10^{-3}, \quad r_3 = 1 \times 10^{-5}$$

$$\boldsymbol{Q} = bd(\boldsymbol{q}_1, \boldsymbol{q}_2, \boldsymbol{q}_3), \quad \boldsymbol{q}_1 = [1 \times 10^{-5}]\boldsymbol{I}_{3\times3} \quad \boldsymbol{q}_2 = [1 \times 10^{-6}]\boldsymbol{I}_{3\times3} \quad \boldsymbol{q}_3 = [1 \times 10^{-6}]\boldsymbol{I}_{3\times3}$$

4.5.2 Robust Testing Scheme

The measured outputs are corrupted with noise which is represented by high-frequency sine signals:

$$y_1 = \delta_1 + 0.0002\sin(250t), \quad y_2 = \delta_2 + 0.0002\sin(350t), \quad y_3 = \delta_3 + 0.0001\sin(400t)$$

Moreover, to evaluate the transient performance of both estimators, different initial conditions (with respect to operation points) have been intentionally considered for the actual MPS model and both estimators, as presented in [42, 68]. The initial transient dynamic response associated with the MPS can be related to the one obtained when the electrical power network considers loads and distributed energy resources with prominent stochastic behaviors [5]. In this way, in the first instance, the convergence of the proposed decentralized estimator is demonstrated against initial condition uncertainties (for comparative purposes, both estimators are not initiated with the same conditions of MPS dynamics). It is a critical advantage compared to the traditional dynamic estimators, usually based on the Kalman filter theory. As stated in [5], if these estimation schemes are not initiated correctly, the estimation error convergence is not guaranteed. An estimator should estimate the actual states even if it is not initiated with the same conditions of the system [82].

Furthermore, in the present comparative study, once the generators are in the steady-state regime, the dynamic state algorithms are tested under a persistent disturbance acting on the rotating shaft of the generator one at t=30 [s] (assumed as a known input for both estimators) and an electromagnetism disturbance entering the excitation winding of the generator three at t=40 [s] (considered as an unknown input for both estimators), both disturbances are modeled as step signals acting 0.5 seconds. Figures 4.3 - 4.8 depicts the performance of estimators, in solid lines, are represented the actual values of the load angle, relative speed, the electric power variation, and the nonlinear interconnection term of every generator unit; on the other hand, the
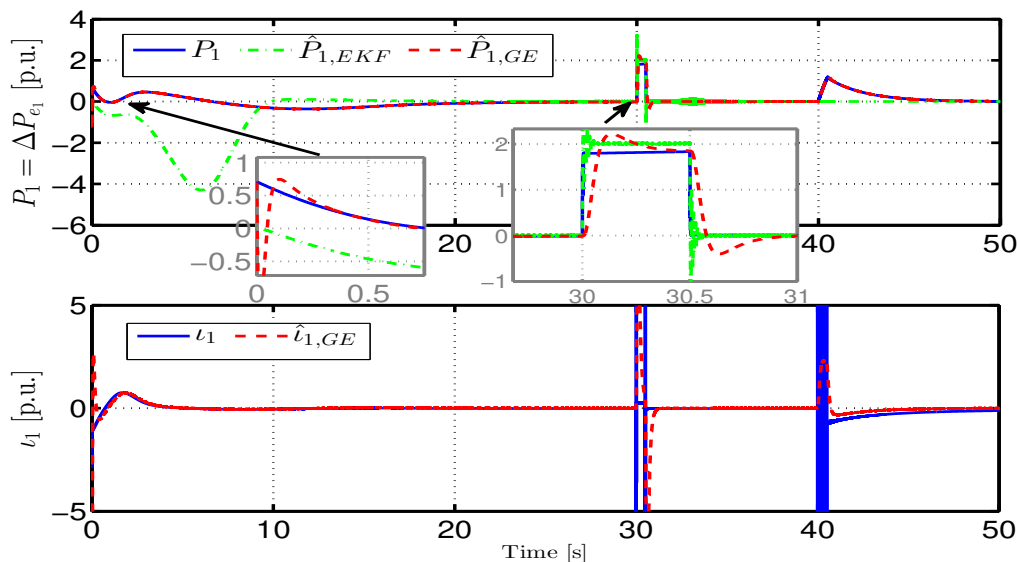
dashed lines are used to show the estimated variables by both the EKF (green) and the proposed GE estimator (red).
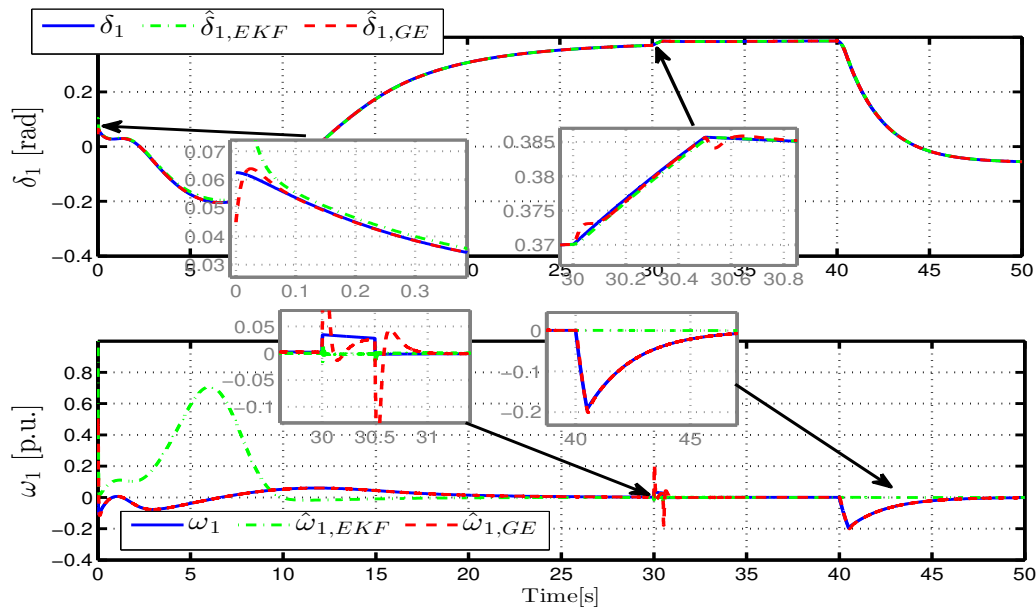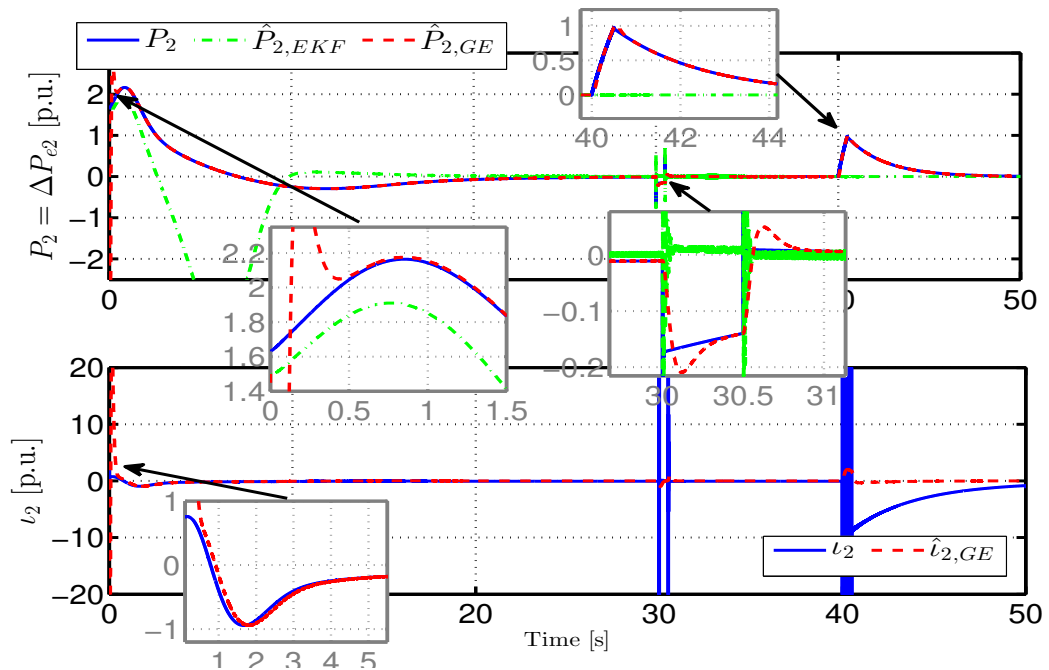

Figure 4.3: Comparison between the GE estimator and the conventional EKF. Load angle and relative speed of generator one.

Figure 4.4: Comparison between the GE estimator and the conventional EKF. The electrical power variation and the nonlinear interconnection term of generator one.
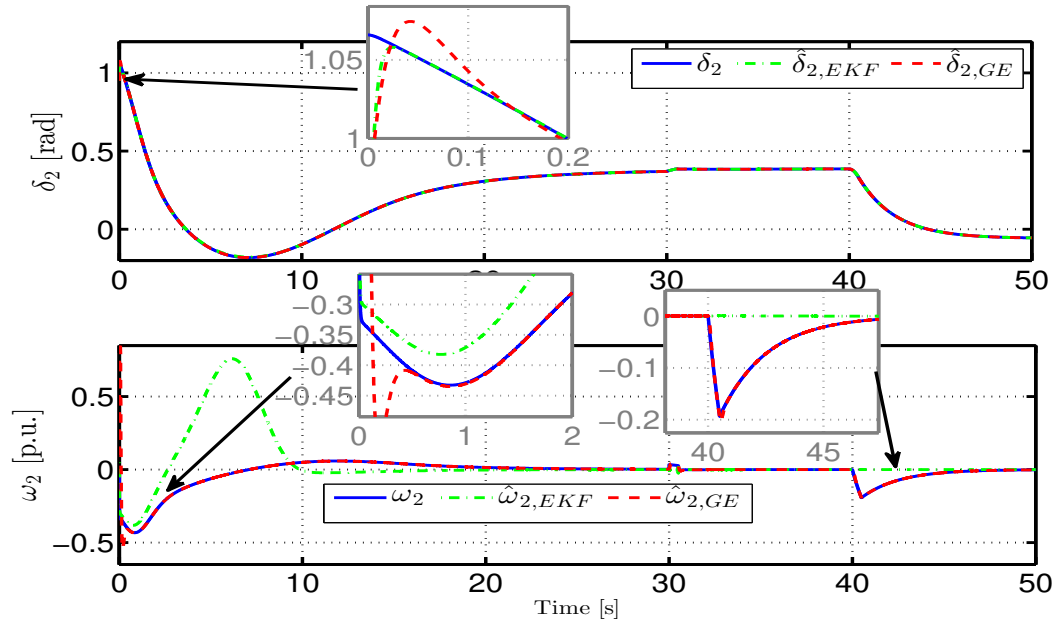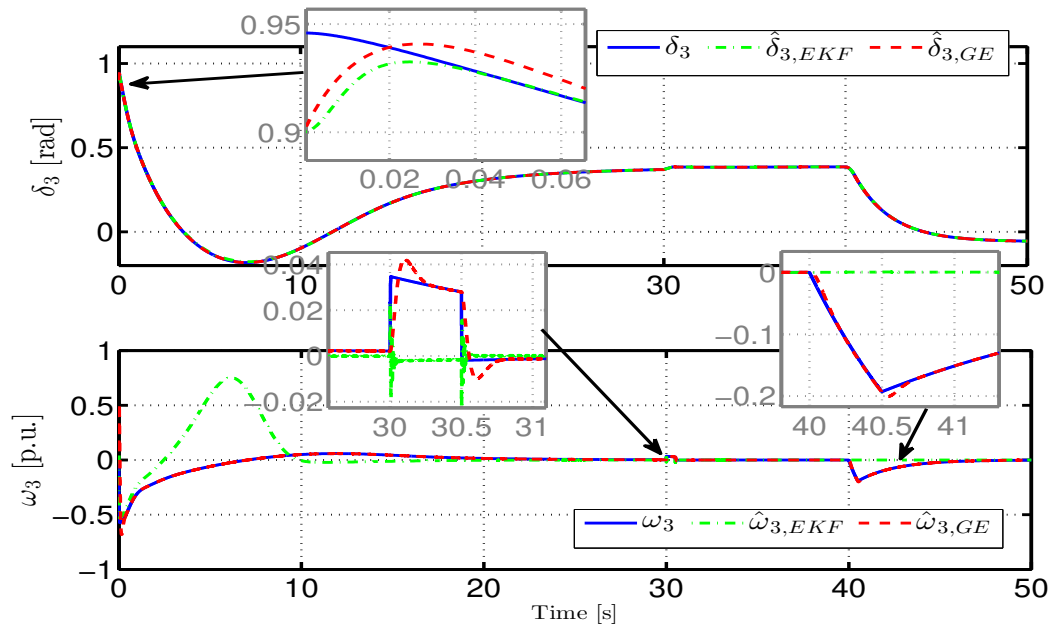
Figure 4.5: Comparison between the GE estimator and the conventional EKF. Load angle and relative speed of generator two.
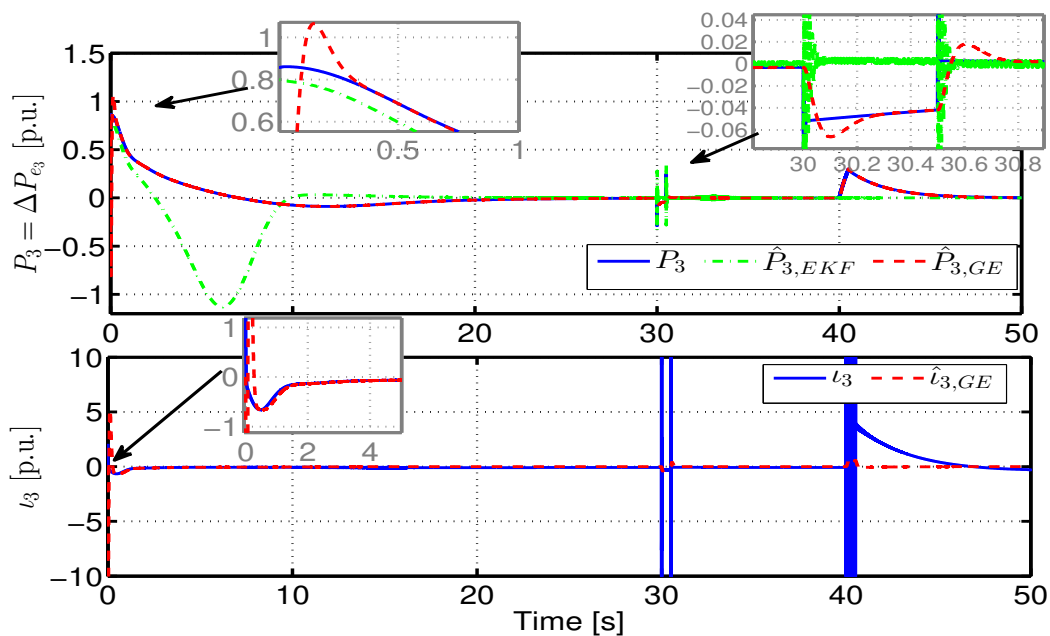

Figure 4.6: Comparison between the GE estimator and the conventional EKF. The electrical power variation and the nonlinear interconnection term of generator two.

Figure 4.7: Comparison between the GE estimator and the conventional EKF. Load
angle and relative speed of generator three.

Figure 4.8: Comparison between the GE estimator and the conventional EKF. The
electrical power variation and the nonlinear interconnection term of generator three.

As can be appreciated, the convergence associated with the proposed GE is considerably faster than the one obtained by the conventional EKF in its centralized version. The transient behavior related to the MPS operation is recovered by the developed GE estimator, an essential strength for monitoring and control purposes. In the opposite case, the EKF cannot assure the reconstruction of the transient behaviors of the generators showing a slow convergence rate to the actual states. Also, specifically for the disturbance that affects generator three at t=40 [s], which also disturbs the behavior of the other two generators. As mentioned above, it is assumed as an unknown exogenous input for both estimators. The EKF performance is not good, recovering this transient behavior. In the opposite case, the proposed GE can estimate the dynamic variables of each generator correctly because the unknown disturbance is included in the nonlinear interconnection term (one per machine), which is reconstructed together with the dynamic variables. It can deal with the unmodeled system dynamics.

Remarks:

R- 4.1 It is necessary to point out that, for the system in the example (Fig. 4.2), the EKF needs to solve 54 ODEs (considering 45 Riccati equations), whereas the GE estimator only solves 12 ODEs.

R- 4.2 The proposed GE estimator only needs local information to achieve its task using load angle as the unique measurement. In contrast, the EKF needs local and neighborhood information. It requires the measurement of the load angle together with the unmeasured vector inputs $\mathbf{w} = [I_{d_i}, E'_{q_i}, E'_{q_j}, \dot{E}'_{q_j}, Q_{e_i}]^\top$ to estimate the state in each machine, in a practical sense, means the use of more sensors.

R- 4.3 The difference among estimators lies in the simplicity of implementation, construction, and computational load of the proposed GE estimator. This estimation scheme is easy to construct and syntonize, presenting a good convergence speed to the actual states.

R- 4.4 In comparison with the centralized approach reported in [68] based on the SM theory, the proposed methodology in this thesis requires fewer measurements to estimate the relative speed together with the electrical power variation whose estimation is only based on the load angle as measured output, thus reducing the number of required sensors. In [68] despite representing the interconnection terms and uncertainties by nonlinear functions of the state, the estimation scheme does not have a systematic construction and requires more local and neighboring information about generators to reconstruct the state.

Table 4.2 are cited some similar state estimation schemes to highlight some critical aspects as construction, convergence proof, and tuning guideline.

Technique	Construction, Tuning & Convergence	Pros & Cons
EKF [31–34, 40, 41]	○ Easy to construct, widely known, and accepted. ○ Without formal convergence analysis.	○ The EKF has not been reached industrial testing, perhaps because of heavy online computational load (especially for control), and it does have a fine and precise tuning. ○ Robust functioning.
Sliding Mode Observer [67, 68]	○ Decentralization and allows detecting and reject model disturbances. ○ Convergence criteria based on Lyapunov functions ideas.	○ It has a severe obstacle for practical applicability, high susceptibility to noise, difficult tuning in the sense of the observer's gains are not parameterized. ○ Robust concerning persistent modeling error, but the fragility to measurement noise is a problem (that is handled with chattering remediation - saturated function).
High Gain [90]	○ Decentralized (the nonlinear interconnection along with the error modeling can be assumed an extra state). ○ The tuning procedure is based on singular perturbation theory and pole placement approach.	○ The MPS is considered as a system that can be fully linearized.
Linear Observer (Luenberger type) [71]	○ The estimator adopts the linear representation of a MPS. Moreover, the nonlinear interconnection terms among generator units are considered. ○ The observer gains are precalculated off-line around a particular equilibrium point (without convergence analysis).	○ The reported state estimation scheme adopts a centralized (wide-area) approach. ○ A set of constants associated with the boundness of the nonlinear interconnection terms must be obtained to compute the observer gains through solving an LMI (Linear Matrix Inequality). ○ The reported observer can deal with uncertainties related to the model.
Nonlinear Observer (Luenberger-Kalman) [69]	○ Based on the fully linearized model of the MPS. ○ The observer gains depend on the Jacobian expression of MPS, and they are computed based on Kalman Filter theory, but there is not any convergence proof documented.	○ The main problem relies that the observer gains directly depends on the accuracy of the used model. ○ The reported observer does not have a fine-tuning, and it does not consider the uncertainties and disturbances of the model.

Table 4.2: State estimation techniques

4.6 Concluding Remarks

A nonlinear geometric (G), Luenberger-like, decentralized, and robustly convergent state estimation design for Multimachine Power Systems (MPSs) has been developed, with emphasis on the attainment of a compromise between reconstruction speed, robustness, computational load, and tuning simplicity that is better than the ones of

previous studies with NL EKF and SMPO designs.

The proposed estimation scheme presents similar advantages to EKF, solves the measurement with noise injection optimally, and Sliding Modes approach the decentralized structure. Moreover, it has a simple and clear to understand pole-placement tuning and low computational load. The robust convergence is formally proved through input-to-state (IS) stability and small gain ideas.

A comparison with the centralized nonlinear EKF (one of the most known estimators in the Electric Power Community) was carried out via numerical simulation. Due to its simplicity, the GE estimator has the advantage of solving considerably fewer equations, almost a quarter of the total ODEs of the EKF, which is reflected in less computational load. Noisy measurements, initial condition uncertainties, and different disturbances were considered in the simulation, showing a better performance by the GE estimator in speed convergence and less impact against measurement noises.

The present study on MPS estimation is a point of departure to address the observer-based output-feedback control design problem with an application-oriented robust-decentralized scheme.

Conclusions and Future Research

The Electric Power System is one of the most complex systems created by humans. The different nature of their components causes complex phenomena that detailed mathematical representations must capture. As previously was mentioned, state estimation is an important tool to deliver information about the system state variables for adequate control, monitoring, and protection purposes. Understanding the system dynamics, the solutions proposed in this dissertation are complete because they solve the estimation problem for IMG structures and MPSs considering different aspects, such as (i) the on-line computational load, (ii) detailed mathematical models, and their respective properties are exploited for estimator design purposes (tailored models are created for this), (iii) identification of observability properties of employed models are presented coupled with the required measurements to estimate the state variables, (iv) specifically for the proposed geometric estimator for MPSs, a formal convergence analysis of estimation error dynamics is presented based on input-to-state stability sense concerning model errors and measurement noise yielding to robust convergence conditions of the type small gains which are sharper, more transparent and with greater interpretability than those based on Lyapunov functions, and (v) the tuning scheme of proposed estimators plays an important role in estimating the state variables clearly and simply. In this way, the proposed dynamic state estimation algorithms show similar or superior performance to other previous alternatives.

The dynamic state estimation in IMG structures is addressed through two estimators based on the Kalman Filter theory, which allows estimating the dynamic variables of generators (load angle, mechanical speeds, and internal voltages) together with those algebraic variables (bus voltage phasors) related to network restrictions using fewer measurements compared to the conventional static estimators. Besides, the estimators can estimate the transient and steady-state regimes associated with the IMG operation following the proposed methodology.

To offer an alternative to those proposed centralized estimators for IMG structures addressing their main drawbacks (computational load, heuristic tuning, global information exchange). For this, a new methodology for the online state estimation of MPS is proposed, through the unknown input-state extension with integral action of the

geometric state estimation, the augmented state (lumping in one fictitious state, after linearization, the combined effect of unmeasured disturbances and state dependency on other machines) is recovered with a non-high gain observer coupled with simple conventional tuning and convergence criteria. Based on a state-unmeasured input observable decentralized model, the dynamic state (load angle, relative speed, and electrical power difference) of every generator is estimated through the local information, using load angle as individual measured output.

This dissertation's dynamic estimators offer a solution to the estimation problem for IMG structures and MPSs. Nevertheless, there are open problems that should be addressed in the future, like validating the proposed dynamic estimators through specialized software and using different electrical networks containing conventional and renewable generation, inverter sources, and dynamic load models. This and other aspects are addressed in the following Section.

5.1 Future Research

Future work can be generalized into the following aspects:

- Dynamic state estimation, whether being carried out in a centralized or distributed/decentralized manner, needs real-time measurements, and this information needs to be transferred to proper locations, such as a control center at transmission or distribution level. Thus, it should be included analysis about which are the data requirements, such as data rates, signals, sensor placement, reliability, redundancy (for wide-area applications), data communication requirements [5].

- Power systems have been improved over time considering complex and different variables (inclusion of different generation sources), diversity between configurations, with mixed slow and fast dynamics. Thus, the estimation algorithms should be improved to work with increasingly complex models to meet the operational requirements of future power systems [5].

- To explore how dynamic state estimation can be compatible with a control room environment in terms of information, technological infrastructure, and human-machine interface [5].

- To implement the developed state estimation algorithms in different electrical networks and validate them with specialized software, such as DIgSilent, PSCAD.

- To implement and adapt the proposed geometric estimator for electrical networks, which can contain conventional and renewable generation, inverter sources, and dynamic load models, similar to those considered in IMG studies. The estimation of dynamic variables associated with generators through local information will allow decentralized control schemes to address the frequency control problem for IMG structures.

○ The present study on MPS estimation is a point of departure to address the observer-based output-feedback control design problem with an application-oriented robust-decentralized scheme.

Nonlinear Maps and Open Loop System Functions

$$g_i(\boldsymbol{x}, \boldsymbol{d}_\gamma) = -c_i(\rho_i - \rho_{t_i})(I_{q_i} I_{d_i}) - c_i P_{m_i} + E'_{q_i} \left[\sum_{j=1}^{N} \dot{E}'_{q_j} B_{ij} \sin(\delta_i - \delta_j) \right.$$

$$\left. - \sum_{j=1}^{N} E'_{q_j} B_{ij} \cos(\delta_i - \delta_j)\omega_j \right] - \alpha_i \bar{\delta}_i \tag{A.0.1}$$

$$\iota_i = \dot{g}_i(\boldsymbol{x}, \boldsymbol{d}_\gamma) = F_i(\boldsymbol{x}, \boldsymbol{d}_\gamma, \dot{\boldsymbol{d}}_\gamma) = \left[\sum_{j=1}^{N} E'_{q_i} \dot{E}'_{q_j} B_{ij} \cos(\delta_i - \delta_j) + \sum_{j=1}^{N} E'_{q_i} E'_{q_j} B_{ij} \sin(\delta_i - \delta_j)\omega_j \right] \omega_i$$

$$- \left[\sum_{j=1}^{N} E'_{q_i} \dot{E}'_{q_j} B_{ij} \cos(\delta_i - \delta_j) + \sum_{j=1}^{N} E'_{q_i} E'_{q_j} B_{ij} \sin(\delta_i - \delta_j)\omega_j \right] \omega_j - \left[\sum_{j=1}^{N} E'_{q_i} B_{ij} \cos(\delta_i - \delta_j)\omega_j \right] \dot{E}'_{q_j}$$

$$- \left[\sum_{j=1}^{N} E'_{q_j} B_{ij} \cos(\delta_i - \delta_j) \right] [a_j \omega_j - b_j P_j + d_{\omega_j}]$$

$$+ \left[\sum_{j=1}^{N} \dot{E}'_{q_j} B_{ij} \sin(\delta_i - \delta_j) - \sum_{j=1}^{N} E'_{q_j} B_{ij} \cos(\delta_i - \delta_j)\omega_j \right] \dot{E}'_{q_i} \tag{A.0.2}$$

$$\boldsymbol{\varepsilon}_i(\boldsymbol{z}, \boldsymbol{v}_i, \dot{\boldsymbol{v}}_i, \boldsymbol{d}_\gamma, \dot{\boldsymbol{d}}_\gamma; \tilde{\boldsymbol{z}}, \tilde{\boldsymbol{v}}_i, \dot{\tilde{\boldsymbol{v}}}_i, \tilde{\boldsymbol{d}}_\gamma, \dot{\tilde{\boldsymbol{d}}}_\gamma, \tilde{\boldsymbol{p}}_i, \pi) =$$

$$\begin{bmatrix} 4\zeta_i e_{y_i}(\pi) \\ (4\zeta_i^2 + 2)w_i^2 e_{y_i}(\pi) \\ (4\zeta_i w_i^3)e_{y_i}(\pi) \\ \Phi_i(\boldsymbol{z}_i, \boldsymbol{v}_i, \dot{\boldsymbol{v}}_i; \tilde{\boldsymbol{z}}_i, \tilde{\boldsymbol{v}}_i, \dot{\tilde{\boldsymbol{v}}}_i, \tilde{\boldsymbol{p}}_i, \pi) + \vartheta_i(\boldsymbol{z}, \boldsymbol{d}_\gamma, \dot{\boldsymbol{d}}_\gamma; \tilde{\boldsymbol{z}}, \tilde{\boldsymbol{d}}_\gamma, \dot{\tilde{\boldsymbol{d}}}_\gamma) + w_i^4 e_{y_i}(\pi) \end{bmatrix} \tag{A.0.3a}$$

$$\Phi_i(\boldsymbol{z}_i, \boldsymbol{v}_i, \dot{\boldsymbol{v}}_i; \tilde{\boldsymbol{z}}_i, \tilde{\boldsymbol{v}}_i, \dot{\tilde{\boldsymbol{v}}}_i, \tilde{\boldsymbol{p}}_i, \pi) = \Psi_i(\boldsymbol{z}_i; \tilde{\boldsymbol{z}}_i, \tilde{\boldsymbol{p}}_i) + \tilde{\phi}_i(t) \tag{A.0.3b}$$

$$\Psi_i(\boldsymbol{z}_i; \tilde{\boldsymbol{z}}_i, \tilde{\boldsymbol{p}}_i) = -\tilde{\gamma}_2^i(z_{2i} + \tilde{z}_{2i}) - \tilde{\gamma}_3^i(z_{3i} + \tilde{z}_{3i}) - \tilde{\gamma}_4^i(z_{4i} + \tilde{z}_{4i})$$

$$= -(\tilde{b}_i + b_i)(\tilde{\alpha}_i + \alpha_i)(z_{2i} + \tilde{z}_{2i}) + [(\tilde{b}_i + b_i)(\tilde{q}_i + q_i) - (\tilde{a}_i + a_i)(\tilde{c}_i + c_i)](z_{3i} + \tilde{z}_{3i})$$

$$- [(\tilde{a}_i + a_i) + (\tilde{c}_i + c_i)](z_{4i} + \tilde{z}_{4i}) \tag{A.0.3c}$$

$$\tilde{\phi}_i(t) = \tilde{c}_i \dot{d}_{\omega_i}(\pi) + (\tilde{c}_i + c_i)\dot{\tilde{d}}_{\omega_i}(\pi) - \tilde{b}_i \dot{u}_i(\pi) - (\tilde{b}_i + b_i)\dot{\tilde{u}}_i(\pi) + \ddot{\tilde{d}}_{\omega_i}(\pi) \tag{A.0.3d}$$

$$\vartheta_i(\boldsymbol{z}, \boldsymbol{d}_\gamma, \dot{\boldsymbol{d}}_\gamma; \tilde{\boldsymbol{z}}, \tilde{\boldsymbol{d}}_\gamma, \dot{\tilde{\boldsymbol{d}}}_\gamma) = b_i \left[F_i(\boldsymbol{z} + \tilde{\boldsymbol{z}}, \boldsymbol{d}_\gamma + \tilde{\boldsymbol{d}}_\gamma, \dot{\boldsymbol{d}}_\gamma + \dot{\tilde{\boldsymbol{d}}}_\gamma) - F_i(\boldsymbol{z}, \boldsymbol{d}_\gamma, \dot{\boldsymbol{d}}_\gamma) \right] \tag{A.0.3e}$$

$$= \left[\sum_{j=1}^{N} b_i(E'_{q_i} + \tilde{E}'_{q_i})(E'_{q_j} + \tilde{E}'_{q_j})B_{ij}\cos(z_{1ij} + e_{1ij}) + \sum_{j=1}^{N} b_i(E'_{q_i} + \tilde{E}'_{q_i})(E'_{q_j} + \tilde{E}'_{q_j})B_{ij}\sin(z_{1ij} + e_{1ij}) \right.$$

$$(z_{2j} + \tilde{z}_{2j})] (z_{2i} + \tilde{z}_{2i}) - \left[\sum_{j=1}^{N} b_i E'_{q_i} E'_{q_j} B_{ij}\cos(z_{1ij}) + \sum_{j=1}^{N} b_i E'_{q_i} E'_{q_j} B_{ij}\sin(z_{1ij})z_{2j} \right] z_{2i}$$

$$+ \left[\sum_{j=1}^{N} b_i(E'_{q_i} + \tilde{E}'_{q_i})(E'_{q_j} + \dot{\tilde{E}}'_{q_j})B_{ij}\cos(z_{1ij} + e_{1ij}) + \sum_{j=1}^{N} b_i(E'_{q_i} + \tilde{E}'_{q_i})(E'_{q_j} + \tilde{E}'_{q_j})B_{ij}\sin(z_{1ij} + e_{1ij}) \right] (z_{2j} + \tilde{z}_{2j})$$

$$- \left[\sum_{j=1}^{N} b_i E'_{q_i} \dot{E}'_{q_j} B_{ij}\cos(z_{1ij}) + \sum_{j=1}^{N} b_i E'_{q_i} E'_{q_j} B_{ij}\sin(z_{1ij}) \right] z_{2j} - b_i c_i(\rho_i - \rho_{t_i})\tilde{I}_{q_i}\dot{I}_{d_i} - b_i c_i(\rho_i - \rho_{t_i})\dot{I}_{q_i}\tilde{I}_{d_i}$$

$$- \left[\sum_{j=1}^{N} b_i(E'_{q_j} + \tilde{E}'_{q_j})B_{ij}\cos(z_{1ij} + e_{1ij}) \right] (z_{3j} + \tilde{z}_{3j}) + \left[\sum_{j=1}^{N} b_i E'_{q_j} B_{ij}\cos(z_{1ij}) \right] z_{3j}$$

$$+ \left[\sum_{j=1}^{N} b_i(\dot{E}'_{g_j} + \dot{\tilde{E}}'_{q_j})B_{ij}\sin(z_{1ij} + e_{1ij}) - \sum_{j=1}^{N} b_i(E'_{g_j} + \tilde{E}'_{q_j})B_{ij}\sin(z_{1ij} + e_{1ij})(z_{2j} + \tilde{z}_{2j}) \right] (\dot{E}'_{q_i} + \dot{\tilde{E}}'_{q_i})$$

$$- \left[\sum_{j=1}^{N} b_i \dot{E}'_{g_j} B_{ij}\sin(z_{1ij}) - \sum_{j=1}^{N} E'_{g_j} B_{ij}\sin(z_{1ij})z_{2j} \right] \dot{E}'_{q_i} - \left[\sum_{j=1}^{N} b_i(E'_{q_i} + \tilde{E}'_{q_i})B_{ij}\cos(z_{1ij} + e_{1ij})(z_{2j} + \tilde{z}_{2j}) \right] (\dot{E}'_{q_j} + \dot{\tilde{E}}'_{g_j})$$

$$+ \left[\sum_{j=1}^{N} b_i E'_{q_i} B_{ij}\cos(z_{1ij})z_{2j} \right] \dot{E}'_{q_j} + \left[\sum_{j=1}^{N} b_i(E'_{q_i} + \tilde{E}'_{q_i})B_{ij}\sin(z_{1ij} + e_{1ij}) \right] (\ddot{E}'_{q_j} + \ddot{\tilde{E}}'_{q_j}) - \left[\sum_{j=1}^{N} b_i E'_{q_i} B_{ij}\sin(z_{1ij}) \right] \ddot{E}'_{q_j}$$

$$- b_i c_i \dot{P}_{m_i} \tag{A.0.3f}$$

where

$$z_{1ij} = z_{1i} - z_{1j}, \qquad \tilde{z}_{1ij} = \tilde{z}_{1i} - \tilde{z}_{1j} \tag{A.0.3g}$$

IMG Parameters

Study cases Sections 3.2.3 and 3.3.3. Parameters given on a 10 MVA base: Synchronous generator power base established on 5 MW, $E_{F_i} = 0.8460$ p.u, $P_{m_i} = 0.2333$ p.u, $D_i = 0.8$ p.u, $H_i = 5$ s, $\tau_1 = 7$ s, $x_{d_i} = 1.35$ p.u, $x'_{d_i} = 0.20$ p.u, $x_{q_i} = 1.39$ p.u, and $x'_{q_i} = 0.3$ p.u. For the simulation of the IG the following data was considered: $R_{r_i} = 0.01$ p.u, $R_{s_i} = 0.01$ p.u, $L_{m_i} = 3.0$ p.u, $L_{s\sigma_i} = 0.10$ p.u, $L_{r\sigma_i} = 0.08$ p.u, $P_{nom} = 0.9$ MW, 50 Hz, 4 pole pairs. Wind turbine data: $R_b = 57$ m, $\rho = 1.225$ kg/m^3, $n_{gb} = 67.5$ m, $c_1 = 0.5$, $c_2 = 116$, $c_3 = 0.4$, $c_4 = 0$, $c_5 = 0$, $c_6 = 5$, $c_7 = 21$, $c_8 = 0.08$, $c_9 = 0.035$, $\beta = 0$, $H_{eq} = 3$ s.

Bibliography

[1] Robert H Lasseter. Microgrids and distributed generation. *Journal of Energy Engineering*, 133(3):144–149, 2007. 5, 13

[2] Huang Jiayi, Jiang Chuanwen, and Xu Rong. A review on distributed energy resources and microgrid. *Renewable and Sustainable Energy Reviews*, 12(9):2472–2483, 2008. 5

[3] Natanael Vieyra, Paul Maya, and Luis M Castro. Dynamic state estimation for microgrid structures. *Electric Power Components and Systems*, 48(3):320–332, 2020. 5, 16, 18, 24, 25, 27, 28, 30, 67

[4] Natanael Vieyra, Paul Maya, and Luis M Castro. Effective dynamic state estimation algorithm for islanded microgrid structures based on singular perturbation theory. *Electric Power Systems Research*, 187:106455, 2020. xv, 5, 16, 18, 24, 37, 40, 49

[5] Junbo Zhao, Marcos Netto, Zhenyu Huang, Shenglong Yu, Antonio Gomez-Exposito, Shaobu Wang, Innocent Kamwa, Shahrokh Akhlaghi, Lamine Mili, Vladimir Terzija, et al. Roles of dynamic state estimation in power system modeling, monitoring and operation. *IEEE Transactions on Power Systems*, 2020. 5, 6, 71, 80

[6] Alcir Monticelli. *State estimation in electric power systems: a generalized approach*. Springer Science & Business Media, 2012. 5

[7] Gianmario Rinaldi, Prathyush P Menon, Christopher Edwards, and Antonella Ferrara. Higher order sliding mode observers in power grids with traditional and renewable sources. *IEEE Control Systems Letters*, 4(1):223–228, 2019. 8

[8] Gildas Besançon. *Nonlinear observers and applications*, volume 363. Springer, 2007. 12

[9] Farid Katiraei, Reza Iravani, Nikos Hatziargyriou, and Aris Dimeas. Microgrids management. *IEEE power and energy magazine*, 6(3):54–65, 2008. xiii, 13, 14

[10] Sungyun Choi and AP Sakis Meliopoulos. Effective real-time operation and protection scheme of microgrids using distributed dynamic state estimation. *IEEE Transactions on Power Delivery*, 32(1):504–514, 2016. 13, 24

[11] Prabha Kundur, Neal J Balu, and Mark G Lauby. *Power system stability and control*, volume 7. McGraw-hill New York, 1994. 14, 16

[12] Peter W Sauer and Mangalore Anantha Pai. *Power system dynamics and stability*, volume 101. Prentice hall Upper Saddle River, NJ, 1998. xiii, 14, 69, 70

[13] John J Grainger, William D Stevenson, William D Stevenson, et al. *Power system analysis*. 2003. 14

[14] Thomas Ackermann. *Wind power in power systems*. John Wiley & Sons, 2005. 15

[15] Leonard L Grigsby. *Electric power generation, transmission, and distribution*. CRC press, 2018. 17

[16] William J Terrell. Observability of nonlinear differential algebraic systems. *Circuits, Systems and Signal Processing*, 16(2):271–285, 1997. 18, 29

[17] Chris J Dafis. An observability formulation for nonlinear power systems modeled as differential algebraic systems. 2005. 18, 29

[18] Gustavo Valverde and Vladimir Terzija. Unscented kalman filter for power system dynamic state estimation. *IET generation, transmission & distribution*, 5(1):29–37, 2011. 18, 29, 40

[19] Long Gao, Lin Chen, Yushun Fan, and Haiwu Ma. A nonlinear control design for power systems. *Automatica*, 28(5):975–979, 1992. 19

[20] Youyi Wang, David J Hill, Richard H Middleton, and Long Gao. Transient stability enhancement and voltage regulation of power systems. *IEEE Transactions on Power systems*, 8(2):620–627, 1993.

[21] Yi Guo, David J Hill, and Youyi Wang. Global transient stability and voltage regulation for power systems. *IEEE transactions on power systems*, 16(4):678–688, 2001.

[22] Youyi Wang, Guoxiao Guo, and David J Hill. Robust decentralized nonlinear controller design for multimachine power systems. *Automatica*, 33(9):1725–1733, 1997.

[23] Tianrui Chen, David John Hill, and Cong Wang. Distributed fast fault diagnosis for multimachine power systems via deterministic learning. *IEEE Transactions on Industrial Electronics*, 2019. 19

[24] Hany EZ Farag, S Saxena, and A Asif. A robust dynamic state estimation for droop controlled islanded microgrids. *Electric Power Systems Research*, 140:445–455, 2016. 24

[25] George N Korres, Nikos D Hatziargyriou, and Petros J Katsikas. State estimation in multi-microgrids. *European transactions on electrical power*, 21(2):1178–1199, 2011. 24, 25, 35

[26] Yanbo Wang, Yanjun Tian, Xiongfei Wang, Zhe Chen, and Yongdong Tan. Kalman-filter-based state estimation for system information exchange in a multi-bus islanded microgrid. 2014. 24, 25, 29, 35

[27] Shivam Saxena, Amir Asif, and Hany Farag. Nonlinear, reduced order, distributed state estimation in microgrids. In *2015 IEEE International Conference on Acoustics, Speech and Signal Processing (ICASSP)*, pages 2874–2878. IEEE, 2015. 35

[28] Md Masud Rana, Li Li, Steven W Su, and Wei Xiang. Consensus-based smart grid state estimation algorithm. *IEEE Transactions on Industrial Informatics*, 14(8):3368–3375, 2017. 24, 25, 29, 48

[29] Natallia Makarava, Guosong Lin, and Sascha Eichstädt. Adaptive quasi-dynamic state estimation for mv and lv grids. *EURASIP Journal on Advances in Signal Processing*, 2019(1):39, 2019. 24

[30] Yang Mi, Yang Fu, Dongdong Li, Chengshan Wang, Poh Chiang Loh, and Peng Wang. The sliding mode load frequency control for hybrid power system based on disturbance observer. *International Journal of Electrical Power & Energy Systems*, 74:446–452, 2016. 25

[31] Zhenyu Huang, Pengwei Du, Dmitry Kosterev, and Steven Yang. Generator dynamic model validation and parameter calibration using phasor measurements at the point of connection. *IEEE transactions on power systems*, 28(2):1939–1949, 2013. 25, 36, 47, 48, 49, 76

[32] Hamed Tebianian and Benjamin Jeyasurya. Dynamic state estimation in power systems: Modeling, and challenges. *Electric Power Systems Research*, 121:109–114, 2015. 49, 51, 52, 67, 69

[33] Esmaeil Ghahremani and Innocent Kamwa. Dynamic state estimation in power system by applying the extended kalman filter with unknown inputs to phasor measurements. *IEEE Transactions on Power Systems*, 26(4):2556–2566, 2011. 48, 49

[34] Lingling Fan and Yasser Wehbe. Extended kalman filtering based real-time dynamic state and parameter estimation using pmu data. *Electric Power Systems Research*, 103:168–177, 2013. 25, 36, 47, 48, 49, 67, 76

[35] Jing Huang, Vijay Gupta, and Yih-Fang Huang. Electric grid state estimators for distribution systems with microgrids. In *2012 46th Annual Conference on Information Sciences and Systems (CISS)*, pages 1–6. IEEE, 2012. 25, 35

[36] Ying Hu, Anthony Kuh, Aleksandar Kavcic, and Dora Nakafuji. Real-time state estimation on micro-grids. In *The 2011 International Joint Conference on Neural Networks*, pages 1378–1385. IEEE, 2011. 25, 35

[37] Md Rana, Li Li, and Steven Su. Kalman filter based microgrid state estimation and control using the iot with 5g networks. In *2015 IEEE PES Asia-Pacific Power and Energy Engineering Conference (APPEEC)*, pages 1–5. IEEE, 2015. 25, 29, 35, 48

[38] MM Rana, Wei Xiang, and Eric Wang. H-infinity-based microgrid state estimations using the iot sensors. In *Smart Power Distribution Systems*, pages 285–295. Elsevier, 2019. 25, 29, 35, 48

[39] Esmaeil Ghahremani and Innocent Kamwa. Online state estimation of a synchronous generator using unscented kalman filter from phasor measurements units. *IEEE Transactions on Energy Conversion*, 26(4):1099–1108, 2011. 25, 36, 47, 48

[40] Zhenyu Huang, Kevin Schneider, and Jarek Nieplocha. Feasibility studies of applying kalman filter techniques to power system dynamic state estimation. In *2007 International Power Engineering Conference (IPEC 2007)*, pages 376–382. IEEE, 2007. 49, 51, 52, 69, 76

[41] Zhenyu Huang, Kevin Schneider, Jarek Nieplocha, and Ning Zhou. Estimating power system dynamic states using extended kalman filter. In *2014 IEEE PES General Meeting— Conference & Exposition*, pages 1–5. IEEE, 2014. 49, 76

[42] Ning Zhou, Da Meng, Zhenyu Huang, and Greg Welch. Dynamic state estimation of a synchronous machine using pmu data: A comparative study. *IEEE Transactions on Smart Grid*, 6(1):450–460, 2014. 48, 49, 67, 71

[43] Yinan Cui and Rajesh Kavasseri. A particle filter for dynamic state estimation in multi-machine systems with detailed models. *IEEE Transactions on Power Systems*, 30(6):3377–3385, 2015. 48

[44] Ning Zhou, Da Meng, and Shuai Lu. Estimation of the dynamic states of synchronous machines using an extended particle filter. *IEEE Transactions on Power Systems*, 28(4):4152–4161, 2013. 48

[45] Junbo Zhao and Lamine Mili. Power system robust decentralized dynamic state estimation based on multiple hypothesis testing. *IEEE Transactions on Power Systems*, 33(4):4553–4562, 2017.

[46] Junbo Zhao and Lamine Mili. A decentralized h-infinity unscented kalman filter for dynamic state estimation against uncertainties. *IEEE Transactions on Smart Grid*, 10(5):4870–4880, 2018. 48

[47] Yang Yu, Zhongjie Wang, and Chengchao Lu. A joint filter approach for reliable power system state estimation. *IEEE Transactions on Instrumentation and Measurement*, 68(1):87–94, 2018. 25, 36, 47

[48] Ravi Kumar Mandela, Raghunathan Rengaswamy, Shankar Narasimhan, and Lakshmi N Sridhar. Recursive state estimation techniques for nonlinear differential algebraic systems. *Chemical engineering science*, 65(16):4548–4556, 2010. 26, 27, 28, 35, 40, 41, 45, 46

[49] Victor Manuel Becerra, PD Roberts, and GW Griffiths. Applying the extended kalman filter to systems described by nonlinear differential-algebraic equations. *Control Engineering Practice*, 9(3):267–281, 2001. 27

[50] Thomas Mazzoni. Computational aspects of continuous–discrete extended kalman-filtering. *Computational Statistics*, 23(4):519–539, 2008. 27

[51] Paul Frogerais, Jean-Jacques Bellanger, and Lotfi Senhadji. Various ways to compute the continuous-discrete extended kalman filter. *IEEE Transactions on Automatic Control*, 57(4):1000–1004, 2011. 27

[52] Kathryn Eleda Brenan, Stephen L Campbell, and Linda Ruth Petzold. *Numerical solution of initial-value problems in differential-algebraic equations*, volume 14. Siam, 1996. 27

[53] Kenneth E Martin. Synchrophasor measurements under the ieee standard c37. 118.1-2011 with amendment c37. 118.1 a. *IEEE Transactions on Power Delivery*, 30(3):1514–1522, 2015. 29

[54] Simon J Julier and Jeffrey K Uhlmann. New extension of the kalman filter to nonlinear systems. In *Signal processing, sensor fusion, and target recognition VI*, volume 3068, pages 182–193. International Society for Optics and Photonics, 1997. 35

[55] Shaobu Wang, Wenzhong Gao, and AP Sakis Meliopoulos. An alternative method for power system dynamic state estimation based on unscented transform. *IEEE transactions on power systems*, 27(2):942–950, 2011. 35, 51, 52, 69

[56] Abhinav Kumar Singh and Bikash C Pal. Decentralized dynamic state estimation in power systems using unscented transformation. *IEEE Transactions on Power Systems*, 29(2):794–804, 2013. 35

[57] M Rana, Li Li, Steven W Su, and Wei Xiang. Microgrid state estimation: A distributed approach. *IEEE Trans. Ind. Inform*, 14(8):3368–3375, 2018. 35

[58] JH Chow, JR Winkelman, MA Pai, and PW Sauer. Singular perturbation analysis of large-scale power systems. *International Journal of Electrical Power & Energy Systems*, 12(2):117–126, 1990. 36

[59] George Peponides, PV Kokotovic, and J Chow. Singular perturbations and time scales in nonlinear models of power systems. *IEEE Transactions on Circuits and systems*, 29(11):758–767, 1982. 36

[60] E Scholtz, P Sonthikorn, GC Verghese, and BC Lesieutre. Observers for swing-state estimation of power systems. In *North American Power Symposium*, 2002. 48

[61] Esmaeil Ghahremani and Innocent Kamwa. Local and wide-area pmu-based decentralized dynamic state estimation in multi-machine power systems. *IEEE Transactions on Power Systems*, 31(1):547–562, 2015. 49

[62] Chong Wang, Zhijun Qin, Yunhe Hou, and Jie Yan. Multi-area dynamic state estimation with pmu measurements by an equality constrained extended kalman filter. *IEEE Transactions on Smart Grid*, 9(2):900–910, 2016.

[63] Shahrokh Akhlaghi, Ning Zhou, and Zhenyu Huang. A multi-step adaptive interpolation approach to mitigating the impact of nonlinearity on dynamic state estimation. *IEEE Transactions on Smart Grid*, 9(4):3102–3111, 2016. 49

[64] Junjian Qi, Kai Sun, Jianhui Wang, and Hui Liu. Dynamic state estimation for multi-machine power system by unscented kalman filter with enhanced numerical stability. *IEEE Transactions on Smart Grid*, 9(2):1184–1196, 2016. 49

[65] Xueyuan Wang, Junbo Zhao, Vladimir Terzija, and Shaobu Wang. Fast robust power system dynamic state estimation using model transformation. *International Journal of Electrical Power & Energy Systems*, 114:105390, 2020. 49

[66] Shahrokh Akhlaghi, Ning Zhou, and Zhenyu Huang. Hybrid approach for estimating dynamic states of synchronous generators. *IET Generation, Transmission & Distribution*, 13(5):669–678, 2018. 49

[67] L Jiang, QH Wu, J Wang, C Zhang, and XX Zhou. Robust observer-based nonlinear control of multimachine power systems. *IEE Proceedings-Generation, Transmission and Distribution*, 148(6):623–631, 2001. 50, 53, 54, 76

[68] Mokhtar Mohamed, Xing-Gang Yan, Sarah K Spurgeon, and Bin Jiang. Robust sliding-mode observers for large-scale systems with application to a multimachine power system. *IET Control Theory & Applications*, 11(8):1307–1315, 2016. 50, 51, 52, 69, 71, 75, 76

[69] Md Apel Mahmud, HR Pota, and MJ Hossain. Full-order nonlinear observer-based excitation controller design for interconnected power systems via exact linearization approach. *International Journal of Electrical Power & Energy Systems*, 41(1):54–62, 2012. 50, 76

[70] Gerasimos Rigatos, Pierluigi Siano, and Nikolaos Zervos. Sensorless control of distributed power generators with the derivative-free nonlinear kalman filter. *IEEE Transactions on Industrial Electronics*, 61(11):6369–6382, 2014. 50

[71] Junjian Qi, Ahmad F Taha, and Jianhui Wang. Comparing kalman filters and observers for power system dynamic state estimation with model uncertainty and malicious cyber attacks. *IEEE Access*, 6:77155–77168, 2018. 50, 76

[72] Jesús Alvarez. Nonlinear state estimation with robust convergence. *Journal of Process Control*, 10(1):59–71, 2000. 50, 52, 55, 64

[73] G Ciccarella, M Dalla Mora, and Alfredo Germani. A luenberger-like observer for nonlinear systems. *International Journal of Control*, 57(3):537–556, 1993. 50, 52, 55

[74] Michael Zeitz. The extended luenberger observer for nonlinear systems. *Systems & Control Letters*, 9(2):149–156, 1987. 50, 52, 55

[75] Xiangjie Liu and Yaozhen Han. Decentralized multi-machine power system excitation control using continuous higher-order sliding mode technique. *International Journal of Electrical Power & Energy Systems*, 82:76–86, 2016. 51, 52, 69

[76] A Colbia-Vega, J de Leon-Morales, L Fridman, O Salas-Pena, and MT Mata-Jiménez. Robust excitation control design using sliding-mode technique for multi-machine power systems. *Electric Power Systems Research*, 78(9):1627–1634, 2008.

[77] Wenzhong Gao and Shaobu Wang. On-line dynamic state estimation of power systems. In *North American Power Symposium 2010*, pages 1–6. IEEE, 2010. 51, 52, 69

[78] Arthur Gelb. *Applied optimal estimation*. MIT press, 1974. 52, 59, 68

[79] Ki Sung You, Min Cheol Lee, and Wan Suk Yoo. Sliding mode controller with sliding perturbation observer based on gain optimization using genetic algorithm. *KSME International Journal*, 18(4):630, 2004. 53

[80] Bo Yang, Tao Yu, Hongchun Shu, Jun Dong, and Lin Jiang. Robust sliding-mode control of wind energy conversion systems for optimal power extraction via nonlinear perturbation observers. *Applied Energy*, 210:711–723, 2018. 53

[81] Marcella Porru, J Alvarez, and Roberto Baratti. Composition estimator design for industrial multicomponent distillation column. *Chemical Engineering Transactions*, 32:1975–1980, 2013. 55

[82] Hassan K Khalil and Jessy W Grizzle. *Nonlinear systems*, volume 3. Prentice hall Upper Saddle River, NJ, 2002. 56, 71

[83] Alberto Isidori. *Nonlinear control systems*. Springer Science & Business Media, 2013. 56, 65

[84] Thomas Kailath. *Linear systems*, volume 156. Prentice-Hall Englewood Cliffs, NJ, 1980. 58, 59

[85] Wilson J Rugh. *Linear system theory*. Prentice-Hall, Inc., 1996. 59

[86] Robert Hermann and Arthur Krener. Nonlinear controllability and observability. *IEEE Transactions on automatic control*, 22(5):728–740, 1977. 59

[87] Jesus Alvarez and Teresa López. Robust dynamic state estimation of nonlinear plants. *AICHE journal*, 45(1):107–123, 1999. 62, 64, 69

[88] Jesús Álvarez and Carlos Fernández. Geometric estimation of nonlinear process systems. *Journal of process control*, 19(2):247–260, 2009. 65, 66, 68

[89] J Carberry James. *Process modeling, simulation and control for chemical engineers*. McGraw-Hill, 1989. 66

[90] Lin Jiang, Q Henry Wu, and JY Wen. Decentralized nonlinear adaptive control for multimachine power systems via high-gain perturbation observer. *IEEE Transactions on Circuits and Systems I: Regular Papers*, 51(10):2052–2059, 2004. 76